Finite Element Design and Manufacturing of a Nylon-String Guitar Soundboard from Sandwich-Structured Composites

Negin Abaeian

Music Technology Area, Department of Music Research

Schulich School of Music

McGill University

Montreal, Canada

December 2017

Abstract

The aim of this project was to use the Finite Element Method (FEM) to design and manufacture the soundboard of a nylon-string guitar from sandwich-structured composites, with reference to an existing wooden soundboard, and to evaluate the accuracy of the numerical models of the wooden soundboard, the brace-less composite top plate and the braced composite soundboard by means of experimental modal analysis.

The modal behaviour of the existing wooden soundboard was studied through experimental modal analysis and numerical simulation. Using FEM, the effects of varying certain physical, geometric and elastic properties of the materials used in the soundboard were determined on its natural frequencies under free and hinged Boundary Conditions (BCs). The composite soundboard that was determined to have natural frequencies relatively similar to those of the wooden soundboard under hinged BCs, and could be built from commercially available materials was constructed. To verify the results predicted numerically, experimental modal analyses were performed on the brace-less composite top plate and the braced composite soundboard under free BCs.

The experimental natural frequencies and mode-shapes of the constructed brace-less top plate were found to match those predicted by the simulation in the frequency range below 200 [Hz], while slightly diverging in the higher frequency range. The experimental results for the braced composite soundboard were also found to be relatively similar to the numerically predicted values, with most mode-shapes matching, and some differences in the mode-frequencies, mostly in the low and mid-frequency ranges. Overall, a reasonable agreement was achieved between the numerical and the experimental results.

Sommaire

L'objectif de ce projet était d'utiliser la Méthode des Éléments Finis (MEF) pour concevoir et fabriquer une table d'harmonie de guitare à cordes en nylon à partir de composites sandwiches en se référant à une table en bois existante; et d'évaluer la précision des modèles numériques de la table d'harmonie en bois, de la plaque supérieure en composite sans renforts et de la table d'harmonie composite renforcée au moyen d'une analyse modale expérimentale.

Le comportement modal de la table d'harmonie existante en bois a été étudié au moyen de l'analyse modale expérimentale et de la simulation numérique. En utilisant la MEF, les effets de la variation de certaines propriétés physiques, géométriques et élastiques des matériaux utilisés dans la table d'harmonie ont été déterminés sur ses fréquences propres en utilisant des Conditions aux Limites (CL) soit libres soit immobiles (c.à-d., sans translations). La table d'harmonie en composite, dont on a déterminé qu'elle avait des fréquences propres relativement similaires à celles de la table d'harmonie en bois sous CL immobiles, et qui peut être construite à partir de matériaux disponibles dans le commerce, a été produite. Pour vérifier les résultats prédits numériquement, des analyses modales expérimentales ont été effectuées sur la plaque supérieure composite et la table d'harmonie en composites sous CL non contraintes.

Les fréquences propres expérimentales et les différents modes propres de la plaque supérieure construite sans renforts correspondent à celles prédites par la simulation dans la gamme de fréquences inférieures à 200 [Hz], tout en divergeant dans la plage de fréquences plus élevées. Les résultats expérimentaux pour la table d'harmonie composite avec renforts se sont également révélés relativement similaires aux valeurs prédites numériquement, la plupart des formes de modes propres correspondantes, et certaines différences dans les fréquences propres, principalement dans les plages de basses et moyennes fréquences. Dans l'ensemble, un accord raissonable a été obtenu entre les résultats numériques et les résultats expérimentaux.

Acknowledgements

Contents

List of Figures

List of Tables

List of Abbreviations

CAD: Computer Aided Design

DOF: Degrees of Freedom

EOM: Equation of Motion

FEM: The Finite Element Method

FRP: Fiber Reinforced Plastics

CFRP: Carbon Fibre Reinforced Plastics

GFRP: Glass Fibre Reinforced Plastics

ODS: Operational Deflection Shape

MSDS: Material Safety Data Sheet

Chapter 1

Introduction

1.1 Motivation

The vibrational behaviour of the nylon-string guitar is a function of different factors that intrinsically affect the sound quality or the musical timbre of the instrument. One of the most important factors is the top plate of the instrument (i.e., the soundboard), since the sound produced by an acoustic plucked-string instrument, such as the guitar, highly depends on the ability of the soundboard to vibrate in response to the strings' excitation [1, p.11].

For hundreds of years, the body of the nylon-string guitar and the braces inside the body have been made mainly from wood. Many tonewoods, however, are now on the verge of extinction [2]. In addition to that, since wood is a natural material, it is not possible to re-produce a wooden guitar with identical elastic properties, vibrational behaviour and consequently the same timbre as another. Different wooden species or parts belonging to the same trunk may not exhibit identical extents of variations, nor do they behave in the same manner under identical excitations. Furthermore, the response of wooden instruments can vary with humidity and temperature [1, p.235].

It is due to this sensitivity to environmental changes, lack of predictability in the instrument sound, and sustainability factors that many acoustic guitar makers have started exploring the possibility of producing instruments from more stable and predictable synthetic materials such as composites. Examples of composite guitars commercially available in the market would include Ovation Guitars, which have been in the market since the 1960's [3], as well as RainSong [4, p.37] and Emerald guitars [5]. Aside from the commercial guitars available in the market, a number of custom-made composite guitars and their acoustic properties have been studied by other researchers as well, e.g. [6] [7] [8].

1

Despite the research done on composite guitars, the musical benefits and acoustic properties of composites as substitute materials for wood are still rather unknown to many musicians. Therefore, the ultimate goal of this project was to expand the research and literature available on the vibrational properties of composite instruments, and to explore the possibility of making composite guitars that sound similar to conventional wooden guitars.

1.2   Project Overview

The aim of this project was to use the Finite Element Method (FEM) to design and manufacture the soundboard of a nylon-string guitar from sandwich-structured composites, with reference to an existing wooden soundboard, and to evaluate the accuracy of the numerical models of the reference and the designed soundboards by means of experimental modal analysis.

The composite soundboard was designed such that it is strong enough to withstand the tension of the strings, light enough to vibrate in response to conventional strings, and under hinged Boundary Conditions (BCs), has natural frequencies similar to those of the wooden soundboard. It was therefor required that the design takes both static and vibrational properties of the soundboard into account. In order to minimize the effect of other factors in this material substitution, the soundboard was treated independently, and the pattern of the braces behind the soundboard was left unchanged.

A wooden soundboard intended for a flamenco guitar was borrowed from Joel Barbeau, a Montreal-based guitar luthier, and was treated as the reference for the design. A numerical model of the soundboard was made and the results of the finite element simulations were regarded as theoretical results. For verification purposes, a series of experimental modal analyses were performed on the wooden soundboard, as well as on the manufactured braceless composite top plate and the braced composite soundboard.

1.3   Thesis Overview

Chapter 2 of this thesis will provide the background information required for understanding the terminology and the theories used throughout the project, from material science to theoretical and experimental modal analyses, followed by a literature review on guitar soundboard acoustics, composite materials and composite instruments.

Chapter 3 will explain the thought process and the steps taken throughout the design, construction and experimentation stages.

Chapter 4 presents and analyzes the theoretical and experimental results obtained at different stages. The analyses will elaborate why certain decisions were made in the design process, and whether the experimental results match those predicted by the simulations. Furthermore, the limitations in the proposed methodology and the design will be discussed, as well as the sources of error.

Chapter 5 will close the report by summarizing the results and the conclusions of the project, followed by the further potential work suggested.

It must be noted that during the first 6 months of this project, I was involved in the design and construction of a composite steel-string guitar soundboard as well, in collaboration with Ulrich Blass, a visiting researcher from the Technical University of Kaiserslautern. He was a part of the Structures and Composites Laboratory of McGill at the time. A portion of the experiments and designs were therefore performed collaboratively, which is why this report is written in a first person plural voice.

1.4   Contributions

The thesis in hand sheds light on the effects of varying certain physical, geometric and elastic properties of the materials used in sandwich-structured composite soundboards on their natural frequencies and mode-shapes. It also discusses the differences observed between the experimental and the numerical results and the possible sources of error.

Another observation that is briefly documented in this thesis is the variations of the modal parameters of the wooden soundboard over time. This phenomena is thought to be caused by environmental factors like temperature and humidity, and it further motivates us to consider producing instruments from synthetic materials that are less sensitive to humidity and temperature.

The outputs of this project broaden our understanding of the factors that affect the modal parameters of a guitar soundboard, providing a more solid ground for further research on numerical modelling of sandwich-structured composites and composite soundboard designs.

Chapter 2

Background

The instruments belonging to the current family of guitars vary in a number of structural aspects that result in variations in the timbre, vibrational and acoustical properties of the instrument. In order to narrow down the scope of this project, the following history and the principles provided will focus on the conventional nylon-string guitar, and more specifically, on their soundboards.

2.1 Relevant History

2.1.1 Nylon-String Guitars

The modern nylon-string guitar as we know it was predominantly the invention of Antonio de Torres in the 19th century [9]. Although the family of lutes, necked string instruments [4, p. 2] and guitar-like instruments date back to centuries prior to that, it was since Torres's designs that a number of features remained standardized in the modern guitar. Despite their variations, the consistent features in his guitars were the presence of 6 strings, the body silhouette, the fretboard being raised above the soundboard [4, p. 14] and joined to the body at the 12th fret, geared tuners and most importantly, the fan bracing behind the soundboard [9].

Aside from Torres' design, many other guitar designs have been explored since the 19th century. Fig. 2.2 shows examples of some bracing pattern variations for the nylon-string guitar that have been developed over the years. Notice that not all bracing patterns used for acoustic guitars have a symmetric layout.
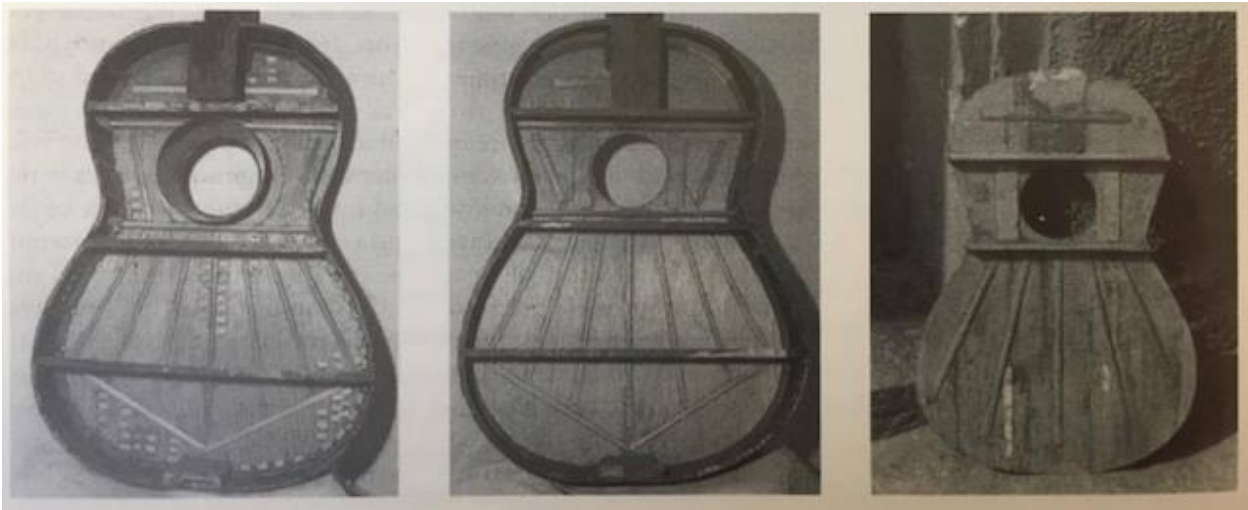
Figure 2.1: Examples of Torres patterns. From left to right: models FE 19, SE 70, SE 147 [10, p. 116].
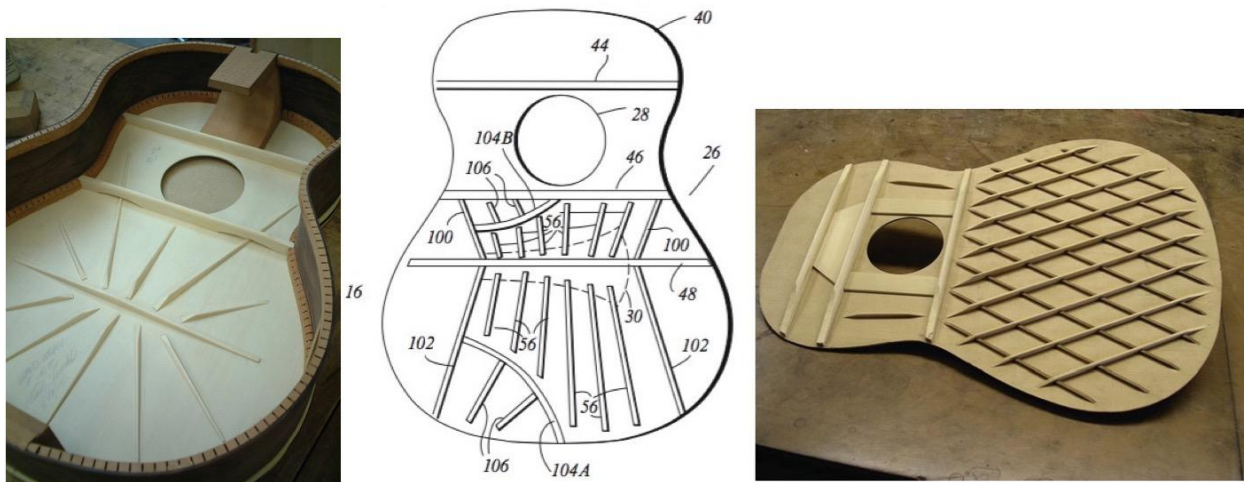
Figure 2.2: Alternate bracing pattern examples. From let to right: Radial bracing by Randy Reynolds [11], Kasha design [4, p. 19], and lattice design by Chris Pantazelos for a 7 string guitar [4, pp. 20].

The ultimate aim of every guitar soundboard is to be light enough to vibrate in response to the excitation of the strings, yet maintain adequate strength and stiffness to not fail under the tension of the strings [4]. Achieving this goal is the art of the luthier and can be achieved in more than one way. Kasha's design in Fig. 2.2, for instance, is intended to distribute the torque caused by the strings across the rest of the body, also causing the different regions of the soundboard to have different resonances. A more recent example is the lattice bracing pattern, that gives a distributed stiffness to the soundboard.

The variations in guitar designs are not limited to the bracing patterns. Instruments belonging to the guitar family can vary in the number of strings, body silhouette and size, the materials used in the different parts, location and size of the sound hole, number of sound holes, scale length, bridge design, etc. Below are a few alternate guitar designs. In Fig. 2.3, the lattice bracing is made of a CFRP/balsa sandwich, providing high stiffness to the soundboard. The second guitar in this figure is an example of a concert guitar with a non-conventional sound-hole location [12], and the soundboard on the right is a *double-top* soundboard. Double-top soundboards are made from a sandwich configuration consisting of two usually dissimilar layers of wood and a thin and light honey-comb layer as the core.

Figure 2.3: Lattice CFRP/balsa bracing [4, p. 114], nylon-string guitar with an unconventional sound hole location [12], Double top guitar [13].

The acoustic results of new designs and variations are rarely predicted prior to construction, and in most cases, they are not analyzed following production either. Although researchers have attempted to come up with more standardized ways of categorizing guitars [14] [15] or assessing their components based on their structural characteristics and vibrational behaviour, luthiers still mainly rely on their experience and qualitative observations in evaluating the make of a guitar and its components.

2.1.2 Composite Instruments

Composites offer a number of desirable material properties, namely, high stiffness, durability, and less sensitivity to humidity and temperature changes, as well as being able to mould to complex shapes. These features make them suitable candidates for applications in many

industries, such as aviation and automobiles. In the realm of musical instruments, although composite materials are not widely used yet, their use in the different parts of string and non-string instruments has been explored by researchers and luthiers in the past several decades. Many of these composite instruments are now available in the market.

The first commercial appearance of composites in musical instruments dates back to the 1960's, when Ovation Guitars started using Glass Fibre Reinforced Plastics (GFRPs) in the body of acoustic guitars. [4, p. 24]. Other composite guitars that have been commercially available since then are produced by Rainsong, since the 1990's, Emerald Guitars, since the 2000's [5], and more recently by Blackbird, Journey Instruments, Mcpherson, The Cargo and KLOS. [16]. The bodies of these acoustic guitars are made from Carbon Fibre Reinforced Plastics (CFRPs), but they vary in size, shape, composite thickness, location and number of sound holes, etc. There are also other acoustic guitars commercially available that are not entirely made from composites, but contain composite components. An example would be the fingerboard of some Gibson Guitars that are made from CFRPs [17].

Figure 2.4: Left: an Ovation guitar with uni-directional GFRP soundboard and the back made of Lyracord [3]. Centre: a brace-less Rainsong guitar with an all-body graphite body [18]. Right: Emerald X20 nylon-string made from a sandwich-structured woven CFRP [19].

Commercial use of composite materials in musical instruments has not been limited to acoustic guitars. Luis and Clark has been producing composite instruments from the violin-family since the year 2000 [20]. Composite violin bows and violin chin rests have also been available in the market for several years. Furthermore, in the realm of non-string instruments, CFRPs are being used in the production of composite flutes, didgeridoos, bagpipes, etc. [21, 22].

Figure 2.5: A composite violin by Luis and Clark [23].

Musicians have taken an interest in the aesthetic and practical features offered by composite instruments so far, but the feedback received on their sound is still largely mixed. Composite instruments from the violin family seem to have been accepted and endorsed by a larger audience than composite guitars. The popular belief appears to be that the sound of composite guitars is richer in the higher harmonics, but that they seem to lack depth in the lower frequency region. Additionally, many have been thought to be too loud. Despite this general belief, however, feedback received on more recent high-end custom-made composite guitars seems to be quite positive. In fact, some are thought to sound better than high-end wooden guitars.

Despite their availability in the market, the amount and extent of research and post-production analysis that has been done on composite instruments is still quite limited. Among the research related to the use of composite materials in acoustic guitars, there are a series of experimental studies published by Teruaki Ono [6, 24, 25] on the acoustical properties of woods and composites, one published study by Charles Besnaino [15] on the desirable characteristics of woods and composites used in musical instruments, as well as the two theses written by Stephen Probert [7] and Max Roest [8], each of which report on the design and manufacturing of a full acoustic guitar from composites. Further use of composites in musical instruments has been explored in academic settings by many more researchers, some of which can be found in [26] [27] [28].

The study published by Charles Besnainou attempts to categorize wooden guitars and violins based on their acoustical properties and introduces principles that must be taken into account when designing acoustic instruments from composites. His statements are later used, verified and extended in the literature of composite instruments that will be presented in Sec. 2.5.

Teruaki Ono's design was the final stage of a series of experimental studies by him and his team that revealed the acoustical properties of different woods and sandwich-structured FRP configurations. His final design is the layup shown below, where CF(L)/UF refers to carbon fiber filaments laid longitudinally in a polyurethane foam matrix, CF(R)/UF refers to carbon fiber filaments laid in the perpendicular direction in a polyurethane foam matrix, and UF is a layer of polyurethane foam alone. The Frequency Response Functions (FRFs) obtained from the produced guitar were found to be very close to those of the reference wooden guitar.
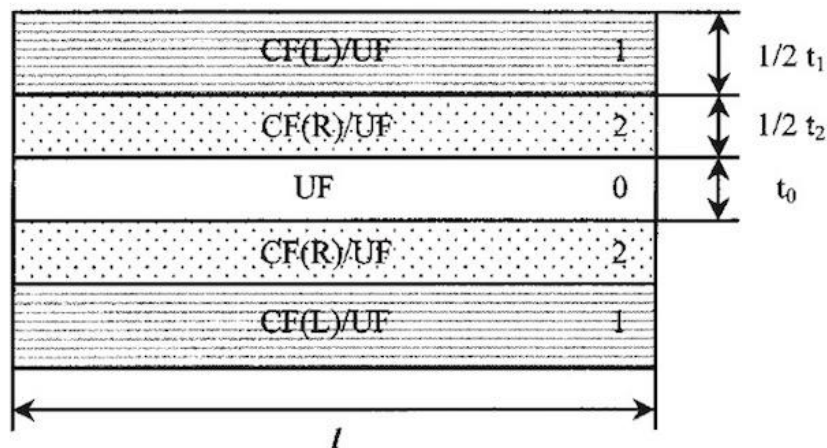
Figure 2.6: Layup of the composite guitar made by Ono [6].

Stephen Probert used numerical simulation to design and manufacture a full steel string guitar in his Master's thesis. His design makes use of a sandwich-structured CFRP with a foam core. On each side of the core, two layers of standard woven CFRPs are used: one at a 0/90° angle, and the other at a 45° angle. It is stated that the guitar made was found to sound "good" to "the average listener". [7].

Max Roest's strategy for designing the composite layup consisted of some pre-calculations followed by multiple stages of experiments. His final composite layup was made from CFRPs laid in a polyurethane foam, which is a gas blown foam. The result of his psychoacoustic

analysis showed that identifying the difference between the sound of that guitar and a wooden one was "extremely difficult".

Figure 2.7: Composite guitars made by Probert [7], Ono et al. [6] and Roest [8].

2.2 Guitar Acoustics

Before starting the design process, it is important that we understand the mechanism of sound generation in an acoustic guitar, where "acoustic" in this context refers to acoustic steel-string and nylon-string guitars, as opposed to electric guitars. It is worth noting that the soundboard has a similar role in almost all acoustic string instruments, such as violins, pianos and guitars, despite being different in the way their strings are excited, and in the geometry and the mechanical properties of the instrument. The aim of this project is to design and build a nylon-string guitar soundboard, and since there are certain structural differences between steel-string and nylon-string guitars, the information provided below is focused on modern nylon-string guitars and their soundboards. Limiting the topic to the soundboard of nylon-string guitars narrows down the components of the guitar and the types of materials we must focus on, the bracing pattern and the range of values we are interested in for the different material properties.

While the nylon-string guitar is commonly referred to as the *Classical guitar*, in order to conform to the terminology of the luthier we collaborated with, it is preferred that we distinguish between *Classical* and *Flamenco* guitars in this document. Both Classical and Flamenco guitars are nylon-stringed, but there are slight structural differences between the two, mainly in the types of woods used in the body of the instrument, the bracing pattern and the thickness of the soundboard, as well as the action of the neck. Classical guitars are generally preferred to have a smoother sound and a longer sustain, while Flamenco guitars are desired to have a more percussive and louder attack, so that they are heard through the sound of dancers' feet. [29]. The signature timbre of the Flamenco guitar is usually achieved by making the soundboard of the instrument thinner - especially in the middle of the lower bout - and making up for the stiffness by adjusting the braces and the bridge. Another factor that makes the timbre of Flamenco guitars so distinct is the low action of the strings[1] which is accompanied with some degree of deliberate "buzzing". Although too much buzzing can negatively affect playability and the timbre of the instrument, some degree of buzzing is generally desired by Flamenco players. The reference soundboard used in this project belongs to a Flamenco guitar.

2.2.1   Basic Physics

When the guitar string is plucked or strummed, the energy received from the finger/pick is stored in the string and is transferred to the body of the instrument over time through the coupling of the string to the soundboard. The string continues to vibrate and transfer energy to the soundboard until all its energy is transmitted to the body and the surrounding air. While being driven by the string, the soundboard vibrates and transmits energy to the ribs, the back of the instrument and the surrounding air, including the air inside the sound box. The vibration of these components will cause propagation of pressure waves in the air surrounding the instrument, causing air pressure to fluctuate. These fluctuations are detected by our ears and our brain perceives them as sound. The sound radiated by the instrument is therefore not a direct result of the string's vibration, but rather a result of the components of the instrument - including the air inside the sound box - vibrating in response to the strings' ongoing vibration [1].

---

[1]Action of the guitar refers to the gap between the strings and the fretboard, so a low action means a smaller gap.

2.2.2 Guitar Components

The guitar is comprised of a number of components, each of which is required for some structural and/or acoustic purposes. The number of components present in different acoustic guitars can differ, depending on whether the instrument is nylon-string or steel. Below, the different components of a conventional nylon-string guitar and their functions are introduced:
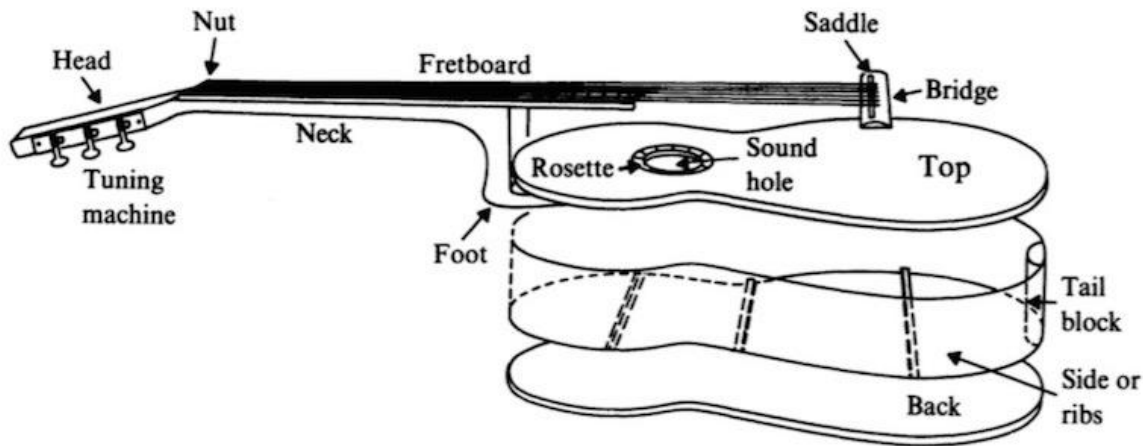
Figure 2.8: Exploded view of a nylon-string guitar [30, p. 240].

The Strings: The strings are the elements that provide vibrational energy to the body of the instrument, upon being excited. In a nylon-string guitar, the 3 lower strings are usually made from nylon or carbon, and the upper three strings are nylon covered in wound metal. The metal windings are there in order to add mass to the string, without affecting the stiffness of the string. The pitch produced by the string varies depending on the mass, length, radius and tension of the string. This explains why placing the finger on the strings can result in different pitches. The fundamental frequency of oscillation of a fixed string is calculated using the equation below:

$$f = \frac{1}{2L}\sqrt{\frac{T}{\rho}}, \tag{2.1}$$

where L is the string length, T is the string tension, and ρ is mass per unit length. [4, p. 62] Note that this equation does not take into account the restoring tension caused by the stiffness of the string. [2]

---

[2]When a cable or a string with fixed ends is bent, the stiffness of the material induces a restoring force that attempts to bring the cable/string back to its original position. [31]

Fretboard and frets: The fretboard provides a space for the player to press on the string and alter the pitch produced by the strings. This pressing therefore allows the player to define new fixed points on the string. The frets on the fretboard serve as both guidelines and facilitators with which the pressing is made easier.

Nut: The nut is the point at which the motion of the strings is terminated. The nut of every guitar is typically a rectangular plastic piece that accommodates every string separately in its allocated slot.

Head and Tuning Pegs: The head provides a secure place for the strings to be fixed. The tuning pegs are then the components in charge of controlling the tension and tuning of the strings.

Neck and Heel: The neck is the component on which the fretboard and the frets are mounted. It is supported by the foot, providing adequate strength so that the fretboard does not fail under the tension of the strings.

Bridge: Located on the front side of the soundboard in the lower bout, the bridge is in charge of holding the other end of the strings in place. In nylon-string guitars, the strings are usually tied to the bridge.

Saddle: Located on the bridge, the saddle is the other termination point for the motion of the string. It is typically a rectangular piece made from plastic, bone or even elephant ivory [32]. The saddle of different guitars have different heights depending on the preference of the luthier and the player, and their upper edge could be straight, slanted, curved, slotted or compensated.

Figure 2.9: Left: The strings tied to the bridge [33]. Notice the compensated saddle between the strings and the bridge. Right: The wooden slots around the ribs are the lining.

The Ribs and the Lining: The ribs are the sides of the instrument, usually made from wood. They transfer the vibrational energy from the soundboard to the back, and provide a semi-closed space for the air inside the sound box. Their curved shape makes it easy for the player to hold the guitar, and they are typically made from hardwoods like rosewood, or laminated wood, which allow easier bending. The lining is installed on the interior outline of the back and the soundboard, to provide more gluing area.

The Back: The back of the guitar helps in sound generation at low frequencies. It is typically made from a thin wooden plate made from rosewood or similar hardwoods.

Sound hole: The sound hole allows the instrument to act as a Helmholtz resonator tuned to about 55.0 Hz for steel-string guitars, 103.8 Hz for Classical and to 92.5-98.0 Hz for Flamenco guitars. [34].

The Rosette: The decorated region around the sound hole, mainly present for aesthetic purposes.

Soundboard and Braces: The soundboard of a guitar is the most important element of the instrument in the production and propagation of sound. It is typically made from a rather thin softwood plate that is stiffened from behind with the help of braces, so that the soundboard is light enough to vibrate in response to the strings' excitation, yet strong enough to withstand the tension of the strings [1, p. 93]. Examples of the types of wood usually used for nylon-string guitar soundboards are from the family of Spruce, Pine, Firr and Redwood [35] [1, p. 37]. It is worth noting that most acoustic guitar soundboards (steel or nylon-string) are not perfectly flat. They are usually shaped in form of a 25-30 inch radius dome. This dome helps the structure in two ways: 1. It adds stiffness to the top plate, allowing the luthier to make the top plate thinner. 2. It prevents the soundboard from rolling up around the bridge due to the tension of the strings. In his book on the life and work of Antonio de Torres [10, p. 114], Romanillos explains that since this doming is initially done by force, if the soundboard is made too thick, it might eventually flatten out due to the tension caused by excessive thickness.

2.3 Material Properties

Before we discuss the literature available on soundboard design and the application of composites in guitars, it is important that we recognize the physical and material properties that play a role in the vibrational behaviour and the acoustical properties of string instruments, and to understand the terminology used.

2.3.1   Basic Definitions and Theories

Young's Modulus: In 1676 Robert Hooke discovered that the normal stress caused by an axial load in an isotropic material[3] is directly proportional to the deformation caused by the load, i.e.:

$$\sigma = E\epsilon, \tag{2.2}$$

where ϵ, referred to as strain, is defined as $\frac{l-l0}{l0}$, i.e. the change in length divided by the original length, σ is the normal stress, and E is a material constant referred to as Young's Modulus. Note that strain is a dimensionless parameter, which means σ and E have the same units of measurement. This linear relationship which is known as *Hooke's Law* holds only when the deformation of the object caused by the normal stress is still in the elastic region. "Normal stresses" in materials are caused by compression, tension or bending, and "elastic region" is the stage in which the shape and the length of the object under stress haven't changed permanently.
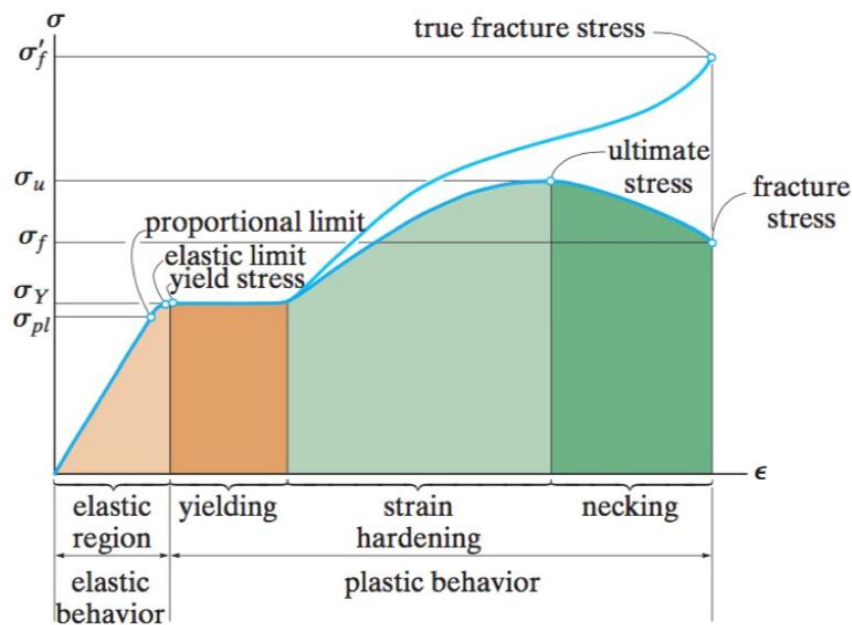
Figure 2.10: A stress-strain curve of a material under loading. [36, p. 84].

E, which corresponds to the slope of the stress-strain graph in the elastic region, is a measure of stiffness in materials. The higher the E of a material, the more load is required to elongate, compress or bend an isotropic object. Engineers generally design parts such

---

[3]Isotropic materials have identical elastic properties in all directions.

that regardless of their function, the parts remain in the elastic region while subject to load.

Shear Modulus of Rigidity (or Shear Modulus of Elasticity): Hooke's law can also be written for materials subject to shear stress, where the shear strain is related to the shear stress by the equation:

$$\tau = G\gamma, \tag{2.3}$$

where τ is the shear stress, γ is the shear strain and G is the shear modulus of rigidity or shear modulus of elasticity. It must be noted that just like normal stresses, Hooke's law for shear stress holds for materials as long as the material under stress is in its elastic region. Also, since γ is in radians (i.e. a dimension-less quantity), G and τ have the same units of measurements.

Poisson's Ratio: When an axial load is applied to a deformable isotropic structure, it causes both the length and the cross sectional area of the body to change, and the longitudinal and lateral strains caused are described as:

$$\epsilon_{long} = \frac{\delta}{L} \tag{2.4}$$

and

$$\epsilon_{lat} = \frac{\delta'}{L}. \tag{2.5}$$

where $\delta = l - l_{inital}$, and δ' is the change in the radius of the cross section, i.e. $r - r_{initial}$. In the early 1800's, Siméon Poisson discovered that the ratio of ϵ_{lat} to ϵ_{long} is constant in the elastic region of materials, based on which the material constant *Poisson's ratio* is defined as:

$$\nu = \frac{-\epsilon_{lat}}{\epsilon_{long}} \tag{2.6}$$
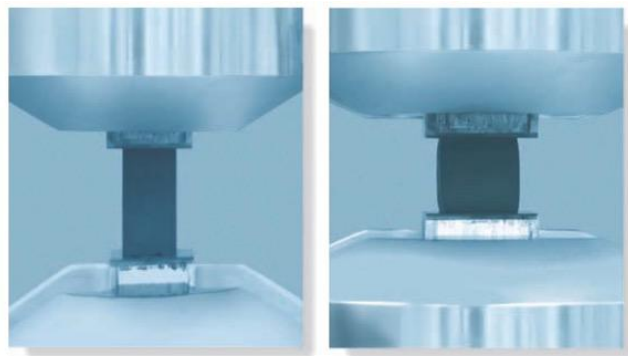
Figure 2.11: Transversal expansion of a specimen caused by axial compression. [36, p. 102].

It is worth noting that for isotropic materials, the three material constants, E, G, and ν, can be related as follows:

$$G = \frac{E}{2(1 + \nu)}. \tag{2.7}$$

Strength: The strength of a material is determined by its ability to withstand an intended load without mechanical failure [36]. Mechanical failure in a material can be due to excessive static load, fatigue, buckling, creep, corrosion or wear. Reference to Fig. 2.10, when some form of load is applied to a material, be it force or moment, if the stress in the material exceeds the elastic limit, i.e. the yield stress, the material will deform plastically and in the case of brittle materials, such as wood, the material will soon fail in the form of fracture. This elastic limit depends on the material and the type of stress it is experiencing, i.e. stress due to bending, compression, tension or torsion. These values, which are material-dependent, are determined experimentally.

Hooke's Law for Anisotropic Materials: Materials that have different elastic properties in different directions are called *anisotropic*. The generalized Hooke's law for anisotropic (and isotropic) materials in 3D can be written[4] in a simplified matrix form, referred to as the Engineering or Voigt notation, as follows:

$$\sigma_i = C_{ij}\epsilon_j, \tag{2.8}$$

where

i: The direction of the normal of the surface upon which the stress components act

j: Direction of the stress itself

σ_i: Generalized stress component which can be normal, σ, or shear, τ

ϵ_j: Generalized strain component, which can be normal, ϵ, or shear, γ

C_{ij}: The stiffness matrix, i.e. a 6x6 matrix comprised of E_x, E_y, E_z, G_{xy}, G_{xz}, G_{yz}, ν_{xy}, ν_{xz}, and ν_{yz}

The number of independent elastic constants required to describe the stiffness matrix of an isotropic material is 2, since the E, G and ν do not vary with direction, and since the three are related to one another according to Eq. (2.7). Anisotropic materials, however, are classified into the following different classes, based on the total number of independent elastic constants that are required to fully describe the material: Triclinic (21 constants), Monoclinic (13 constants), Orthotropic (9 constants), Transversally isotropic (5 constants),

---

[4]The original form of 3D notation is in a tensor form. Engineering notation only makes use of certain symmetries in the tensor form and is more compact than the original tensor notation.

and cubic (3 constants) [37]. In this project, we are mainly interested in orthotropic and transversely isotropic materials.

Flexural Rigidity: When a load is causing bending in a beam, a plate or a structure, the deflection caused by the load is not only a function of the material properties and the amount of the load, but also the geometry of the structure. One measure of bending stiffness is referred to as "flexural rigidity", i.e. EI, where I is the area moment of inertia of the cross section of the structure being bent.

2.3.2 Introduction to Composites

Composite materials are made up of a combination of two or more materials, with properties superior to those of the constituents when separate. Unlike metal alloys, materials combined in composite form preserve their physical, chemical and mechanical properties [38]. They generally consist of a fibre or a particulate phase, laid in a matrix phase. The fibre or particulate phase, referred to as the *reinforcement phase*, is what provides stiffness and determines the strength of the composite. Elastic properties of a composite material, therefore, mainly depend on the dimensions, properties, weave, direction and the volume of the reinforcement phase, and to a lower extent on the properties of the matrix. It is understandable that depending on the weave of the fibres, different types of anisotropy can exist among composites.

Composites offer high strength and stiffness, low cost, as well as resistance to corrosion and environmental changes, and have been widely used to replace metals and ceramics in many industries, such as aerospace, automotive, naval, infrastructure, wind turbines, electrical towers, etc. [38]. Typical fibres used in composites are carbon, glass and aramid, used both in continuous and discontinuous forms [38]. On the other hand, the types of materials commonly used for the matrix phase are polymer, ceramic and metals, depending on the application and the range of elastic properties desired for the application.

In this research, we are interested in a family of composites referred to as Fibre Reinforces Plastics (FRPs). As the name suggests, FRPs are made from fibres laid in a polymer matrix. Laying the fibres in the matrix can be done manually or using filament winding machines. Initially, both the matrix and the fibres are quite flexible, and it is through curing that the FRPs become a stiff and strong solid. Curing in this case is the process of heating the FRPs up to and holding it in a specified temperature for a specified amount of time, depending on the type of fibre and polymer used. Since the curing process is the stage in which the shape

of the FRPs is finalized, while being cured, the FRPs are laid inside or over a mould that determines the desired final shape. It is worth noting that FRPs can be *thermoplastic* or *thermosetting*, where the former means the composite can be cured, melted and re-moulded without its physical properties being affected, and the latter means the FRPs can be moulded and cured only once.
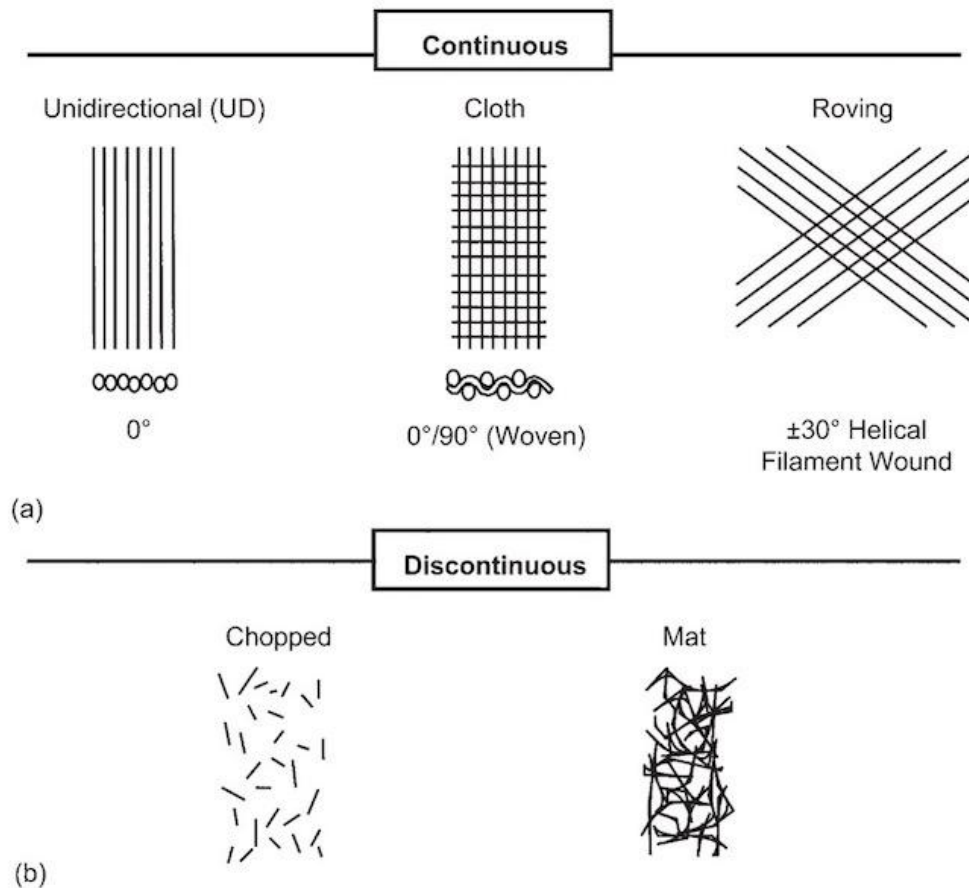
Figure 2.12: Typical reinforcement types [38].

The fibres and the matrix materials required for FRPs can be found in the market separately, but in the past couple of decades, many *pre-impregnated* (or *pre-preg*) continuous-fibre reinforced plastics have been produced in *lamina* or *ply* form as well. Pre-preg sheets are partially cured, which makes them easier to handle. To prevent the pre-preg FRPs from further curing, however, it is required that the sheets are kept in cold temperatures. Pre-preg plies can then be stacked on top of each other and cured together, which would result in thicker and stiffer FRP parts.

2.4   Modal Analysis

Modal analysis is the process of determining the dynamic properties of a structure under dynamic loading or vibrational excitation [39]. Dynamic properties in this context are the natural frequencies, mode-shapes and modal damping values. These properties can be determined analytically or experimentally.

When a linear time-invariant structure is excited by means of some harmonic load, the structure can take different complex shapes to it, depending on the frequency of excitation. The complex shapes the structure takes due to vibrational excitations are referred to as Operating Deflection Shapes (ODS). At certain frequencies, the structure can experience maximum deformation. Those frequencies are referred to as "resonances", "natural frequencies" or "eigen-frequencies" of the structure, and the ODS of the structure at those specific frequencies are referred to as "mode-shapes". The modal properties of the structure, i.e. mode-shapes, eigen-frequencies and modal damping values, depend on its geometric and material properties as well as its Boundary Conditions (BCs). Modal analysis is established on the fact that the vibration response of a linear structure can be expressed as the linear combination of its normal modes of vibration. The dynamic properties calculated or measured are then features associated with the normal modes, and can be used to describe the vibrational response of a structure.

2.4.1   The Mathematical Model

The simplest mechanical system that can be considered in a real vibration problem is a mass-spring-damper, also referred to as a *harmonic oscillator*.
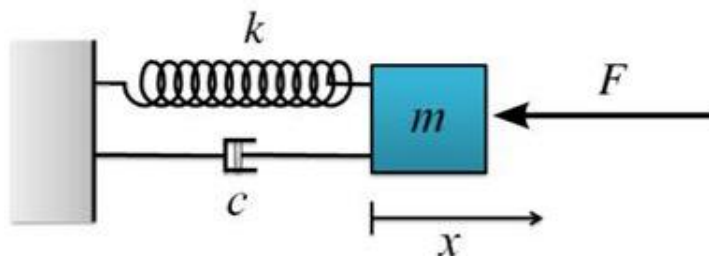
Figure 2.13: A 1DOF damped harmonic oscillator [40].

The Equation of Motion (EOM) for this system is as follows:

$$m\frac{d^2x}{dt^2} + c\frac{dx}{dt} + kx = F(t), \tag{2.9}$$

where m is the mass, c is the damping ratio of the damper, k is the spring constant, x is the displacement and $F(t)$ is the applied force. Since a system's natural frequencies are independent of the applied load, they can be determined under free vibration, i.e. $F(t) = 0$. The damping term is also usually disregarded in calculations of natural frequency, which reduces Eq. (2.9) to:

$$m\frac{d^2x}{dt^2} + kx = 0. \tag{2.10}$$

The natural frequency of such a system is then equal to

$$w_n = \sqrt{\frac{k}{m}}. \tag{2.11}$$

Now, consider the two coupled oscillators below:
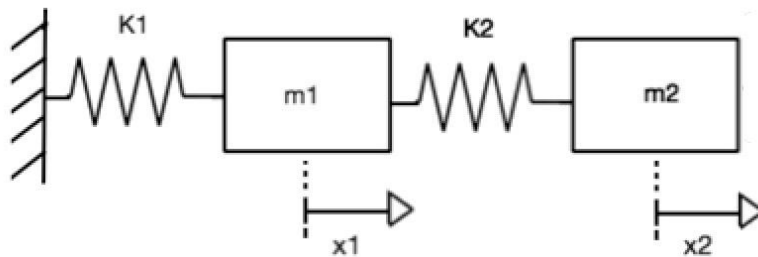
Figure 2.14: Coupled undamped harmonic oscillators.

The EOM of coupled undamped oscillators can be written as:

$$[M]\{\ddot{X}\} + [K]\{X\} = 0, \tag{2.12}$$

where [M] is the mass matrix for the system, and [K] is the stiffness matrix for the system, defined as:

$$\left[K_1\right] = \begin{bmatrix} k_1 & -k_1 \\ -k_1 & k_1 \end{bmatrix} \qquad \left[K_2\right] = \begin{bmatrix} k_2 & -k_2 \\ -k_2 & k_2 \end{bmatrix} \tag{2.13}$$

and

$$\begin{bmatrix} M_1 \end{bmatrix} = \begin{bmatrix} m_1 & -m_1 \\ -m_1 & m_1 \end{bmatrix} \qquad \begin{bmatrix} M_2 \end{bmatrix} = \begin{bmatrix} m_2 & -m_2 \\ -m_2 & m_2 \end{bmatrix}; \tag{2.14}$$

therefore,

$$\begin{bmatrix} M \end{bmatrix} = \begin{bmatrix} m_1 & -m_1 & 0 \\ -m_1 & m_1 + m_2 & -m_2 \\ 0 & -m_2 & m_2 \end{bmatrix} \tag{2.15}$$

$$\begin{bmatrix} K \end{bmatrix} = \begin{bmatrix} k_1 & -k_1 & 0 \\ -k_1 & k_1 + k_2 & -k_2 \\ 0 & -k_2 & k_2 \end{bmatrix}. \tag{2.16}$$

The solution of such a system is assumed to be of the form:

$$\{x\} = \{v\}e^{j\{w\}t}, \tag{2.17}$$

where $\{x\}=\{{}^{x_1}_{x_2}\}$, $\{v\}$ is the eigen-vector of the solution, $\{w\}$ is the vector of eigen-frequencies to be determined, and t is time. Substituting the solution into Eq. (2.12) results in:

$$([K] - \lambda[M])\{X\} = 0, \tag{2.18}$$

where $\lambda = w^2$. For Eq. (2.18) to have non-trivial solutions, the following should hold:

$$det([K] - \lambda[M]) = 0. \tag{2.19}$$

$[K]$ and $[M]$ for the system are known, so the set of λ's obtained will lead us to the natural frequencies of the system, such that:

$$w_{ni} = \sqrt{\lambda_i}, \tag{2.20}$$

where i is the subscript of the i'th mass. The different v_i's (eigen-vectors) are then calculated by inserting the different λ_i's in the following equation:

$$([K] - \lambda_i[M])\{v_i\} = 0. \tag{2.21}$$

Defining M and K is relatively simple in the case of discrete coupled oscillators, but most

of the systems we deal with in reality are continuous structures, rather than discrete sets of oscillators. It is possible to simplify and approximate linear continuous structures as sets of coupled harmonic oscillators, whose equations of motion determine the approximate dynamic behaviour of the structure as a whole. To be able to analytically determine the natural frequencies and eigen-modes (eigen-vectors) of a linear continuous structure, however, the structure must be simplified to a great extent, and this simplification must take into account the Degrees of Freedom (DOF) that are most significant in determining the vibrational and dynamic behaviour of the structure. *Degrees of Freedom* in this case refer to the masses whose dynamic motions are described by the EOM. The more accurate this approximation is, the more difficult it would be to determine the solution to the differential equations analytically.

In his book, *The Science of String Instruments*, Rossing states that at low frequencies, the soundboard, the enclosed air and the back plate contribute to the sound radiation of the instrument, but at higher frequencies, most of the sound is radiated by the soundboard [1, p. 20]. A 2-DOF representation of the acoustic guitar was first proposed by Caldersmith in 1978 [41], where the ribs and the back plate of the instrument are assumed fixed, while the soundboard and the enclosed air are regarded as the two DOF determining the dynamic behaviour of the instrument. In this model, presented in Fig. 2.15, $[K]$ would be defined in terms of the elastic properties of the soundboard and the enclosed air. It is therefore understandable that the volume and the properties of the air inside the sound box will play a role in the modal characteristics of the instrument model, as would the geometric, physical and material properties of the soundboard.
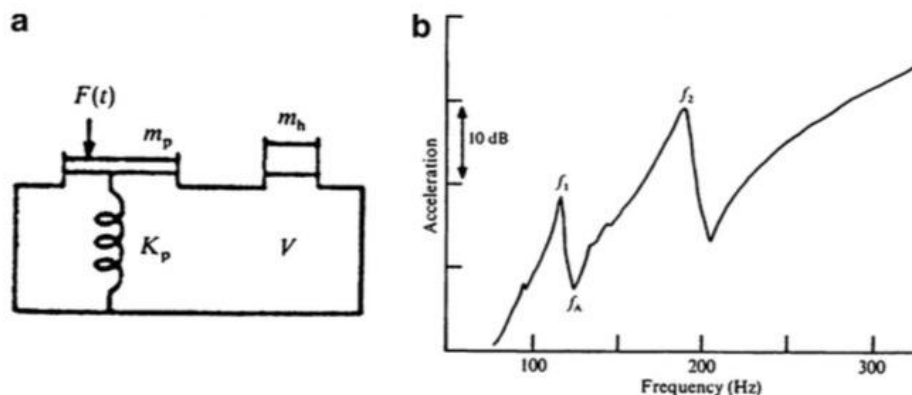
Figure 2.15: (a) The 2DOF guitar model, (b) Frequency response of a Martin D-28 with its backplate and ribs fixed in sand [1, p. 26].

Later, a 3DOF model of the guitar was proposed by Christensen [42], taking the back

plate into account, and a 4DOF model proposed by John Popp [43], with the ribs added to the model. As you can notice, the common components present in all these models are the soundboard and the enclosed air. Since the harmonics present in the sound of the guitar in a large range of frequencies are generated by the soundboard, the behaviour of the guitar, to a first approximation, is thought to be dominated by the behaviour of the soundboard. This is why the soundboard was chosen as the first component of the instrument that is made from alternative materials and monitored through this design and material replacement.

2.4.2   The Finite Element Method

While simplified mathematical models are a good starting point for modelling instruments, a much larger set of differential equations is required to accurately model a complex structure like the guitar. The more complex the structure, the more analytical equations are required to describe the behaviour of a structure, and the more difficult it is to analytically solve them. It is in fact not practical to represent such complex structures analytically and to look for exact analytical solutions to these equations. In such cases, engineers use the Finite Element Method (FEM) to discretize the structure, and numerically determine the static or dynamic behaviour of the structure under different circumstances.
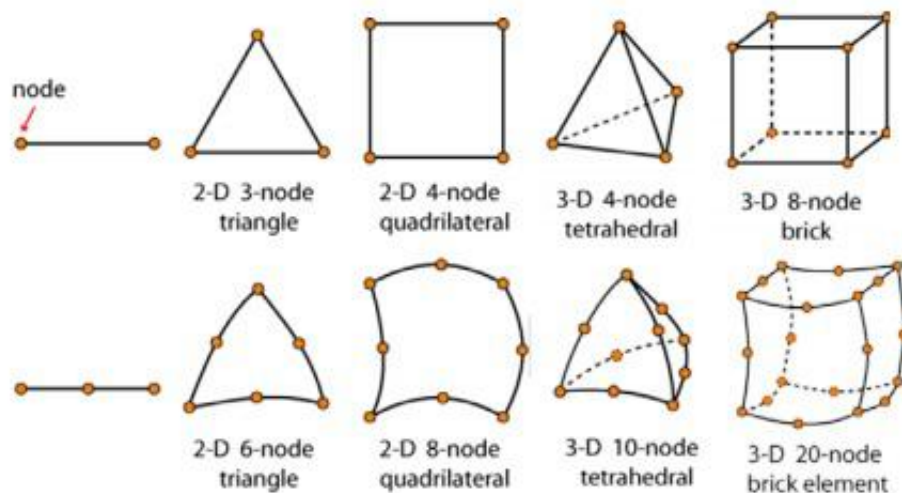
Figure 2.16: Some common element types used in FEM [44]. 1st line: linear elements. 2nd line: quadratic elements.

In every FEM representation, the structure is approximated using a large but finite set of *elements*. The elements can be 1D, 2D or 3D, and can be linear, quadratic, cubic, etc.

Depending on the dimension and the order of the elements, each element will consist of a limited number of nodes. The solution to the differential equation is computed at nodes and interpolated between them. Interpolation is done by functions referred to as *shape function*, N_i. Shape functions are usually polynomials of some order n, and essentially act as *weights* on the nodal solutions, making the solution for every element of the form:

$$u(x) \approx N_1(x)u_1 + N_2(x)u_2 + N_3(x)u_3 + ... + N_n(x)u_n = \sum_{i=1}^{n} N_i(x)u_i, \qquad (2.22)$$

where n is the order of the element (not its dimension), i is the node subscript, x is the independent global variable, and $u(x)$ is the parameter of interest, i.e. the solution to the differential equation at x. Therefore although the solution is computed for a discrete set of points, with the help of shape function, it can be computed for the continuous domain of x within every element. Fig. 2.16 is an example of the solution - in this case temperature profile - being represented using two quadratic 1D elements.
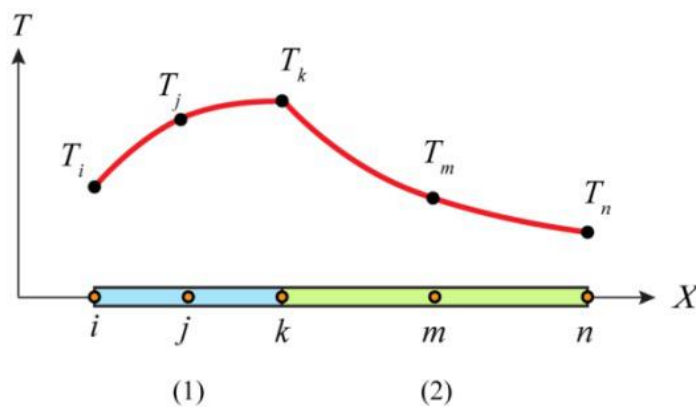
Figure 2.17: Temperature profile represented across two quadratic elements [44].

Once the structure is discretized, the K and the M for every element j will be defined as:

$$[M_j] = \iiint_V [N_i]\rho[N_j]^T \delta V \qquad (2.23)$$

$$[K_j] = \iiint_V [B_j]^T E_j[B_j]\delta V, \qquad (2.24)$$

where $[B_j] = \frac{\delta}{\delta x}[N_j]$, and E_j is the elasticity matrix of the element, in compliance[5] form. For an orthotropic material, like wood, E_j of its elements would be described as:

$$[E_j] = \begin{bmatrix} \frac{1}{E_x} & -\frac{v_{yx}}{E_y} & -\frac{v_{zx}}{E_z} & 0 & 0 & 0 \\ \frac{-v_{xy}}{E_x} & -\frac{1}{E_y} & -\frac{v_{zy}}{E_z} & 0 & 0 & 0 \\ \frac{-v_{xz}}{E_x} & -\frac{v_{yz}}{E_y} & -\frac{1}{E_z} & 0 & 0 & 0 \\ 0 & 0 & 0 & \frac{1}{2G_{yz}} & 0 & 0 \\ 0 & 0 & 0 & 0 & \frac{1}{2G_{zx}} & 0 \\ 0 & 0 & 0 & 0 & 0 & \frac{1}{2G_{xy}} \end{bmatrix}. \tag{2.25}$$

Given M and K for every element, the eigen-frequencies and eigen-vectors can be determined for the system of elements, as described in Sec. 2.4.1.

2.4.3 Experimental Modal Analysis

Experimental modal analysis is the process of determining the dynamic properties of a structure experimentally. While there are different possible forms of dynamic loads that can be applied to a structure, the two useful forms of loading which can reveal important information about the structure are applied using a shaker or an impact hammer. The shaker test provides information on the response of the structure to cyclic loading only at the frequency of the input, while the impact hammer test provides information on the response of the structure at a large range of frequencies. The impact hammer test is useful when the natural frequencies of the structure are unknown.

The method used in this project is the impact test, which consists of applying a single impulse to the structure with a hammer-shaped force transducer in the direction normal to the deflecting surface, while simultaneously measuring the response at another location on the structure. The ratio of the measured response to the input force is considered, and the Fourier Transform of this ratio is what is referred to as the Frequency Response Function (FRF). The resulting FRF will be a complex function which carries magnitude and phase information. The response parameters that can be measured are the velocity and acceleration, and the FRFs corresponding to these measurements are respectively referred to as mobility (admittance), and accelerance. It is worth noting that these functions are algebraically related, and measuring one allows calculation of the other two. The FRFs used in this thesis were mobility FRFs, calculated as follows:

---

[5]Hooke's law in compliance form is $[\epsilon] = [C][\sigma]$, where [C] is the stiffness in compliance form.

Normalizing the EOM of a damped 1DOF oscillator, Eq. (2.12), results in

$$\ddot{x} + 2\zeta w_0 \dot{x} + w_0^2 x = \frac{F}{m}, \tag{2.26}$$

where $w_0 = \sqrt{\frac{k}{m}}$, and ζ is the damping ratio of the oscillator. From this point, the mobility function of the oscillator will be:

$$\frac{V(w)}{F(w)} = [\frac{1}{k}][\frac{jww_0^2}{w_0^2 - w^2 + j(2\zeta ww_0)}], \tag{2.27}$$

where w is the frequency of excitation, and the magnitude and the phase expressions are, respectively:

$$|\frac{V(w)}{F(w)}| = [\frac{1}{k}][\frac{ww_0^2}{\sqrt{(w_0^2 - w^2)^2 + (2\zeta ww_0)^2}}] \tag{2.28}$$

and

$$\theta = \arctan(\frac{-w_0^2 + w^2}{2\zeta w_0}). \tag{2.29}$$

As long as the impact location and the measurement point are not located on the nodes of any mode, one perfect impulse would be adequate to reveal most of the natural frequencies of the structure. However, for the mode-shapes to be known, it is required that the response is measured at a set of pre-selected locations across the structure, while the impact location is kept constant, or the other way around. This would create a map of the whole structure that determines the vibrational behaviour of the structure at a large range of frequencies. [39] Ideally, this is done under free boundary conditions, but in reality it is not possible to do so, so the structure is set up such that there are minimal constraints applied to the structure and the boundaries.

In the past, mode shapes were determined using Chladni's method [45], and more recently using holographic interferometry [46], or visualized using modal analysis software. The response data can be obtained using an accelerometer or a Laser Doppler Vibrometer (LDV). The input and the response data are then sent from the force transducer and the measurement instruments to a Data Acquisition unit (DAQ), on to the software where the set of FRFs obtained are assigned to the different selected points, and the mode shapes are visualized. The visualization is done by making use of the real (i.e. magnitude) and the imaginary parts (i.e. phase information) of the measured FRFs, and the dynamic property extraction is done by curve fitting. Further procedural details on the experimental modal analysis will be discussed in the methodology chapter.

2.5 Literature Review: Determining the Quality of a Soundboard

Over the past several decades, a considerable amount of research has gone into identifying the factors that affect the acoustical properties of materials, the extent of their effects, and the parameters that determine the quality of string instruments. Though the larger portion of these studies is not specifically on guitars, the relationships between mechanical properties and acoustical properties of soundboards hold for all acoustic string instruments such as violins and guitars. The range of mechanical and acoustical properties that make the timbre of the instrument more desirable, however, differ depending on the instrument. The following review of the literature will list the mechanical properties that affect acoustical properties of guitar soundboards in particular.

Wood is the most widely used material for soundboard construction, but what makes certain woods better candidates for soundboards? And what determines if other materials have the potential to replace wood in the soundboard of acoustic string instruments? Wood is an orthotropic material with a high Young's modulus in the longitudinal direction (i.e. along the direction of its grains), E_L, and a much lower Young's modulus in the two directions perpendicular to the grains, E_R and E_T.
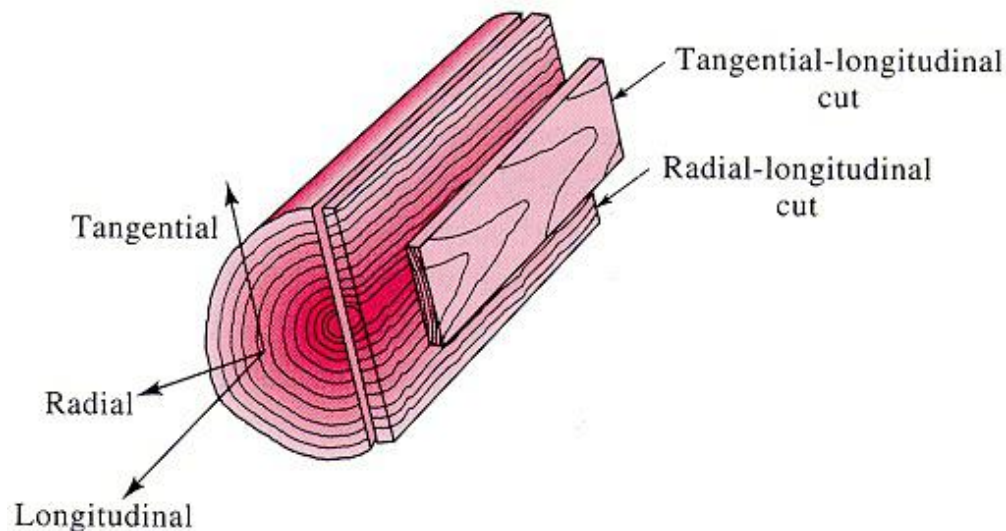
Figure 2.18: Material direction notation in wood [47]. Note that radial-longitudinal cuts (LR) must pass through the centre, while tangential-longitudinal cuts (LT) do not. Soundboards are ideally made from LR cuts. [24, 48].

In his paper on *Frequency Response of Woods for Musical Instruments* [24], Ono states that the high anisotropy in wood is one of the factors that makes wood a good candidate for use in soundboards. In this study, he experimentally evaluates various acoustical properties of a number of boards made from different materials. The experiments consist of exciting boards made from different materials, including some softwoods (e.g. sitka spruce) and some hardwoods (e.g. maple), and recording the pressure changes caused by their vibration, using a microphone. The result of his experiments showed that the qualities that make softwoods suitable for soundboard construction are:

- **High anisotropy**, i.e. high E_L/E_R

- **High E_L/ρ**, where ρ is density

- **Low ρ**

- **Low internal friction in the L direction** (Q_L^{-1}), i.e. the vibratory energy lost in the form of heat.

Ono's study suggests that the response of the soundboard in the high frequency region is associated with the high E_L of the soundboard material, and the low frequency responses are associated with its low E_R. It is worth noting that although high anisotropy is a desirable feature in the soundboard woods, the preferred ratio of this anisotropy is different for different string instruments. Upon collaborating with some guitar and violin luthiers, Charles Besnainou had found that guitar luthiers prefer a $E_L/E_R \approx 20$, while violin luthiers prefer a ratio of ≈ 10 [15].

Finally, Ono introduces $(E/\rho^3)^{\frac{1}{2}}$ as an "easy measure" of quality in acoustic materials, i.e. the higher this fraction, the better the quality of a soundboard. This fraction is later on used by many researchers [35, 49] and referred to as the *Acoustic Coefficient* or *Sound Radiation Coefficient*. Ono's study also clarified that softwoods have a higher overall power level, and the peaks in their frequency responses are further apart than in hardwoods.

Ono was not the only researcher to study the acoustical properties of woods. In his paper titled as *Wood for sound* [35], Wegst starts off by reminding us that many mechanical and physical properties are correlated. For instance, Young's modulii and shear modulii of wood in both radial and longitudinal direction are correlated with density, ρ. He then explains that in selecting materials for acoustic instruments, the most important acoustical properties that must be considered are as follows:

Speed of Sound (c): Speed of sound is defined as

$$c = \sqrt{\frac{E_L}{\rho}}. \tag{2.30}$$

It decreases as temperature or moisture content increase. It also decreases slightly as frequency and amplitude of vibration increases. Higher values of c are desired for woods used in the construction of acoustic instruments.

Characteristic Impedance (z): Characteristic impedance is defined as

$$z = c\rho = \sqrt{E_L \rho}. \tag{2.31}$$

It characterizes the ratio of the energy that gets reflected back at the coupling of two media. Impedance is most important when vibratory energy is being transmitted from one medium to another, where the impedances differ. Note that the reciprocal of impedance is admittance, and that in musical instruments, a low z is desirable, i.e. a high admittance.

Sound Radiation Coefficient or Acoustic Coefficient (R): This parameter describes the extent to which the instrument body gets damped due to sound radiation, and is defined as

$$R = \sqrt{\frac{E_L}{\rho^3}}. \tag{2.32}$$

A large sound radiation coefficient is desired.

Loss Coefficient (η): It is a measure of the extent of vibratory energy that is dissipated in form of internal friction. Unlike the previous properties, loss coefficient is independent of density and Young's modulus, and is frequency dependent. It is defined as:

$$\eta = 1/Q = \frac{\delta}{\pi} = tan\psi, \tag{2.33}$$

where ψ is the loss angle [6], δ is the logarithmic decrement[7], and Q is the quality factor.

Acoustic Conversion Efficiency (ACE): Quoting Barlow (1997), Wegst states that if we wish to increase the average loudness of the instrument, the parameter that needs to

---

[6]A measure of the material damping in viscoelastic materials.

[7]Natural logarithm of the ratio of the amplitudes of every two consecutive peaks of a motion in the time domain.

be maximized is the sound radiation coefficient, but if we wish to increase the peak response of a soundboard, what needs to be maximized is the ratio of the sound radiation coefficient to the loss coefficient. In 2014, in a study done by Jalili on the acoustical properties of FRPs [49], this ratio is referred to as the Acoustic Conversion Efficiency (ACE):

$$ACE = \frac{R}{tan(\delta)}$$

Finally, Wegst organizes different materials in terms of the above parameters by means of graphical representations. Two of those important graphs are provided below.
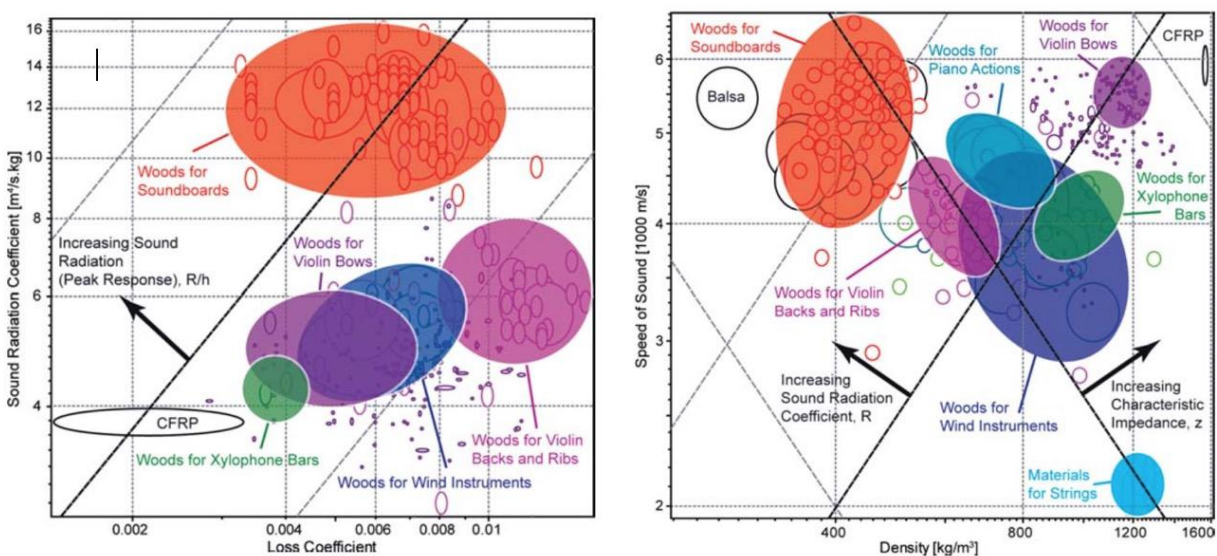
Figure 2.19: Left: R vs. η for different materials. Right: c vs. ρ. Notice soundboard woods and CFRPs on the graphs. [35].

In addition to the findings presented on the acoustical properties of woods, there is a fair amount of literature available on the vibrational behaviour of string instruments (e.g. [26] [50], etc.). In a series of studies done on the vibrational behaviour of a classical guitar, Elajabarrieta et al. [51–54] studied the evolution of modal parameters of the guitar, i.e. resonance frequencies, admittance, quality factors and mode-shapes through the different stages of consturction. The first study consisted of an experimental modal analysis on the soundboard of the guitar, and it reported on the changes in modal parameters along its construction phases. The succeeding studies made use of the FEM to model the soundboard, the back, the enclosed air and the guitar as a whole. The ideas and the results presented in these studies were taken into account in the design and analysis process of this project, and will be further explained in the following chapters.

Chapter 3

Methodology

The specific goal in this project was to design and manufacture a composite soundboard that would have similar natural frequencies to those of a reference wooden one under hinged Boundary Conditions (BCs). Ideally, the two soundboards would have similar natural frequencies, mode shapes and acoustical properties, but as a starting point, natural frequencies were used as the primary determining factor in the design of the composite soundboard, while the mode-shapes and modal-damping values were also being monitored. In addition to the above goal, it was important that the soundboard designed fulfills a number of static functional requirements, i.e., to have adequate strength to withstand the tension of the strings, and to be light enough to vibrate in response to conventional strings.

The wooden soundboard was borrowed from a guitar luthier based in Montreal, Joel Barbeau, who shared some of his knowledge with us and allowed us to perform experiments on two nylon-string guitar soundboards he had built, one of which was used as the reference for our design. The top plate of this soundboard was made from Picea Abies, and the braces from Sitka Spruce.

In order to meet the above goals and functional requirements, the bending stiffness, mass and the strength of the wooden top plate were first used as guidelines for an initial top plate design. A number of materials were considered for potential use in the top plate and the bracing sandwiches. Using the Finite Element Method (FEM), the effect of varying certain physical, geometric and elastic properties of the materials were then determined on the natural frequencies and mode-shapes of the soundboard under free and hinged BCs. The composite soundboard that was determined to have natural frequencies relatively similar to those of the wooden soundboard under hinged BCs was then manufactured. For verification purposes, experimental modal analysis was performed on the wooden and the composite

soundboards.

It is worth noting that the criteria of matching natural frequencies does not guarantee similarity in acoustic properties, especially from a perceptual point of view, as the relative amplitude and damping ratios of the modes affects the timbre of the instrument to great extent as well. Furthermore, in the higher frequency range, the frequency spacing between the modes tends to decrease, causing interaction between the normal modes and also making it difficult for us to distinguish between them. The significance of the instruments' natural frequencies in their timbre, however, is well known and has been looked at by many scientists in the study of the timbre of instruments. Moreover, the modes of an instrument and its soundboard are some of the few parameters that can be determined and monitored prior to construction, through numerical modelling. Matching the natural frequencies, therefore, seemed to be a reasonable starting point in the realm of the use of synthetic materials in musical instruments.

As explained in Sec. 2.4.1, since the harmonics present in the sound of a guitar in a large range of frequencies are generated by the soundboard, the behaviour of the guitar, to a first approximation, is thought to be dominated by the behaviour of the soundboard. This is why the soundboard was chosen as the first component of the instrument that is made from alternative materials and monitored through this design and material replacement.

This chapter will provide the description of the steps taken in the course of the project. Keep in mind that most of the decisions made throughout the design process were based on simulation results of the wooden and the composite top plates under free BCs, and those of the wooden and the composite soundboards under free and hinged BCs, most of which will be further elaborated in Chap. 4. Furthermore, in the methodology proposed, we must understand that it is not always possible to taylor a material to have the optimum geometric, physical and elastic properties we are interested in, as many of these properties are correlated (e.g. density and Young's modulus). The practical design, therefore, comes down to choosing available materials that would result in the best *possible* solutions.

3.1   Experimental Modal Analysis - Wood

It was important to identify certain modal characteristics of the wooden soundboard experimentally, in order to have a reference for the numerical model of the wooden soundboard, and the design of the composite one. The experiments aimed to monitor the natural frequencies, mode-shapes and modal damping values of the soundboard, and were performed in

the Computational Acoustic Modelling Laboratory (CAML) in the Music Technology suite of the Schulich School of Music, McGill University. The experimental set up was as follows:

The soundboard was hung from the ceiling using two long lightweight threads. The ends of the threads were knotted, sandwiched and glued between two small pieces of paper, in order to increase the contact surface between the threads and the tape. The sandwiches were then attached to the soundboard using adhesive tape in a symmetric manner, as shown in Fig. 3.1.
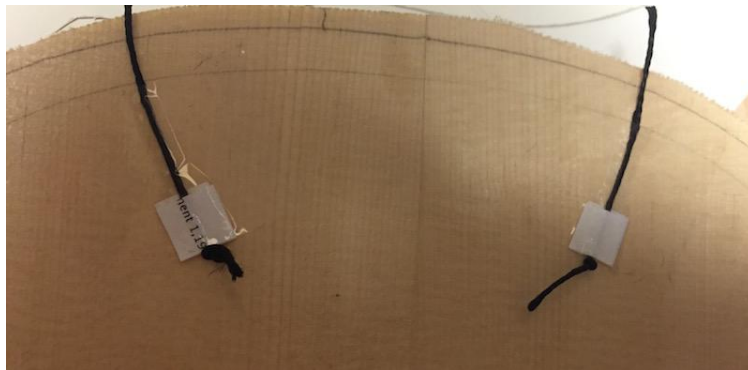
Figure 3.1: The threads from which the soundboard is hung.

The hammer used for the impact was a PCB 084A14 miniature hammer fitted into a custom-built aluminum holder mounted on a lab stand (Fig. 3.2). The bearing installed in the holder allowed for smooth rotation of the hammer. Once the hammer was fitted into the holder, the stand was placed close enough to the soundboard such that giving an initial angle to the hammer resulted in a hit on the soundboard with a consistent impact force. Note that the signal recorded by the force transducer in the hammer is weak and was therefore always amplified by a specified factor (in our case, a factor of 40), using a PCB signal conditioner. It was important to make sure that no hit exceeds the signal range accepted by the software, otherwise the signal would be clipped and the Frequency Response Function (FRF) calculations would be stopped. This meant making sure the amplification factor was not too high, and the initial angle of the hammer was not too large.

Figure 3.2: The PCB 084A14 miniature hammer.

Ideally, the hammer must hit the soundboard only once, but due to the elasticity of wood, a double-hit or multi-hit might be observed in the time-domain signal of the impact hammer. Normally, one would monitor this and adjust the setup to minimize the effect of a double hit. That being said, the force signal is deconvolved from the measured velocity, so the extra forces are taken into account in the input signal.
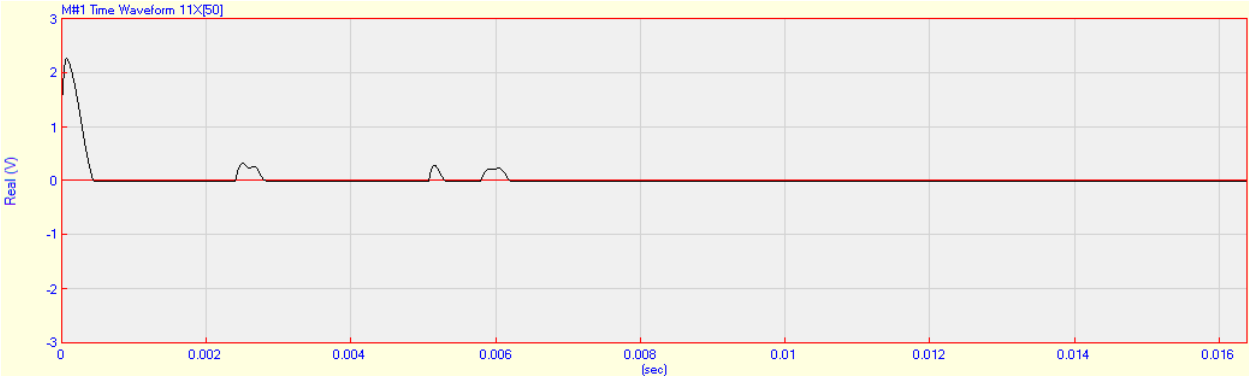
Figure 3.3: Example of a multi-hit time-domain signal from the hammer.

Mobility measurements were performed using an Polytec portable digital vibrometer LDV (PDV 100). The laser was perpendicularly placed at a 23 cm distance from the soundboard surface, as 23cm was listed as the shortest optimal stand-off distance in the LDV manual. For best results, the lens had to be adjusted until the focus of the laser was optimal.

In our experiments, the impact point was kept constant while the laser was moved from one measurement point to another. A total of 41 points were selected as measurements points. Note that we were not allowed to mark on the borrowed wooden soundboard, so the locations of the impact point and the measurement points were marked on a paper cutout of the soundboard instead. The cut out was attached to the soundboard using large paper clips, and the hammer and the laser were placed based on the marks on the cutout. Once the locations of the hammer and the laser were set, the cut out was removed. Every hit was repeated 3 times, as the LDV measured the responses of the three hits. Between the hits, we waited until the soundboard was stabilized before applying the next impact. The average of the FRF's obtained from the three hits were saved as the FRF corresponding to that measurement point. Note that while performing the experiments, the relative humidity of the laboratory was also monitored using a humidity sensor.

Both the hammer and the LDV signals, i.e. the input and the response signals respectively, were sent to a National Instruments DAQ (PCI-4472). The DAQ transferred the data to ME'scope, a software capable of analyzing and visualizing vibratory data. ME'scope was used in our experiments to allow us to monitor the time-domain data received from the hammer, the mobility FRFs, the modal damping values, the coherence between the averaged signals, and to visualize the Operational Deflection Shapes (ODSs) at all frequencies.

Using BNC splitters, the input and the output signals were sent to a secondary digital DAQ (USB-4431) that simultaneously sent the hammer and the LDV data to MATLAB. This was done mainly in case we needed to access and process the raw time-domain data later on, which is easier done on MATLAB. The MATLAB code developed for acquiring and plotting the received data was written by Gary Scavone and Jim Woodhouse.

On ME'scope, the "frequency span" was set to 21,376.46 [Hz] [1], since the range of audible frequencies for humans is 20,000 [Hz]. For adequate resolution of the FRFs, the number of time-domain samples was set to 32768 per 0.766 seconds, so that it would result in 1.3 [Hz] frequency increments, and the three FRFs corresponding to every measurement point were averaged "linearly".

---

[1]Note that this value is technically beyond the range the hammer practically captures, as it does not impart significant energy above 9 kHz.

On ME'scope, a "structure" file, an "acquisition" file and a "BLK" file (referred to as "data block") were created. The structure was made up of the surface triangles connecting the measurement points. The acquisition file was the platform through which the DAQ and the software communicated, and where the different measurements were stored as "measurement sets". The data block was the file containing all the FRFs, coherences and the time domain data. Note that other types of plots can be stored and analyzed in ME'scope as well, e.g. correlation, but that the three mentioned were those we were interested in, in our experiments.

The experimental natural frequencies were obtained by selecting the peaks observed in both the amplitude and phase plots, i.e. the frequencies at which a peak had occurred in both plots.
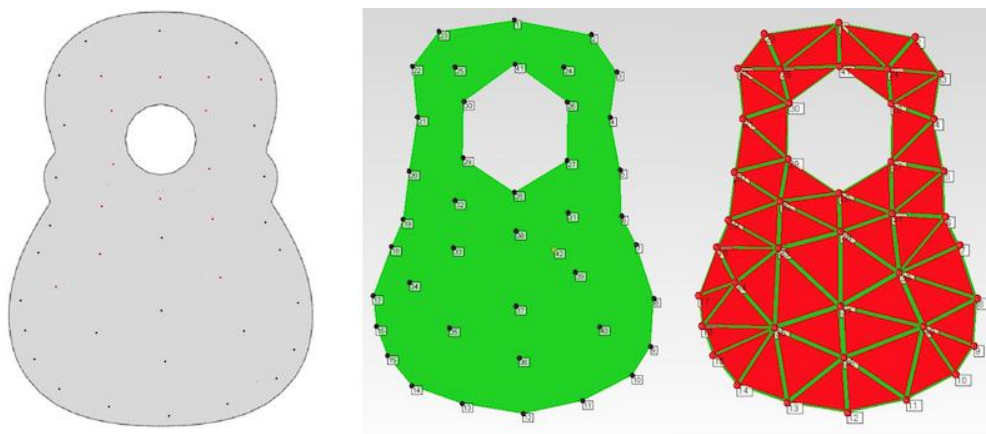
Figure 3.5: Left: Map of the measurement points on the wooden soundboard. Centre: Measurement points defined on ME'scope. Right: Surface triangles created on ME'scope.

3.2 The CAD Model

This step involved developing a 3D Computer Aided Design (CAD) model of the soundboard that would represent its geometry as accurately as possible. The model was made on Autodesk Inventor, based on the drawing and the soundboard borrowed from the luthier, and was made in two steps: 1. The brace-less top plate (to be referred to simply as the top plate). 2. The complete soundboard with the braces added and trimmed to their real shape.

Figure 3.6: Left: the drawing of the soundboard. Centre: the braces behind the wooden soundboard. Right: The front side of the wooden soundboard. The top plate is made from Picea Abie, and the braces from Sitka Spruce.
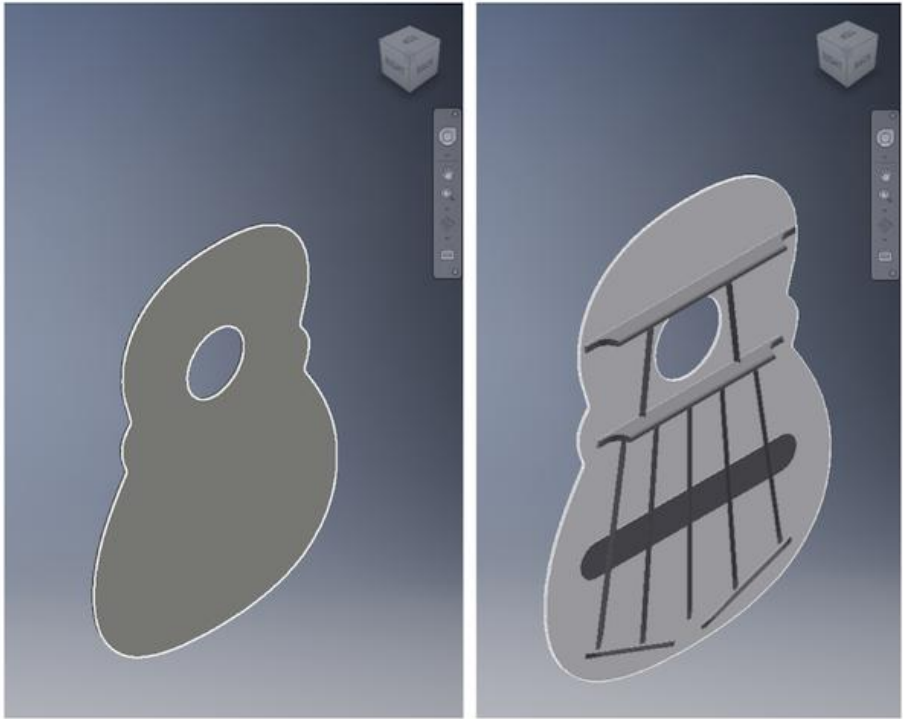
Figure 3.7: Left: The 3D CAD model of the wooden top plate. Right: The 3D CAD model of the complete wooden soundboard.

3.3   Simulating the Modal Behaviour - Wood

The modal behaviour of the soundboard was determined using Abaqus CAE, a software capable of performing Finite Element Analysis (FEA) [2]. It features pre-processing (i.e. basic CAD modelling), simulation, and post-processing (i.e. visualization and plotting) capabilities. As explained earlier, the pre-processing was done on Autodesk Inventor, commonly used for CAD modelling purposes, and the simulation and post-processing steps were performed on Abaqus. The following tasks were performed once for the brace-less wooden top plate, and once for the full wooden soundboard.

3.3.1   The Wooden Top Plate

1) **Importing the Model**: The CAD model of the top plate was imported from Inventor into Abaqus as a 3D "part" in a .stp format.

2) **Material Properties and Section Assignment**: In the *Property* module, a material directory had to be created in which certain properties of the materials used are defined. For a frequency analysis, the density and the elastic properties of the material were required. Picea Abies, as an orthotropic material, was therefore defined with its density and the 9 elastic constants listed in Table 3.1 (referred to as "Engineering Constants" on Abaqus).

Note that Abaqus does not require us to specify units for the values we enter, so it is important to use a consistent system of units. The system used in our simulations is presented in Table 3.2. For reference, the density and Young's modulus of steel are listed. For other possible systems of consistent units, refer to [55].

For the numerical model to implement the correct material anisotropy, *material coordinates* must be defined. In case of assemblies, different coordinates must be defined for the different constituent parts. In case of the top plate, however, only one material coordinate was required. The top plate was then chosen as the *section* to which Picea Abies was assigned.

---

[2]Abaqus is also capable of performing Computational Fluid Dynamics (CFD), Computational Electromagnetics and in general, Computer Aided Engineering (CAE).

Table 3.1: Density and Elastic Properties of Picea Abies and Sitka Spruce. S_b, l and S_b, r are the longitudinal and the radial bending strengths. Values marked with * were given to us by the Luthier.

Properties	Picea Abies	Sitka Spruce
$\rho^*\ [kg/m^3]$	353	360
$E_1^*\ [MPa]$	10200	11880
$E_2^*\ [MPa]$	1020	927
$E_3\ [MPa]$	1600	927
ν_{12}	0.51	0.467
ν_{13}	0.38	0.372
ν_{23}	0.31	0.245
$G_{12}\ [MPa]$	754	724.68
$G_{13}\ [MPa]$	812	760.32
$G_{23}\ [MPa]$	36	35.64

Table 3.2: System of consistent units used. For reference, the density and Young's modulus of steel are listed.

Mass	Length	Time	Force	Stress	Energy	Density	Young's Modulus	Gravity
tonne	mm	s	N	MPa	N-mm	7.83E-09	2.07E+05	9.81E+03

3) **Assembly**: To perform computation on a part or a set of parts, Abaqus requires us to define an *Instance*. In this case, the whole top plate was chosen as an *independent* instance, in the *Assembly* module.

4) **Step**: In the *Step* module, the type of analysis we wish to perform is specified, e.g. *frequency*, *heat transfer*, etc., as well as the solution method and further specifications, e.g. frequency range, increment size, etc. Our analysis was a *frequency* type for which we inquired all the modes between 1-1000 Hz, and the eigen-solver was chosen to be *Lanczos*. Note that the lower bound was specified in order to ignore the zero modes, and the upper bound was

roughly the highest fundamental pitch playable on a nylon-string guitar[3]. Since 32 modes were obtained for the wooden soundboard in this range, all the following modal analyses on the full composite soundboard was also concerning its first 32 modes.

5) **Interaction, Constraints and Boundary Conditions**: In the case of assemblies or multiple parts in contact, the type of interaction the parts have must be defined, e.g. *fixed*, *surface-to-surface contact*, etc. Different BCs can also be applied to the model, e.g. free-translation fixed-rotation. In the modal analysis of the top plate, no BCs, constraints or loads were required.

6) **Mesh**: In the *Mesh* module, the size, type and order of the elements of the numerical model can be selected. The approximate global mesh size was chosen to be 3 with a maximum 0.1 deviation factor. The smaller the mesh size, the more accurate the results, but also, the more time consuming the simulations can be. We found 3 to be sufficiently small. For a more detailed explanation on selecting element size, refer to footnote [4].

7) **Simulation**: Every *job* created will contain the analysis results and *field outputs* requested in the *steps*. If there are multiple *steps* defined in the step module, running the job will perform all the computations requested and present all the results. Once the job is completed, it will be possible to perform certain post-processings on the results, e.g. FRF plots.

8) **Visualization of the Results**: Once the *Job* is completed, the eigen-modes are reported and the mode-shapes can be visualized.

3.3.2   The Wooden Soundboard

The soundboard assembly was imported into Abaqus as a single 3D *part*. It was introduced as one independent assembly, and the above steps were performed on the full wooden soundboard under free BCs. The eigen-frequencies and mode-shapes obtained from this simulation were then compared to those obtained experimentally.

---

[3]One can argue that the higher partials of all notes are important, but the more important issue is that the modal density starts to get too high above 1-2 kHz for us to properly discern individual modes.

[4]In his article on discretization requirements [56], Marburg states that the minimum number of nodes required in acoustic computations of numerical models must go beyond fulfilling Shannon's sampling theorem [57]. He believes that while adequate for wave "detection", this number is not enough for approximating the shape of the elements, and he suggests a minimum of 6 to 10 nodes per wavelength of the highest frequency of interest, i.e. equivalent to 3 to 5 linear elements.

In a series of studies done by Elajabarrieta et al. [51–54], it is stated that the boundary conditions of a real soundboard attached to the ribs can be approximated as a fixed-translation free-rotation boundary condition, referred to as "hinged" boundary conditions. It was therefore decided to determine the natural frequencies of the soundboard under hinged BCs as well. This required us to create a second *job* in which the new BCs were defined, after having run the first job.
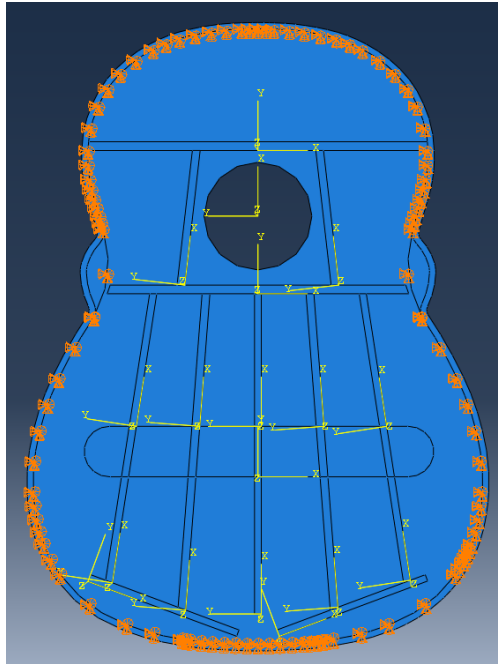
Figure 3.8: The numerical model of the soundboard is "hinged" along the final soundboard silhouette.

Comparing Experimental and Numerical Mode-frequencies

In order to make correct comparisons between the numerical and the experimental results, it was important to understand the difference between how mode-frequencies are determined numerically, and how they are obtained experimentally. In the experiments, the mode-frequencies were simply chosen by selecting the peaks that appeared in both the magnitude plot and the imaginary plot of the mobility FRFs. The mode-frequencies reported by Abaqus, however, are determined through computation of eigen-vectors and eigen-values of the numerical model. Some of these eigen-vectors (or modes) might not have enough amplitude to appear as "peaks" in the FRFs. This could be either because the excitation point has happened to fall on a nodal point of those modes, or due to the uncertainties and errors associated with the impact testing. Examples of these errors are those associated with

humidity or boundary conditions not accounted for.

Consider a mode-frequency vs. mode-number plot representing the experimental and the numerical mode-frequencies (Fig. 3.9). With the above explanation, a correct comparison between the two would be one in which the mode-frequencies obtained numerically are plotted strictly sequentially, while those determined experimentally are not. In this case, every mode-frequency from the experimental set would be compared with a numerical mode-frequency in its vicinity. The point of the comparison would therefore be to observe whether for every predicted eigen-frequency, a natural frequency is obtained experimentally, and if so, how different are the experimental modes from the predicted modes, in terms of frequency and mode-shape.
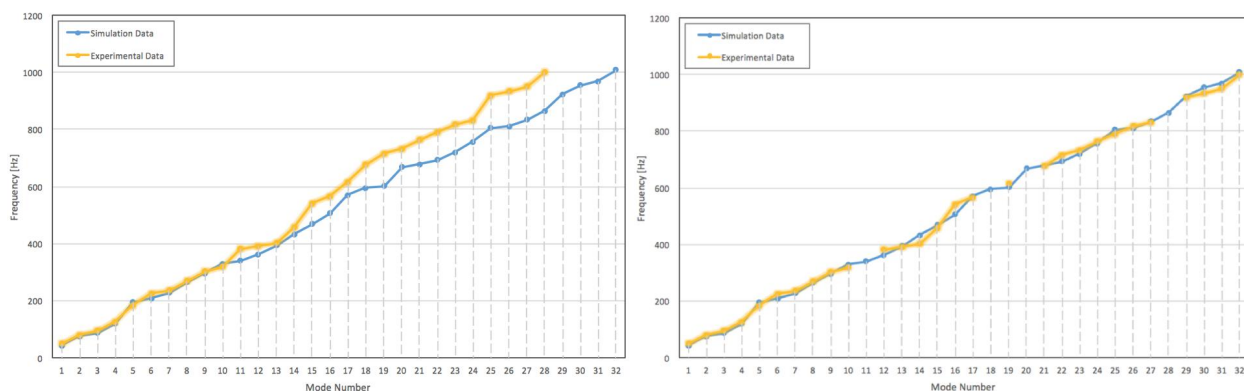
Figure 3.9: Graphical comparison of simulation and experimental natural frequencies. Left: Strictly sequential plotting. Right: Non-strictly sequential plotting. The yellow plot represents the experimental natural frequencies, and blue represents eigen-frequencies obtained through simulation.

3.4 Top Plate Simulation: From Wood to Composite

As explained earlier, every guitar soundboard must fulfill certain functional requirements. It must have adequate strength to withstand the tension of the strings, and must be light enough to vibrate in response to conventional strings. But aside from these requirements, in this project, we were interested in making a composite soundboard whose natural frequencies would also be similar to those of the reference wooden one.
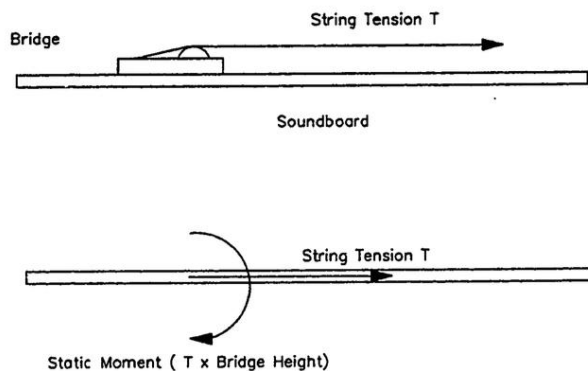
Figure 3.10: The tension and moment caused by the strings [9].

We know that the natural frequencies of structures highly depend on their mass and stiffness matrix, i.e., a function of E, G and ν in the different directions. We are also aware that according to the Euler beam theory, the natural frequencies of a free suspended beam are related to its bending stiffness according to Eq. (3.1) [58], i.e.:

$$D_n = \frac{Mw_n^2 L^3}{[(n+1/2)\pi + k_n]^4},\tag{3.1}$$

where D_n is the bending stiffness, M and L are, respectively, the mass and the length of the beam, w_n is the n'th natural frequency of the beam (in $[rad/sec]$), and k_n is a mode-dependent constant that can be found in [58, p. 64]. In more complex structures, however, finding an analytical relationship between the bending stiffness and the natural frequencies would not be as easy. Eq. (3.1) was, nevertheless, a hint for us to recognize a link between natural frequencies and mechanical properties of a structure.

Furthermore, the mathematical relationships between vibrational frequencies and elastic properties of simple structures, such as beams and pins, have long been used in optimization problems and mechanical design techniques such as Ashby's method [59]. In Ashby's method, the *function* of the structure is first defined, e.g. withstanding compression, or resisting bending. Then considering the constraints (e.g. dimensional constrains), the function defined allows us to find the optimal material properties for the structure, e.g. mass or cost.

When designing sandwich structures, however, with a vast range of potential materials and their variability in properties, it may be more difficult to treat the project as an "optimization" problem, especially considering the little research that has been done on the use of composites in guitar soundboards, unless the potential materials are narrowed down and many variables are treated as constraints, e.g. the thickness of the plate. Nonetheless,

Ashby's approach and Eq. (3.1) led us to a meaningful starting point for our design process.

3.4.1 Why Sandwich Structures?

Sandwich structures have been used in many industries and applications in the recent decades, due to their lightweight and high in-plane flexural stiffness [60]. In addition to that, as mentioned in Chap. 2, their use has been explored in the literature of composite guitars as well [6] [7] [8]. That, combined with the fact that producing sandwich structured-composites manually is relatively easy, motivated us to explore the option.

3.4.2 Initial Proposition

To have a reference for our sandwich design, it was important to analyze certain mechanical properties of the wooden top plate first. The top plate was approximated as a rectangular plate made from Picea Abies, with the length, width and thickness of the wooden sound-board, i.e. $l = 490$ [mm], $b = 360$[mm] and $h = 2.3$ [mm] respectively.
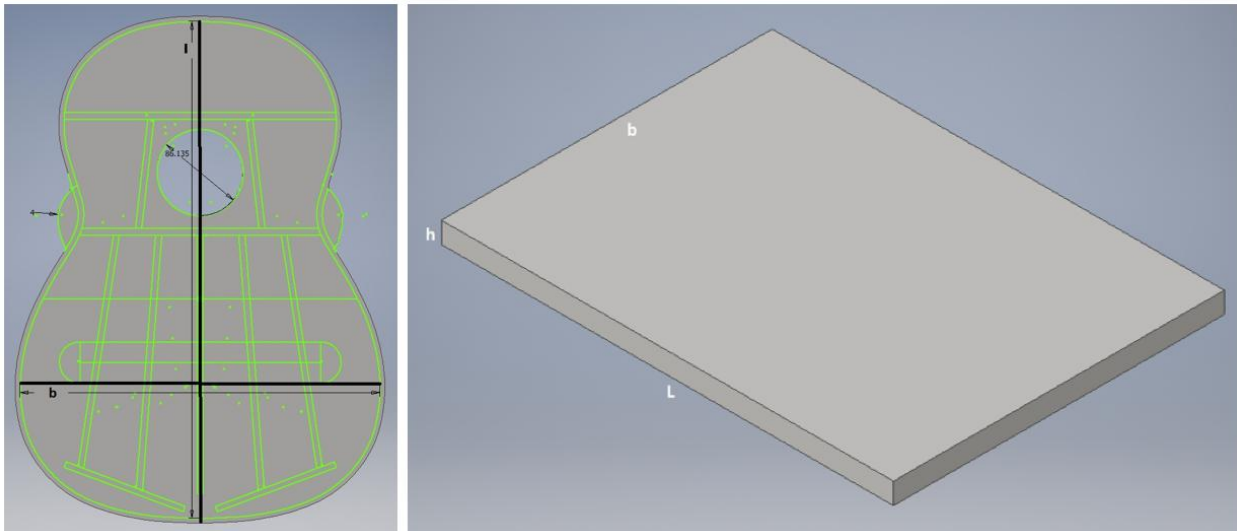
Figure 3.11: Left: the Inventor CAD model of the wooden top plate. Right: The rectangular approximation of the wooden top plate, with length $l = 490mm$, width $b = 360mm$ and thickness $h = 2.3mm$.

As a starting point, the materials available to us in the composites lab were considered for use in a sandwich arrangement as depicted below. Among the available materials, it was decided to consider the unidirectional composites for use in the sandwich structure, since their anisotropy would be more similar to wood. Table 1 lists the uni-directional composites

that were available to us in the composites lab, as well as their required properties. In this table, NCT321-UD (Unidirectional Newport 321) is made from uni-directional carbon fibres pre-impregnated in epoxy resin, and was provided to us in form of pre-preg plies. Similarly, Lineo FUD180 plies are made from pre-preg uni-directional flax fibres with epoxy resin [61].
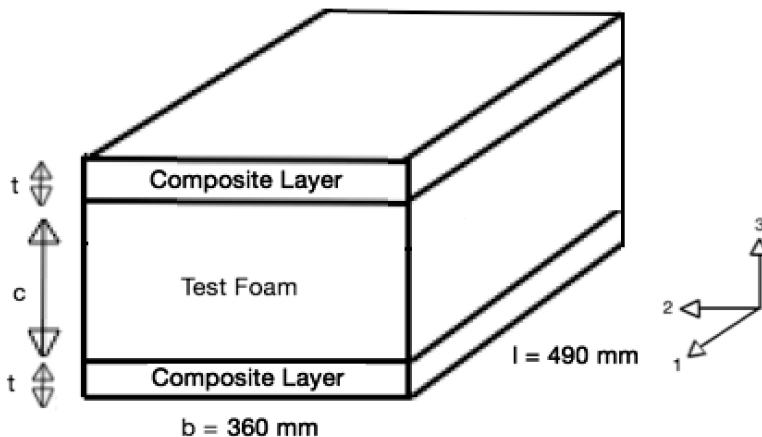
Figure 3.12: The initial sandwich arrangement proposed for the top plate. Note that uni-directional fibres would be laid parallel to axis 1. Note: Diagram is not to scale.

Table 3.3: Elastic properties of the uni-directional materials considered. t is thickness and $S_{b,l}$ and $S_{b,r}$ are the longitudinal and radial bending strengths.

Material	E_1	E_2	ν_{12}	G_{12}	G_{13}	G_{23}	t	ρ	$S_{b,l}$	$S_{b,r}$
	[MPa]	[MPa]		[MPa]	[MPa]	[MPa]	[mm]	$[kg/m^3]$	[MPa]	[MPa]
NCT321-UD	128242	8274	0.3	4137	4137	2000	0.16	1500	1186.8	220.8
FUD180	28200	3310	0.34	27.1	27.1	10000	0.294	1330	286	11.8

Based on the requirements and the goals stated earlier, the design process for the brace-less top plate sandwich was then as follows:

I. The bending stiffness and the mass of the approximated rectangular plate were used as guidelines to come up with an initial sandwich design.

II. The composite top plate with the proposed sandwich arrangement was modelled on Abaqus, where its mode-frequencies and mode-shapes were determined, as the different physical and elastic properties of the sandwich were varied.

III. A strength analysis was then performed on the rectangular plate with the modified sandwich arrangement, to make sure the proposed top plate sandwich has sufficient strength to withstand the tension of the strings.

3.4.3   I. Bending Stiffness and Mass as Considerations

In monolithic materials[5], the bending stiffness of a rectangular plate is calculated simply as:

$$D = E \times I \tag{3.2}$$

where I is the area moment of inertia of the plate cross section. So in an orthotropic monolithic material, like wood, $I_l = (bh^3)/12$ is the I in longitudinal bending (bending along the wood grains, i.e. about axis 2), and $I_r = (lh^3)/12$ in radial bending (bending perpendicular to the wood grains, i.e. about axis 1). The longitudinal and the radial bending stiffness of the Picea Abies rectangular plate were therefore calculated as:

$$D_{wood-l} = 10200[MPa] \times \frac{360[mm] \times (2.3[mm])^3}{12} = 3.72 \times 10^6 \quad [N.mm^2] \tag{3.3}$$

and

$$D_{wood-r} = 1020[MPa] \times \frac{490[mm] \times (2.3[mm])^3}{12} = 5.07 \times 10^5 \quad [N.mm^2]. \tag{3.4}$$

(a)   (b)
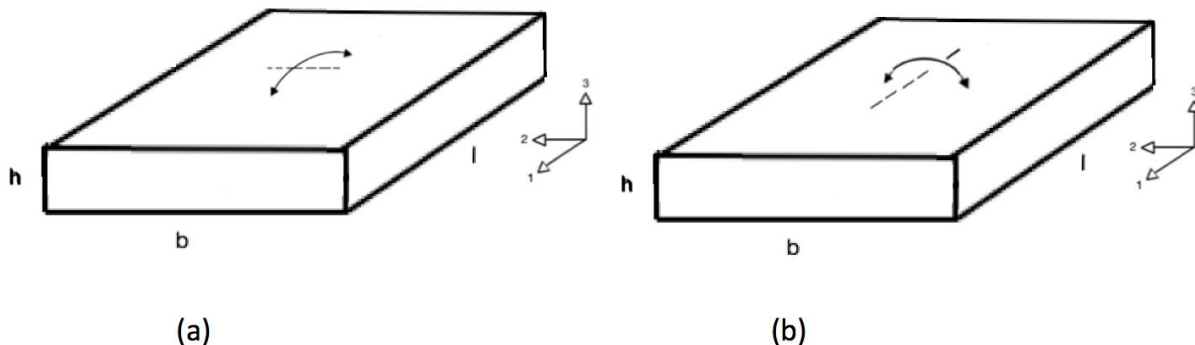
Figure 3.13: Monolithic rectangular plate subject to bending. (a): Longitudinal bending. (b): Radial bending.

---

[5]Monolithic materials are made from two or more different materials, combined in such a way that they are not easy to distinguish, so the combination is best treated as one single-phase material. [8]

Now consider the sandwich arrangement proposed earlier, which is an example of a non-monolithic structure. The equivalent bending stiffness of sandwich structures can be calculated as:

$$D_{eq} = \sum (EI)_i, \tag{3.5}$$

where i corresponds to the ith layer. In a symmetric sandwich like Fig. 3.9, if the compressive and tensile moduli of the face layers are assumed equal, the neutral axis[6] can be assumed at the centre of the core. The area moment of inertia of every face layer with respect to this neutral axis, I_f, can therefore be calculated using the parallel axis theorem as:

$$I_f = I_{ff} + Ad^2, \tag{3.6}$$

where A is the cross sectional area of the face layer, i.e. $A = b \times t$, d is the distance between the neutral axis and the centre of that face layer, i.e. $d = (c + t)/2$, and I_{ff} is the area moment of inertia of the face layer about its own neutral axis.
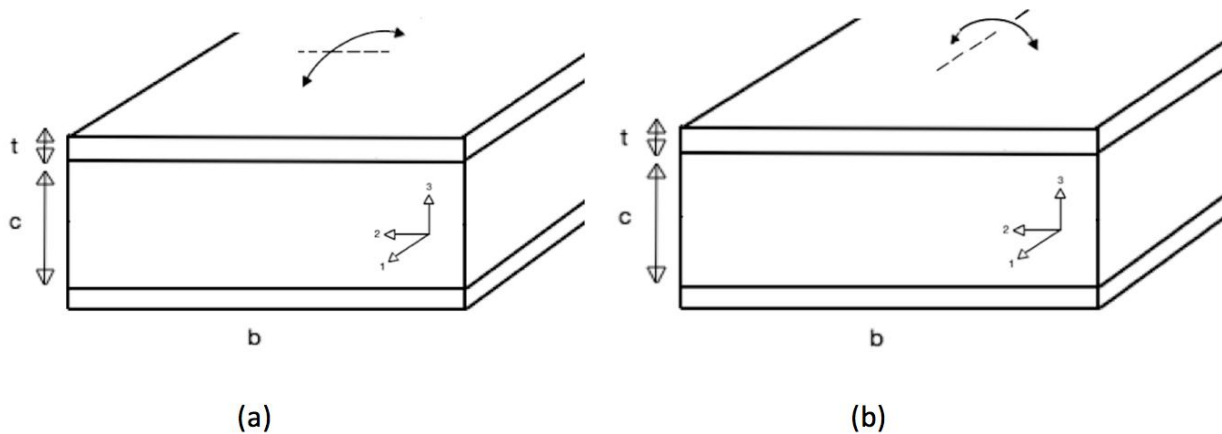
Figure 3.14: Sandwich structure subject to bending. (a): Longitudinal bending. (b): Radial bending. Note: Diagrams are not to scale.

The equivalent bending stiffness of the sandwich will then be:

$$D_{eq} = E_c I_c + 2E_f I_f, \tag{3.7}$$

where c subscripts correspond to the *core* material, and f subscripts to the *face* material.

---

[6]The axis along which the compressive and tensile stresses within the material cancel each other.

Eq. (3.1) for longitudinal bending can then be written as:

$$D_{eq,l} = E_c \frac{bc^3}{12} + E_{f,l}[\frac{bt^3}{6} + \frac{btd^2}{2}]. \tag{3.8}$$

Since the Young's moduli of foams are generally orders of magnitude smaller than those of composites, the first term in Eq. (3.9) can essentially be ignored. The equation will therefore be reduced to:

$$D_{eq,l} \cong E_{f,l}[\frac{bt^3}{6} + \frac{btd^2}{2}]. \tag{3.9}$$

Similarly, the radial bending stiffness can be determined as:

$$D_{eq,r} \cong E_{f,r}[\frac{lt^3}{6} + \frac{ltd^2}{2}]. \tag{3.10}$$

In the initial design, the total thickness of the sandwich was chosen to be that of the wooden soundboard, and the face layers were chosen to be FUD180. Therefore $t = 0.294$ [mm], $c = 1.712$ [mm] and $E_f = 28200$ [MPa]. Using Equations (3.9) and (3.10), the longitudinal and radial bending stiffnesses of the sandwich were calculated to be:

$$D_{eq,l} \cong 6.05 \times 10^6 [N.mm^2] \text{ and } D_{eq,r} \cong 9.66 \times 10^5 [N.mm^2].$$

As explained earlier in the literature of guitar soundboards, a high longitudinal stiffness is generally desired along the length of the soundboard. Based on that, the longitudinal bending stiffness in these initial design calculations was used as the factor determining the similarity between the wooden top plate and the composite one. Therefore given the longitudinal bending stiffness obtained above, the bending stiffness of the sandwich rectangular plate needed to be reduced. An easy way to reduce these values was to reduce the thickness of the core foam. It was determined that with FUD180 as the face layers, a core thickness of $c = 1.275$ [mm] would result in the same longitudinal bending stiffness as that of the wooden plate, i.e.:

$$D_{eq,l-FUD} \cong 3.72 \times 10^6 [N.mm^2] \text{ and } D_{eq,r} \cong 5.94 \times 10^5 [N.mm^2].$$

The other available material for face layers was the uni-directional Newport 321 with a thickness of $t = 0.16$ [mm] and $E_f = 128242$ [MPa]. The optimal foam thickness was found to be $c = 0.84$ [mm] in this case, and the bending stiffnesses as follows:

$$D_{eq,l-NCT} \cong 3.72 \times 10^6 [N.mm^2] \text{ and } D_{eq,r} \cong 3.27 \times 10^5 [N.mm^2].$$

So far, with the above preliminary calculations, the thickness of the foam core was determined for potential sandwiches with two different potential composite face layers. The above results were to be regarded as a starting point for our simulations. We now had to choose a foam whose physical and elastic properties would result in mode-frequencies similar to those of the wooden top plate. This required us to start from an existing foam and vary certain material properties of the core and the face layers, and to determine the effects of their variations on the mode-frequencies and mode-shapes of the top plate.

Note that in this process, it was not our intention to have the lightest possible soundboard, but one that was light enough to be excited by conventional strings, while simultaneously exhibiting similar mode-frequencies. The initial density of the core foam was therefore chosen such that the thicknesses discussed would result in the sandwich top plate having the same mass as the wooden one.

3.4.4   II. Using Simulation to Monitor the Eigen-frequencies

In Sec. 3.1.3, we simulated the modal behaviour of the wooden top plate and the wooden soundboard. In this 2nd stage of the design, we simulated the modal behaviour of the composite top plate as it was being designed.

The 3D CAD model of the top plate was imported into Abaqus as a 2D part. The composite layers were introduced into the software as *Lamina*, and the foams were introduced via *Engineering Constants*. For a *frequency* analysis, the density and 6 elastic constants needed to be entered into the material directory, and material assignment was done using *composite layup*. Under *composite layup*, the laminate materials were chosen from the material directory, and were assigned to the layers in order. It was also in *composite layup* that the thickness of every layer was entered, as well as their orientation.

The goal here was to simulate and monitor the eigen-frequencies of the proposed sandwiches, as the ρ, E, G and ν of the core and the face layers were varied, as well as the thickness of the core. The boundary conditions at this stage were still free.

Foam Selection

The simulations started by exploring the foam options offered by Evonik's Rohacell foams, since we had previously used their products and were aware of the wide range of material properties they offer. In doing so, we had to keep the following in mind:

○ The core foam must be able to withstand high curing temperatures of at least 121°C, since FUD180 and NCT321 are cured at temperatures higher than that.

○ The foam must be rigid, so it transfers vibratory energy between the composite layers. This would also make sure that the foam doesn't change shape under high vacuum pressures during vacuum bagging.

○ The foam must absorb enough resin to adhere to the pre-preg material in the curing process. It should, however, not absorb too much resin to the extent that its properties are affected.

○ The foam must be suitable for manually laying up pre-preg carbon fibres.

Properties Varied

After studying the properties of some existing composites and rigid foams, it was decided to vary the specified material properties in the ranges practically available (Table 3.4).

Table 3.4: Range of the properties varied in the design of the top plate.

Layer	E_1	E_2	ν_{12}	G_{12}	G_{13}	G_{23}	t	ρ
	[MPa]	[MPa]		[MPa]	[MPa]	[MPa]	[mm]	$[kg/m^3]$
Core	30 - 180	30 - 180	0.20 - 0.50	10 - 92	10 - 92	10 - 92	0.80 - 2.00	31 - 180
Face	60000 - 130000	1000 - 8500	0.30 - 0.50	2000 - 4500	2000 - 4500	1000 - 3000	0.08 - 0.294	990 - 2500

Practical Limitations

Throughout the calculations and the simulations, some of the potential sandwiches had core foams of less than 1 [mm] thicknesses. Despite being theoretically optimal in some cases, after an extensive search in the market, it was discovered that rigid foams are not commercially produced in thicknesses of less than 1 mm.

To overcome this problem, it would have been possible to use spray foams instead, and manually make the core foam with less than 1 [mm] thickness, but that would have required a more complex moulding system which would make the manufacturing process more time consuming and exhausting. The other option was to choose other core materials, such as honey-comb Nomex which is already being used in double-top guitars. That idea was briefly explored with the help of the honey-comb Abaqus plug-in, and while possible, modelling the honey-comb layer was found to be highly time consuming.

With the issues stated, it was eventually decided to settle for higher than optimal thicknesses, and compensate for the excess stiffness of the top plate by making the braces less stiff.

The Modified Sandwich

After varying the properties stated and comparing the eigen-frequencies of the wooden top plate with those of the composite top plate, it was decided to make the core from Rohacell Rist 110 with a thickness of $c = 1$ [mm], and the face layers from one ply of uni-directional NCT321 on each side of the foam.

Table 3.5: Properties of Rohacell Rist 110.

Material	E_1[MPa]	E_2[MPa]	ν_{12}	G_{12}[GPa]	G_{13}[GPa]	G_{23}[GPa]	ρ [kg/m^3]
Rohacell Rist 110	180	180	0.3	70	70	70	110

3.4.5 III. Strength Criteria

Now that we had some idea about the arrangement of the top plate sandwich, it was time to assess whether the sandwich proposed would have sufficient strength to withstand the tension of the strings. The moment caused by the strings of the guitar were described by:

$$M_{max,wood} = \frac{S_b I_{wood}}{y}, \tag{3.11}$$

where S_b is the bending strength of Picea Abies, and y is the distance from the neutral axis to the location of maximum stress (i.e. the surface), hence $y = h/2$. Note that this equation is applicable only to monolithic materials.

Most guitar soundboard woods are cured to have less than 12% moisture contents therefore the strength values for 12% were used in the calculations. Based on the longitudinal and radial bending strengths listed in Table 3.6 (found in [62] and [63] respectively), the maximum moment the rectangular wooden piece could withstand was then calculated as:

$$M_{wood,l} = \tfrac{75 \times 360 \times 2.3^2}{6} = 23.81 \times 10^3 \text{ [N.mm]}$$

and

$$M_{wood,r} = \frac{6.4 \times 490 \times 2.3^2}{6} = 2.76 \times 10^3 \text{ [N.mm]}$$

Table 3.6: Longitudinal and radial bending strength values of Picea Abies. Note that where the radial bending strength is marked with *, the moisture content of the Picea Abies specimen was listed as 10.5±0.5%, and not 12%.

Moisture Content [%]	$S_{b,l}$ [MPa]	$S_{b,r}$ [MPa]
12	75	6.4*
30	43	-

In sandwich structures, depending on the relative thickness and the relative stiffness of the skin and the core layers, the structure can have different possible modes of failure. For a sandwich structure with relatively thin and stiff skin layers and low core stiffness, the most probable failure modes are failures due to *face-sheet compression*, or if the stiffness of the core is too low, due to *face-sheet wrinkling*. [64, p. 209]

The maximum moment the composite sandwich experiences during compressive failure of the face-sheet can be described as:

$$M_{comp,l} \cong b S_{b,l} h_f (h_f + h_c), \tag{3.12}$$

where h_f is the thickness of the face layer and h_c the thickness of the core. Therefore based on the properties of NCT321 listed in Table 3.3:

$$M_{comp,l} \cong 360 \times 1186.8 \times 0.16 \times (0.16 + 1.00) = 79.30 \times 10^3 \text{ [N.mm]}.$$

and

$$M_{comp,r} \cong 490 \times 220.8 \times 0.16 \times (0.16 + 1.00) = 20.08 \times 10^3 \text{ [N.mm]}.$$

Assuming that our rectangular approximation of the top plate is valid, the maximum moments the wooden rectangular plate experiences at its highest stress in the longitudinal and the radial directions are smaller than the moments the composite rectangular plate can experience. Therefore, if the moment caused by the strings is applied to the composite top plate, the composite top plate is not likely to fail due to facesheet compression:

$$M_{max-comp,l} > M_{max-wood,l} \text{ and } M_{max-comp,r} > M_{max-wood,r} \implies \text{Composite rectangular}$$
$$\text{plate will not fail due to face-sheet compression.}$$

On the other hand, the stress at which face-sheet wrinkling occurs can be determined by Eq. (3.14) [64, p. 209]:

$$\sigma_{cr,l} \cong c\sqrt[3]{E_{f1}E_{c3}G_{c13}} \tag{3.13}$$

and

$$\sigma_{cr,r} \cong c\sqrt[3]{E_{f2}E_{c2}G_{c23}}, \tag{3.14}$$

where c is a coefficient between 0.5 and 0.8 determined experimentally, so:

$$\sigma_{cr,l} \cong c\sqrt[3]{128242 \times 180 \times 70} = c \times 1173.46 \text{ [MPa]}$$

and

$$\sigma_{cr,r} \cong c\sqrt[3]{8274 \times 180 \times 70} = c \times 470.65 \text{ [MPa]}.$$

Since the sandwich is not built yet at this stage, the worst case scenario (i.e. if $\sigma_{cr,l}$ is the smallest) was computed in the longitudinal and the radial directions as:

$$\sigma_{cr,l} \cong 0.5 \times 1173.46 = 586.73 \text{ [MPa]}.$$

and

$$\sigma_{cr,r} \cong 0.5 \times 470.65 = 235.33 \text{ [MPa]}.$$

Notice that the critical stresses at which the sandwich fails due to face-sheet wrinkling in the longitudinal and radial directions are larger than the longitudinal and radial bending strength of Picea Abies respectively (i.e. 75 [MPa] and 6.4 [MPa]). This means that the allowable stress before face-sheet wrinkling occurs is sufficiently high, therefore face-sheet wrinkling will not occur in the composite rectangular plate under the tension of the strings.

$$\sigma_{cr,l} > S_{b-wood,l} \text{ and } \sigma_{cr,r} > S_{b-wood,r} \implies \text{Composite rectangular plate will not fail due to}$$
$$\text{face-sheet wrinkling.}$$

3.5 Adding the Braces - Simulation

The above results and considerations provided a starting point for the design of the complete composite soundboard. It was now time to design the braces, in order to increase the eigen-frequencies of the soundboard and match those of the wooden one. It is worth noting that at this point, the design of the top plate sandwich was not considered finalized and could be subject to change, if the simulation of the full soundboard suggested so.

Adding the braces to the composite top plate numerical model required us to have the layout of the braces projected on the top plate plane. This was done by importing the 3D CAD model as a 3D *part*, and creating *partitions* on one face of the top plate, by tracing the bracing pattern. In Abaqus, 3D *parts* are visualized as empty 3D shells, and the *faces* of the shell can be removed. When the bracing *partitions* were completed on one face of the top plate, all the braces and the other faces of the soundboard were removed. The top plate face with the partitions was then used as the base for the *composite layup*.

Just as was explained in Sec. 3.4, certain physical, geometric and elastic properties of the constituent materials in the bracing sandwiches were varied in the simulations, while their effects on the eigen-frequencies of the soundboard were monitored. Note that the simulations were first run with free boundary conditions, so we knew the inherent natural frequencies of the soundboard, and then with hinged BCs. In both cases, the eigen-frequencies were monitored up to 1000 Hz, and the mode-shapes up to the 10th mode.
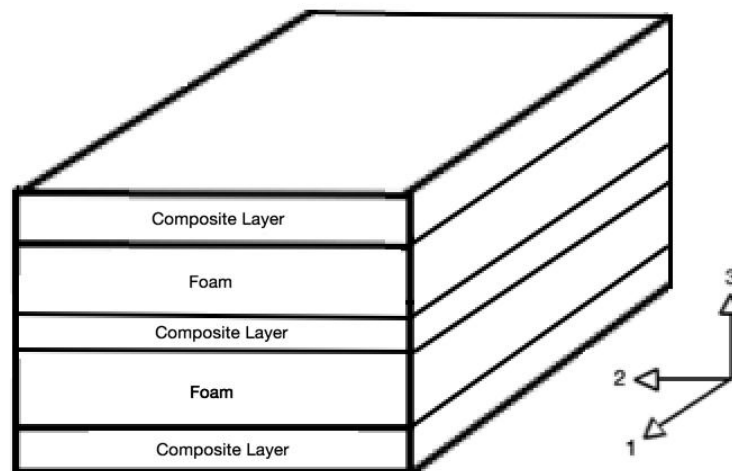
Figure 3.15: Sandwich arrangement proposed for the braces.

The material properties were varied in a range similar to those listed in Table 3.4, but larger foam thicknesses and other composite ply orientations were considered for use in the bracing sandwiches. It was also noticed that using a sandwich arrangement with three composite plies and two foam layers resulted in a better match of the eigen-frequencies (Fig. 3.14).

Based on to the simulation results that will be discussed in Chap. 4, Rohacell HF 71 was found suitable for use in the bracing sandwiches, with the arrangements shown in Fig. 3.15. The top plate sandwich remained as was decided in Sec. 3.4. Figures 3.16 and 3.17 show the

sandwich arrangements determined for the different parts of the soundboard.
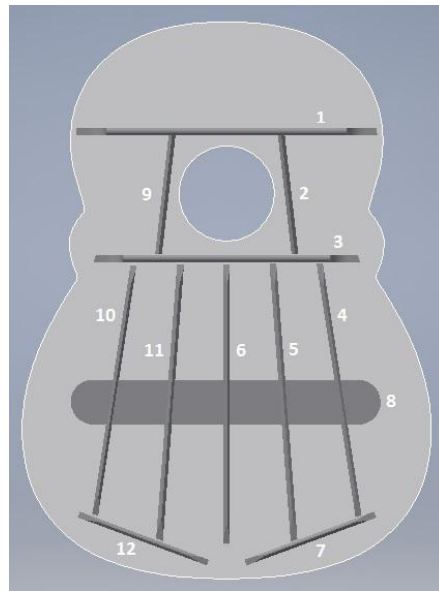
Figure 3.16: Soundboard with the braces numbered.
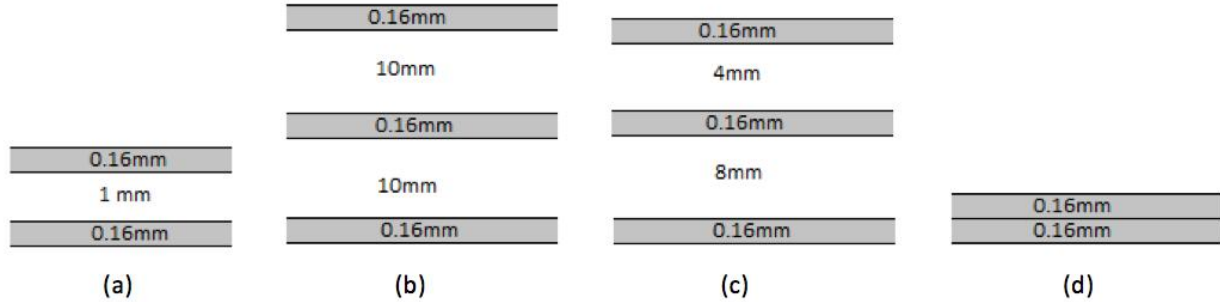
Figure 3.17: Finalized sandwich arrangements. In the diagrams, grey corresponds to NCT321-UD, and white to foams. The foam used in all the braces is Rohacell HF 71, and the foam used in the top plate is Rohacell Rist 110. (a): The top plate sandwich. (b): Sandwich arrangement for braces 1 and 3. (c): Sandwich arrangement for braces 2, 4, 5, 6, 7, 9, 10, 11, 12. (d): Sandwich arrangement for brace 8. Note: Diagrams are not to scale.

Table 3.7: Properties of Rohacell HF 71.

Material	E_1[MPa]	E_2[MPa]	ν_{12}	G_{12}[GPa]	G_{13}[GPa]	G_{23}[GPa]	$\rho\ [kg/m^3]$
Rohacell HF 71	92	92	0.3	29	29	29	75

3.6   Construction

This stage consisted of laying up the sandwich layers in the planned order on top of a flat aluminium mould, curing the sandwiches and finally, cutting them to the desired shapes. The carbon fibre plies were available to us in form of large ply rolls at the *Structures and Composite Materials Laboratory*, and the foams were delivered to us by Evonik Foams Inc. as a courtesy to our research. The final materials used and their required properties are listed below. Note that in Table 3.8, the Poisson's ratios for the foams and NCT321 were not listed in the data sheet of the products and were therefore selected to be 0.3 as a generic value commonly reported for stiff foams and composites, based on a map adapted from Milton [65].

Table 3.8: Elastic properties of the materials analyzed.

Material	E_1[MPa]	E_2[MPa]	E_3[MPa]	ν_{12}	ν_{13}	ν_{23}	G_{12}[MPa]	G_{13}[MPa]	G_{23}[MPa]
NCT321-UD	128242	8274	-	0.3	-	-	4137	4137	2000
Rohacell Rist 110	180	18	-	0.3	-	-	70	70	70
Rohacell HF 71	92	92	-	0.3	-	-	29	29	29
Picea Abies	10200	1020	1600	0.51	0.38	0.31	754	812	36
Sitka Spruce	11880	927	927	0.467	0.372	0.245	724.68	760.32	35.64

Table 3.9: Physical and geometric properties of the materials used.

Material	Thickness [mm]	ρ [kg/m^3]	Max. Temp. [°C]
Newport 321	0.16	1500	-
Rohacell Rist 110	1	110	180
Rohacell HF 71	4, 8, 10	75 ± 15	130

To work in the composites lab, all students are required to pass a Workplace Hazardous Materials Information System (WHMIS) test first. They are also required to follow the safety rules of the labs and have safety gloves and goggles on at all time, especially when handling uncured pre-preg carbon fibres. In addition to goggles and safety gloves, however, it is required to have face respirator and protective clothing on while performing dry or wet cutting on carbon fibres.

3.6.1 Cleaning the Mould

The mould used for the top plate and the braces was essentially a rectangular aluminium plate of $90 \times 70 \times 1$ $[cm^3]$ dimensions. The mould surface was pre-sanded by the students working in the composites lab, but to ensure carbon fibres do not stick to the mould, the surface of the mould had to be cleaned with Zyvax mould cleaner, sealer and release agent in order, according to their manuals. The mould was then used once in curing the top plate, and once in curing the bracing sandwiches. Since the mould could accommodate all the bracing sandwiches, they were all cured together.

3.6.2 Sandwich Layups

Both Rohacell Rist and Rohacell HF were stated to have low but satisfactory levels of resin uptake, which ensures sufficient adhesion between the foam and the face layers, in this case NCT321 [66] [67]. This means that as long as the core and the NCT321 layers are cured together under the right amount of pressure, there will be no need for additional adhesives to create a bond between the core and the NCT321 plies.

The clean mould was placed horizontally on a stable surface. The NCT321 and the foam layers were then manually laid on top of one another on top of the clean mould in the designed arrangements. It was important that the sandwiches were laid far from the edges of the mould. Considering how much material was required for the braces overall, the bracing materials (uncured pre-preg NCT321 sheets and Rohacell HF 71 foams) were initially cut to large rectangles and placed in the desired arrangements. It was important to make the rectangles bigger than we needed them to be, to leave enough margin for errors in cutting, material that would fade away by the blade, and material that we needed to hold on to when cutting the braces. The top plate materials, however, were cut out in a rough silhouette of the guitar shape, slightly larger than needed. The sandwiches were to be cut to the correct size later on, after being completely cured.

3.6.3 Vacuum Bagging

Vacuum bagging is the most common technique used for laminating sandwich-structured composites. The process of vacuum bagging is as follows:

1) Place the mould horizontally on a stable surface and apply one row of sealant tape along the edge of the mould, leaving 1-2 cm free margins outside the tape bounds. You should

end up with a rectangular tape running around the face of the mould. Do not remove the top plastic cover of the tape yet.

2) Make sure the sandwich layups are placed inside the tape bounds, and that there is some uncovered mould surface within the tape bounds, where the valve can be placed later on. Note that once cured, the side of the sandwich that is in contact with the mould will have a flatter surface.

3) Cut a piece of perforated release film and place it flat on top of all the parts. Make sure the release film is large enough to cover all the parts, but not too large to overlap with the sealant tape.

4) Cut a piece of breather and place it on top of the release film. Stay within the tape bounds.

5) Cut a large rectangular piece of vacuum bag. The piece must be a few inches larger that the taped area.

6) Locate the lower part of the valve between the breather and the vacuum bag, not overlapping the part. Place the vacuum bag on top of all the layers (including the sealant tape). Remove the top plastic cover of the tape little by little, and start attaching the vacuum bag from one corner. It is best if the vacuum bag is loose and not perfectly flat, so the bag can deform without altering or damaging the sandwich, when the vacuum pump is turned on. In order to avoid air passages forming between the tape and the vacuum bag, insert a small ball of sealant tape in the gap between the bag and the tape, before removing the last parts of the tape (Fig. 3.18).

7) Make a small cut in the vacuum bag, where the hole of the valve lies. Insert the upper part of the valve inside the lower part (through the vacuum bag) and lock the valve.
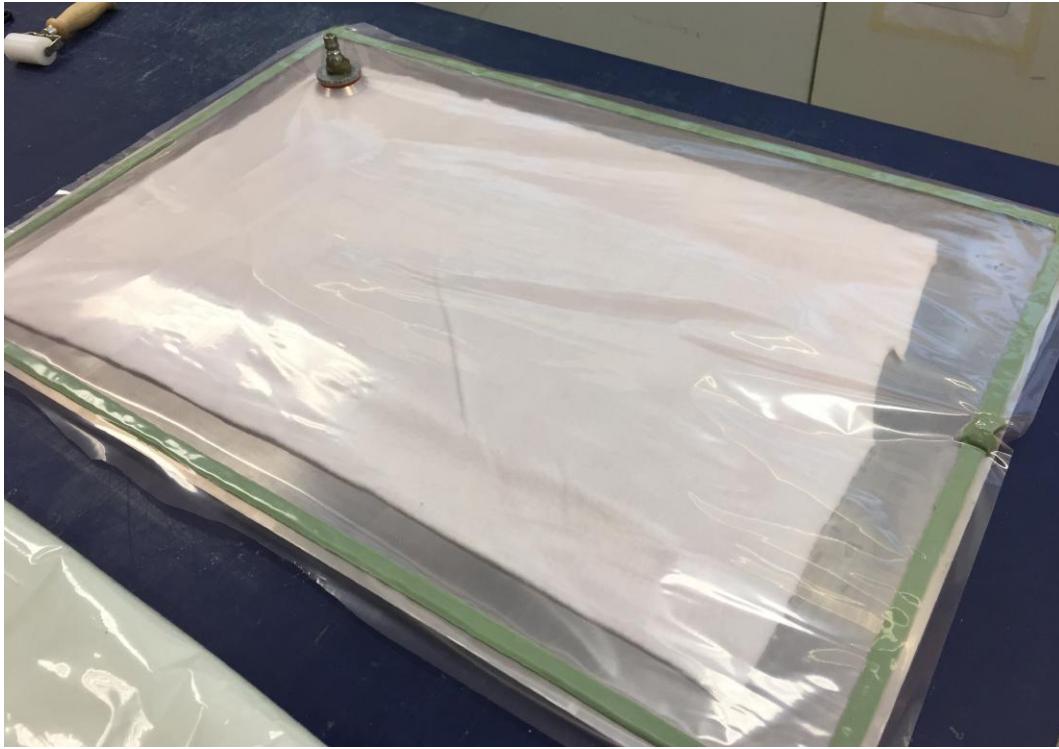
Figure 3.18: The vacuum bag before attaching the vacuum pump. Notice the inserted ball of sealant tape on the right, and the valve at the top corner.

8) Attach a vacuum pump to the valve and observe as the air is removed from the bag. Watch out for air gaps that make noises during vacuuming, and seal the gaps by applying pressure on the sealant tape.

9) Remove the air pump and attach a pressure gauge to the valve. Observe the pressure gauge for about half a minute. If the pressure value is stable, the bag has been sealed properly. If not, look for possible air passages and block them by applying further pressure on the tape or adding more tape to the sides. Apply vacuum and measure the pressure again. Repeat until the bag is fully sealed.

3.6.4 The Curing Process

Once the vacuum bag was ready, it was placed in a 24 cu ft Blue M oven. The vacuum pump was attached to the valve before closing the oven doors, in order to remove all air and maintain the pressure desired for the mould throughout the cure cycle.

Newport 321 can be cured in temperatures between 121-149°C, depending on the time spent at the peak cure temperature. Since Rohacell Rist and Rohacell HF could be handled

in temperatures of up to 180°C and 130°C, respectively, there was no need to worry about their mechanical properties altering, as long as the sandwiches were cured at temperatures below 130°C. To be on the safe side, however, it was decided to cure the sandwiches at the minimum recommended cure temperature of 121°C.

While there was one specific cure cycle mentioned in the specifications sheet of NCT321, there are other cure cycles that could be used to cure the NCT321 plies to the same degree-of-cure. The cure cycle chosen was as shown in Fig. 3.19.

Figure 3.19: Ramp up from 25°C to 121°C in 1 hour (i.e. rate of 1.6°C/min), hold for 6 hours, and cool down to 25°C in one hour.
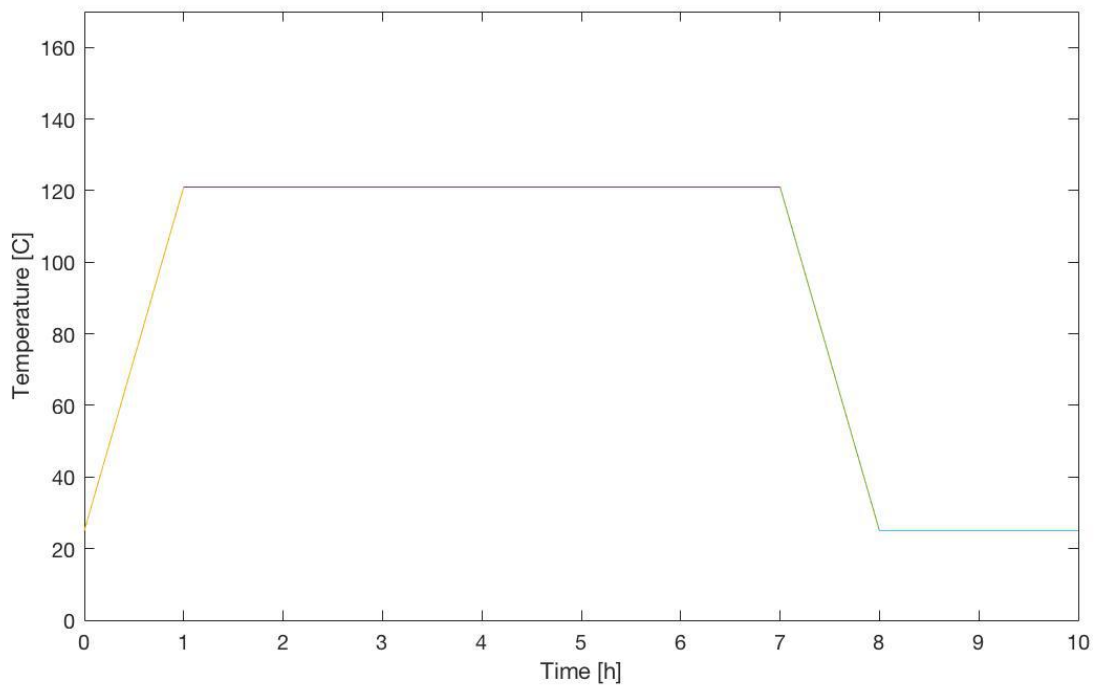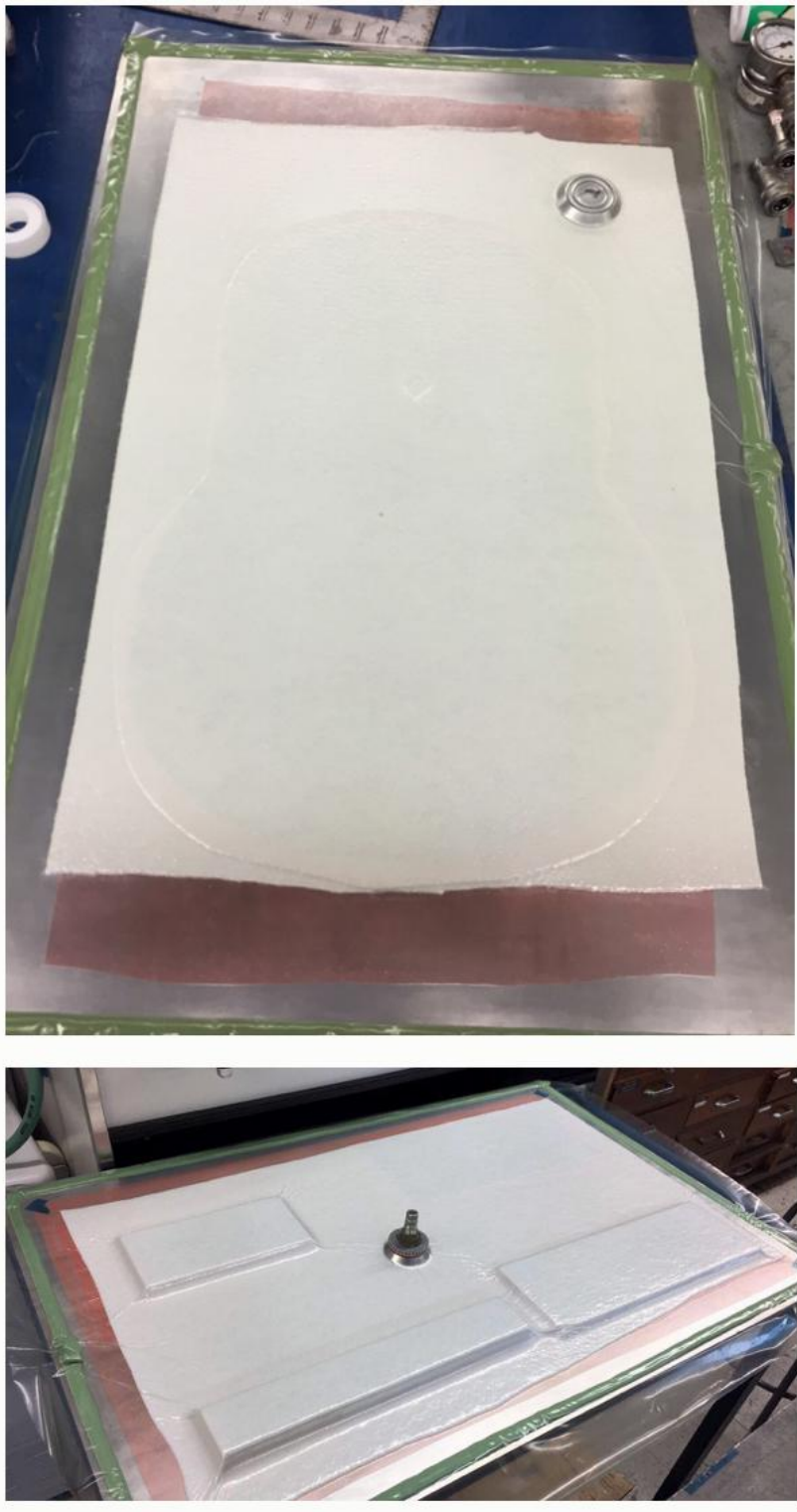
Figure 3.20: Vacuum bags after the cure. Top: The vacuum bag containing the top plate. Bottom: The vacuum bag containing the bracing sandwiches. Notice that the silhouette of the top plate is slightly larger than the desired shape, and that it is yet to be trimmed.

3.6.5 The Cutting Process

The braces were cut out of the cured rectangular sandwich plates using a RUBI DX-350 wet bridge saw. The saw was quite large and was not an optimal tool for cutting to such small dimensions with little room for error, but since carbon dust is extremely invasive, it was important that the parts were either cut in a specific dry-cutting booth, or are done through wet cutting. Given the circumstances, it was decided the best tool available for straight cutting was the wet bridge saw.

Figure 3.21: The wet bridge saw RUBI DX-350 [68].

The cured top plate on the other hand, could not be cut using the saw, and was manually trimmed using a Dremel, i.e a rotary cutting and trimming tool. The Dremel was also used to trim the edges of some of the braces to the exact angles and curves required. Note that the Dremel, and in fact any other dry-cutting tool, had to be used in a designated space with adequate ventilation power, to suck the carbon dust away. For that purpose, the designated booth for dry-cutting carbon fibres was used, located in the Faculty of Engineering of McGill university.

It is worth noting that we were aware of the fact that manually cutting the silhouette of the soundboard was not an optimal technique. A better choice would have been to use a water jet cutter to cut the top plate to the exact desired shape. It was decided not to pursue this choice, however, simply due to lack of time and because it was not available to us on campus.

Figure 3.22: The booth designated for dry cutting carbon fibres and composites.

Figure 3.23: Dry cutting the edge of the braces using the Dremel.

Figure 3.24: The manufactured composite top plate and the braces.

3.7   Experimental Modal Analysis - Composite Top Plate

In order to verify the eigen-frequencies and the mode-shapes obtained from the composite simulations, it was required that an experimental modal analysis was performed on the brace-less composite top plate, before attaching the braces. The procedure performed was as explained in Sec. 3.1.1. One thing to take into account this time, however, was that the side of the composite top plate that had been in contact with the mould now had a flatter surface compared to the other side. The side that had been covered with the release film was now more irregular, yet also very reflective, which could cause the laser to reflect faulty phase data. We managed to notice this early on by monitoring the coherence of the response signals, so we made sure the laser pointed to the flatter surface of the top plate. Note that ignoring poor coherence could have resulted in faulty mode-shapes.
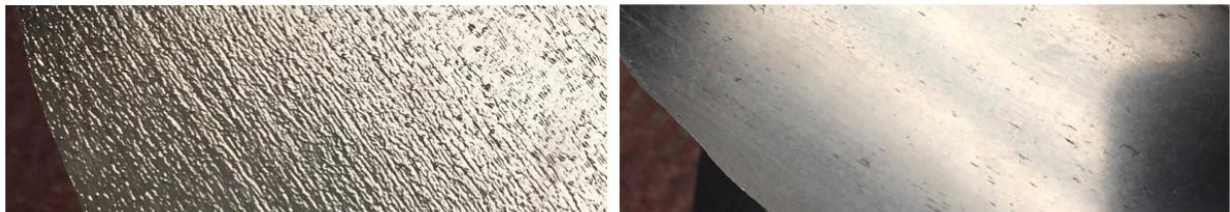
Figure 3.25: Close up shot of the two surfaces of the top plate. Left: The side facing the vacuum bag. Right: The side in contact with the aluminium mould.

After considering the first 10 mode-shapes of the soundboard (determined by the simulation), the measurement points were selected with the intention to capture at least the first 10 mode-shapes and to not fall on their nodes[7].

3.8 Attaching the Braces

The rougher side of the top plate was chosen as the front of the soundboard, simply for aesthetic reasons, and the braces were attached to the composite top plate using Magnobond 56, an epoxy glue by Magnolia Plastics. The glue comes in a part A and part B that must be mixed according to the MSDS of the glue. The cure time of the glue was stated to be overnight in room temperature, though leaving the glue for longer would have resulted in even stronger bonds.

Since the glue was not introduced in the numerical model of the soundboard, we did our best to apply as little glue as possible, so that the final mass of the soundboard is not far from that of the numerical model. We then left a number of heavy objects on the braces, for better adhesion. The excess glue pushed out from under the braces was removed, and the assembly was left to sit over night.
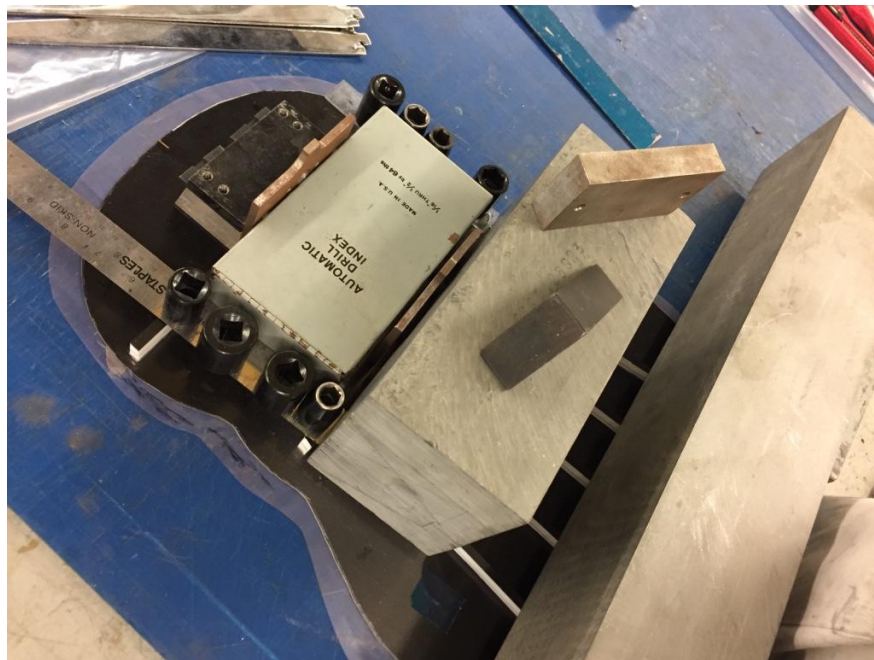
Figure 3.26: The braces were left under a number of heavy object over night for better adhesion of the glue.

---

[7]Nodal points are the points that have zero displacement values in the mode-shapes.

3.9 Experimental Modal Analysis - Composite Sound-board

Since the rougher side of the top plate was chosen as the front, the measurements had to be taken from the back side of the soundboard, where the braces were attached. The measurement points therefore had to be selected such that no point would fall on a brace or on the nodal regions of the first 10 modes. Taking these into account, the experiments were done as explained in Sec. 3.1.1. The natural frequencies and the mode-shapes of the composite soundboard were then compared with those obtained from the composite simulation results and will be discussed in the next chapter.

Figure 3.27: Left: Measurement points marked on the composite soundboard. Right: The measurement setup for the composite soundboard.

Figure 3.4: The experimental setup.

Chapter 4

Results and Discussion

4.1 The Wooden Soundboard

In this chapter, you will find the simulation and the experimental results obtained throughout the design process. Keep in mind that in describing the results, *mode-frequencies* is the general term used for the resonance frequencies obtained numerically and experimentally, *natural frequencies* refer to the mode-frequencies obtained experimentally, and *eigen-frequencies* are the mode-frequencies determined by the numerical model.

4.1.1 Effect of Environmental Factors

The first set of experiments on the wooden soundboard were performed in a span of 3 hours, during which the natural frequencies were seen to shift by a 0-2 [Hz], depending on frequency. To have an idea about the extent of these variations over time, the experiments were repeated on two more days, the first two being 9 days apart, and the last two, 1 day.

Observing the Frequency Response Functions (FRFs) on different days revealed that natural frequencies of a wooden structure like the soundboard can vary to large extents over time. As shown in Fig. 4.1, the number and the frequency of the different peaks observed in the FRFs are different on the first and the third day. This was believed to be due to the variations of humidity and temperature over time.

Considering the frequency shifts of the modes over time, it was decided that the average of the results obtained on the last two days were regarded as our reference. On the 2nd and the 3rd day of the experiments, the relative humidity and temperature values of the laboratory were recorded, but their significance and their exact effect on the natural frequencies remain

unknown, as it is not only the humidity and the temperature values at the time of the experiments that affect the natural frequencies, but more their variations over time.
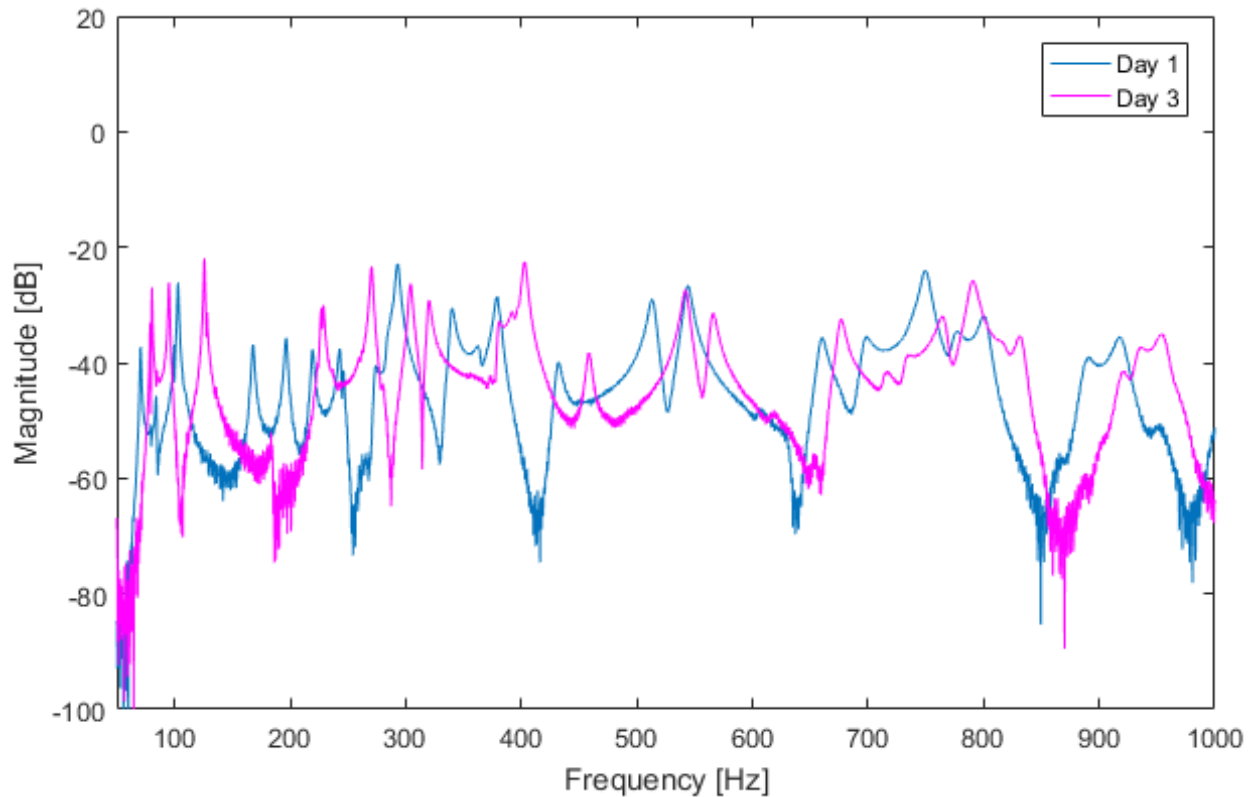
Figure 4.1: FRFs representing the modal behaviour of the soundboard on the first and the last day. The impact point and the measurement point corresponding to these FRFs were kept constant between the two day.

To quantify and better understand the extent of the changes in the FRFs over the days, the natural frequencies and damping ratios of the first 10 modes were compared on the different days. Figure 4.2 presents the frequency and damping values associated with the modes observed on the 1st and the 3rd day. These parameters were extracted using the *curve fit* and *modal parameters* features available in ME'scope, where the *mode indicating* method was chosen as *CMIF*, and frequency and damping values were obtained using *global polynomial* fitting [1]. Notice the extent of variations in the natural frequencies and the damping ratios on these two days.

To make sure the shift in the natural frequencies was not due to the the differences in the experimental set up on different days, the test was repeated with longer and shorter

---

[1]For more information on the different curve fitting options available in ME'scope, refer to [69].

threads and also with different attachment points on each day. It was observed that changing
the length of the threads or the attachment point of the threads did not affect the natural
frequencies of the structure.

	Select Mode	Frequency (Hz)	Damping (Hz)	Damping (%)
1	No	31.6	0.342	1.08
2	No	70.7	0.485	0.687
3	No	84.3	0.489	0.58
4	No	103	0.801	0.781
5	No	104	0.69	0.664
6	No	130	0.0597	0.0458
7	No	167	1.25	0.747
8	No	196	1.23	0.629
9	No	220	1.33	0.607
10	No	243	0.952	0.392

(a)

	Select Mode	Frequency (Hz)	Damping (Hz)	Damping (%)
1	No	49.3	0.207	0.42
2	No	80.1	0.538	0.671
3	No	95.2	0.54	0.567
4	No	126	0.598	0.475
5	No	184	1.18	0.638
6	No	228	1.03	0.451
7	No	237	1.21	0.511
8	No	271	1.25	0.46
9	No	304	1.68	0.551
10	No	320	1.8	0.562

(b)

Figure 4.2: Experimental natural frequencies and modal damping values of the wooden
soundboard under free BCs. (a) Day 1. (b) Day 3.

4.1.2 Simulation vs. Experimental Results

The natural frequencies of the wooden soundboard obtained experimentally were compared
with the eigen-frequencies determined through simulation on a mode-by-mode basis, ac-
cording to the explanation provided in Sec. 3.3.2, i.e. the eigen-frequencies were plotted in
a strictly sequential manner, whereas the experimental natural frequencies were not. The
comparison (Fig. 4.3) showed a general agreement between the experimental and simulated
mode-frequencies in the range of 1-1000 [Hz], with the the exception of four modes missing
in the experimental results, and the central modes (13 to 18) appearing at lower frequencies
than expected. This is thought to be mostly caused by humidity and temperature varia-
tions. Table 4.1 lists the absolute differences associated with every two mode-frequencies
being compared from the simulated and the experimental sets.
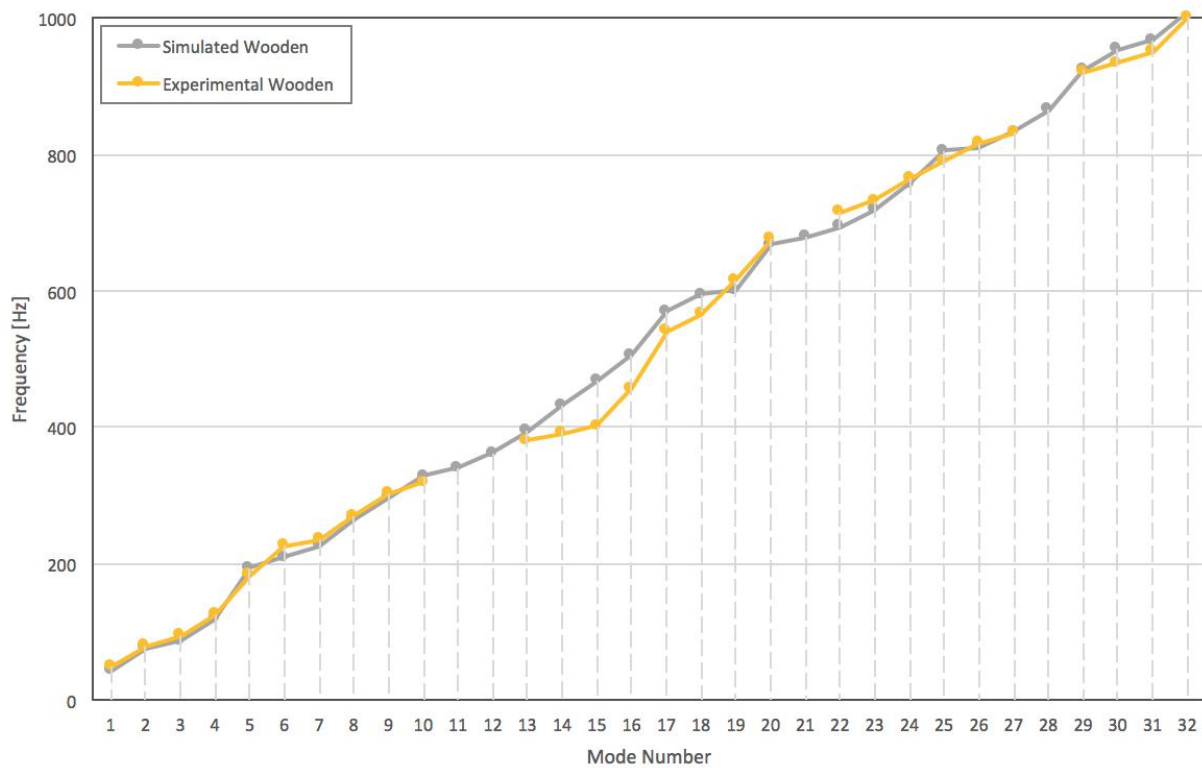
Figure 4.3: Experimental and simulated mode-frequencies of the wooden soundboard under free BCs, plotted vs. mode number.

Next, the first 10 mode-shapes obtained numerically and experimentally were compared. As shown in Fig. 4.4, the two sets were found to be in agreement. Note that the visual accuracy of the experimental mode-shapes is a function of the number of measurement points defined on the structure, and how the points are connected to one another using *surface triangles* (Fig. 3.5). A finer representation of the mode-shapes would have required a higher number of measurement points. In this case, the measurement points defined for the wooden soundboard seemed sufficient for representing the first 10 mode-shapes.
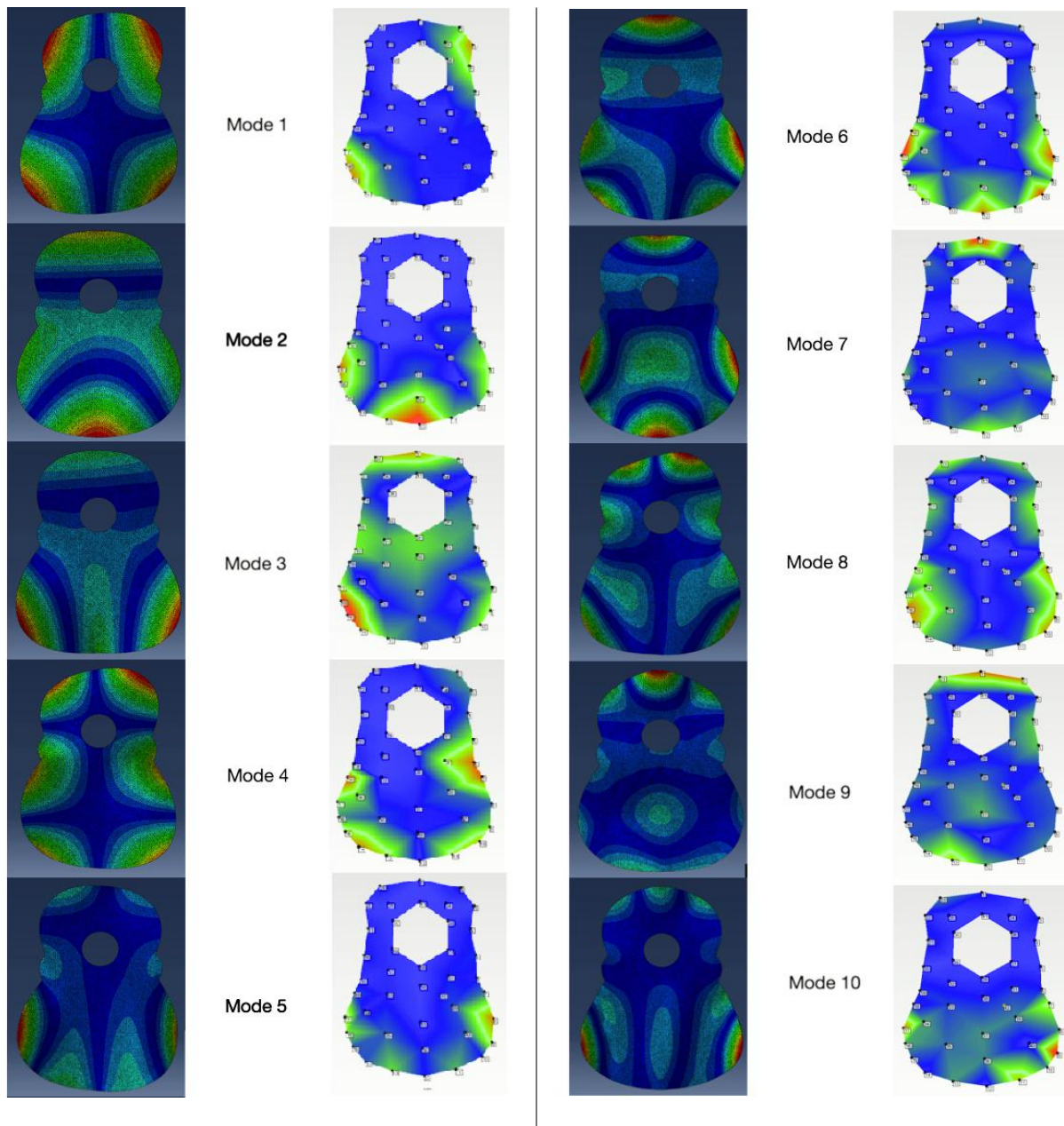
Figure 4.4: Experimental and simulated mode-shapes of the wooden soundboard under free BCs.

It is perhaps worth mentioning that the mode-shapes obtained for the wooden sound-board were found to be quite comparable with the mode-shapes previously reported by Elajabarrieta [51] [52], with the exception of modes 4 and 5 appearing in the opposite order (Fig. 4.5). This could be due to the woods of the two soundboards being different, the bracing patterns being different, and the fact that silhouette of the soundboard studied

in this thesis is slightly larger than its final intended shape. Furthermore, note that the wooden soundboard studied in this thesis has 5 modes in the 0-200 [Hz] range, whereas the soundboard studied by Elajabarrieta has 7.
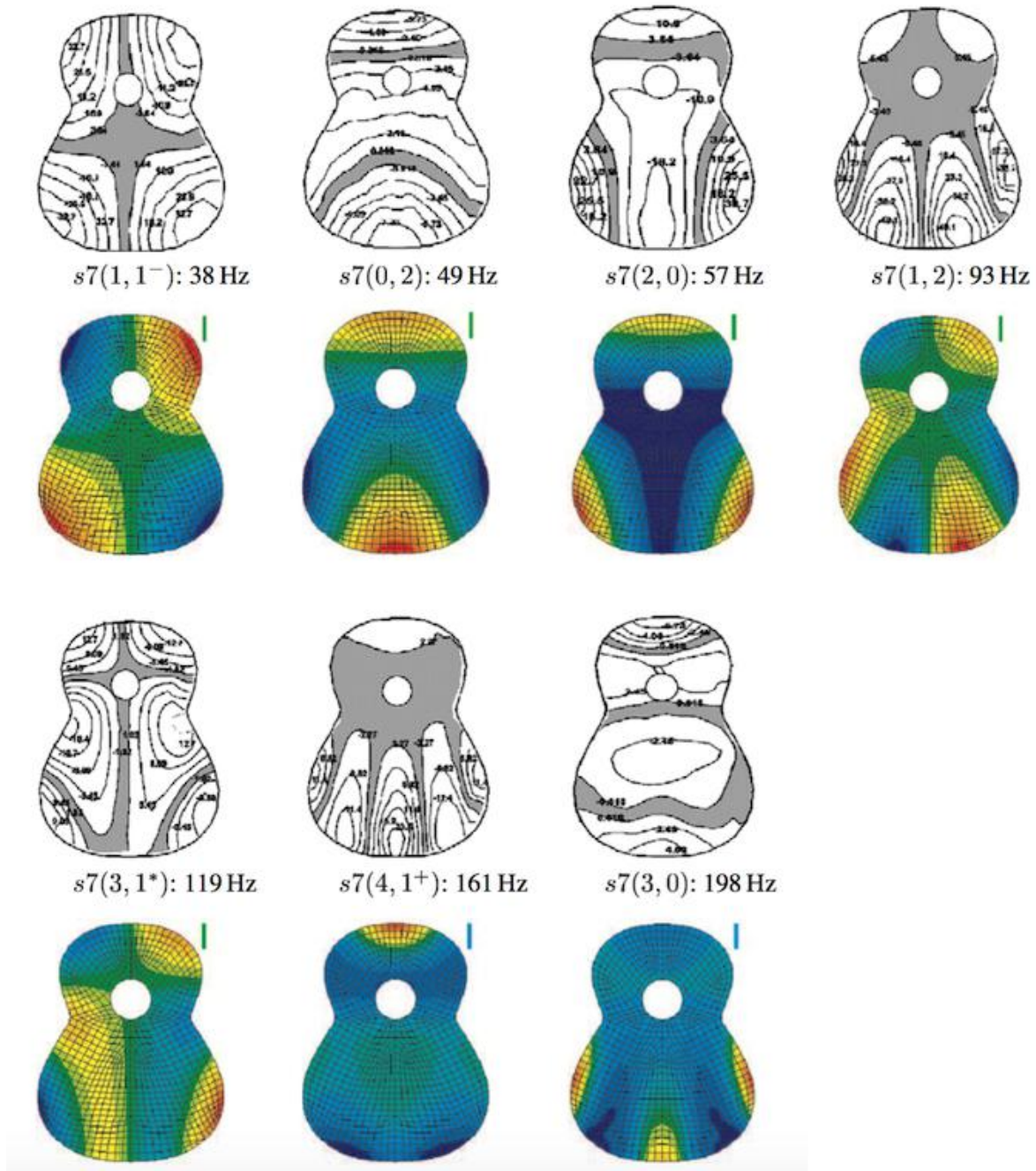
Figure 4.5: The first 7 Experimental and simulated mode-shapes reported in [52].

4.2 The Top Plate: Simulation Results from Wood to Composite

As part of the design process, the eigen-frequencies and the mode-shapes of the composite top plate designed needed to be monitored and compared with those of the simulated brace-less wooden top plate. In doing so, the effect of varying the thickness, ρ, E, G and ν of the core were monitored on the natural frequencies of the composite top plate, while the available pre-preg composites were considered for use in the top plate sandwich.

FUD180

As explained in Sec. 3.4.3, a top plate made from FUD180 face layers and a 1.275 [mm] core foam was first considered as a potential top plate layup. For the top plate to have a mass equal to that of the wooden top plate, the foam (with a 1.275 [mm] thickness) would have needed to have a ρ of about 25 $[kg/m^3]$. However, among the lightest rigid foams offered by Rohacell, the lowest density was 32 $[kg/m^3]$. This foam (Rohacell HF 31) was inserted in the numerical model of the top plate as the core foam. The eigen-frequencies of this sandwich layup are presented in Fig. 4.6.

Figure 4.6: Visualizing the effect of varying the core thickness on eigen-frequencies of the top plate, when the face layers are FUD180 and the core foam HF 31.

The eigen-frequencies of the mentioned composite top plate were found to be much lower than those of the wooden top plate, which is why the modal behaviour of a sandwich top plate with a higher core thickness (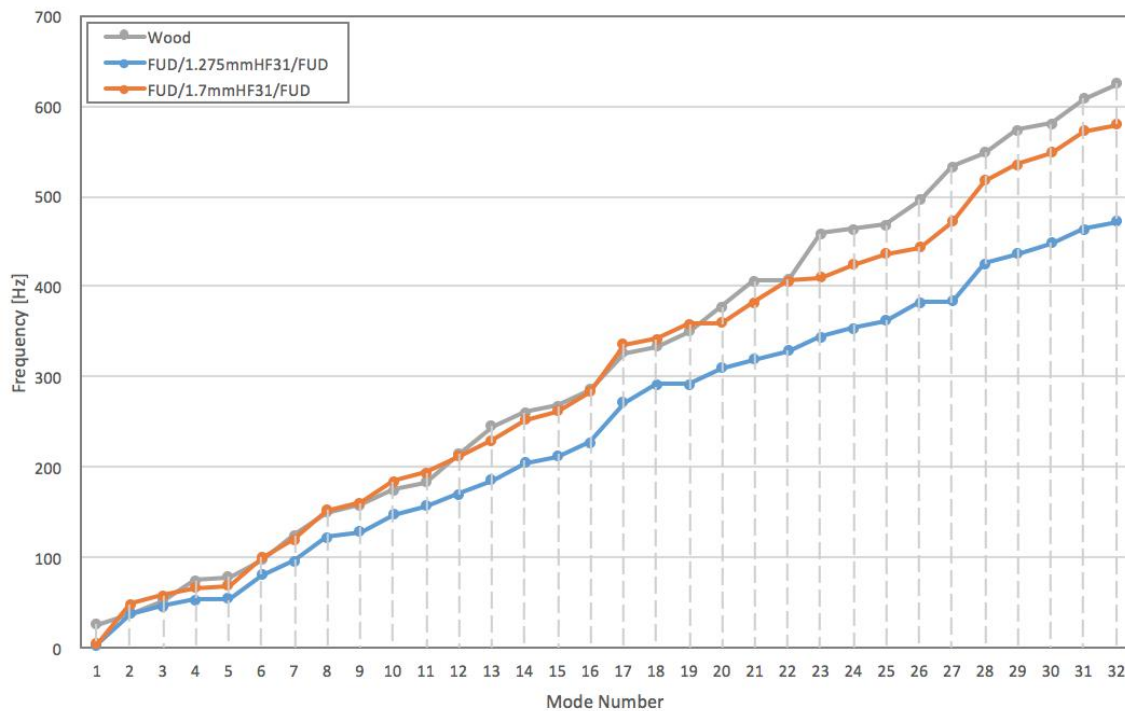1.7 [mm]) was also simulated and presented. Notice that an in crease in the thickness (and hence the stiffness) of the top plate results in an increase in the slope of the Frequency vs. Mode Number curve. This means that as a result of increasing the thickness of the core foam, higher eigen-frequencies are increased by a larger amount, than the lower eigen-frequencies are.

Considering Ono's comments about the effect of G on higher eigen-frequencies [24], the eigen-frequencies of the FUD/1.7mmHF31/FUD top plate being low in the higher modes was believed to be due to the G of HF 31 being low. It was therefore of our interest to better understand the effect of varying the different properties of the core foam on the eigen-frequencies. To do so, the E, G, ν and the ρ of the HF 31 were varied to hypothetical values, while the thickness of the core was kept constant, i.e., 1.7 [mm]. The original material properties of the foams discussed in this chapter are presented below. Figure 4.7 then presents the effect of varying certain elastic properties of HF 31 to the hypothetical values specified.

Table 4.1: Properties of the Foams Considered.

| Material	E_1[MPa]	E_2[MPa]	ν_{12}	G_{12}[GPa]	G_{13}[GPa]	G_{23}[GPa]	ρ $[kg/m^3]$
Rohacell HF 31	36	36	0.3	13	13	13	32
Rohacell HF 51	70	70	0.3	19	19	19	52
Rohacell HF 71	92	92	0.3	29	29	29	75
Rohacell Rist 51	75	75	0.3	24	24	24	52
Rohacell Rist 110	180	180	0.3	70	70	70	110
Rohacell IG 110	160	160	0.3	50	50	50	110
Rohacell Hero 150	124	124	0.3	75	75	75	150
Rohacell Hero 200	180	180	0.3	109	109	109	205
Rohacell SL 200	306	306	0.3	123	123	123	205
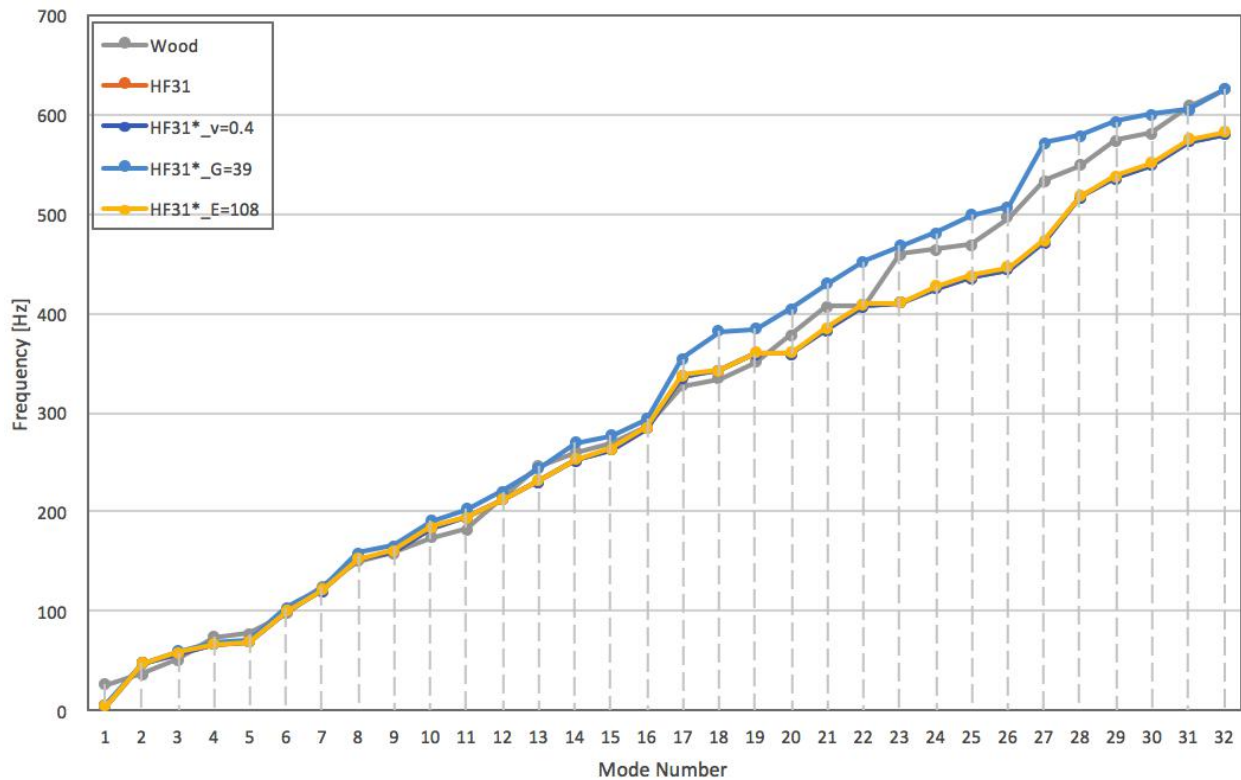
Figure 4.7: Visualizing the effect of varying the elastic properties of the top plate core foam, when the core foam is a 1.7 [mm] HF 31, and the face layers are FUD180. Note that the foams marked with a star have the same elastic properties as those of HF 31, with the exception that the property specified for each foam is changed to the hypothetical value specified. The orange and the dark blue curves fall under the yellow curve.

As can be seen in Fig, 4.7, increasing the E of the core foam has had almost no effect on the eigen-frequencies of the top plate, which was expected for a sandwich structure with high-stiffness face layers and low-stiffness core. This is while increasing the G has caused the eigen-frequencies to increase, especially in the higher frequency region, which confirms Ono's statement on the matter. Changing the ν of the foam from 0.34 to 0.4 has also had no significant effect on the eigen-frequencies of the top plate[2].

As expected, it can be seen in Fig. 4.8 that when the elastic properties are kept constant, increasing the density of HF 31 core foam from 32 $[kg/m^3]$ to a hypothetical value of 75 $[kg/m^3]$ will result in a decrease in the eigen-frequencies of the top plate. In reality, however, an increase in the density of the foam is accompanied with an increase in the E and the G of the foam. The eigen-frequencies of the top plate were therefore monitored when HF 71 was used as the core foam instead, which is an available foam with a density of 75 $[kg/m^3]$.

---

[2]The value of ν for non-rubbery materials is usually in the range between 0.3 and 0.5 [65].
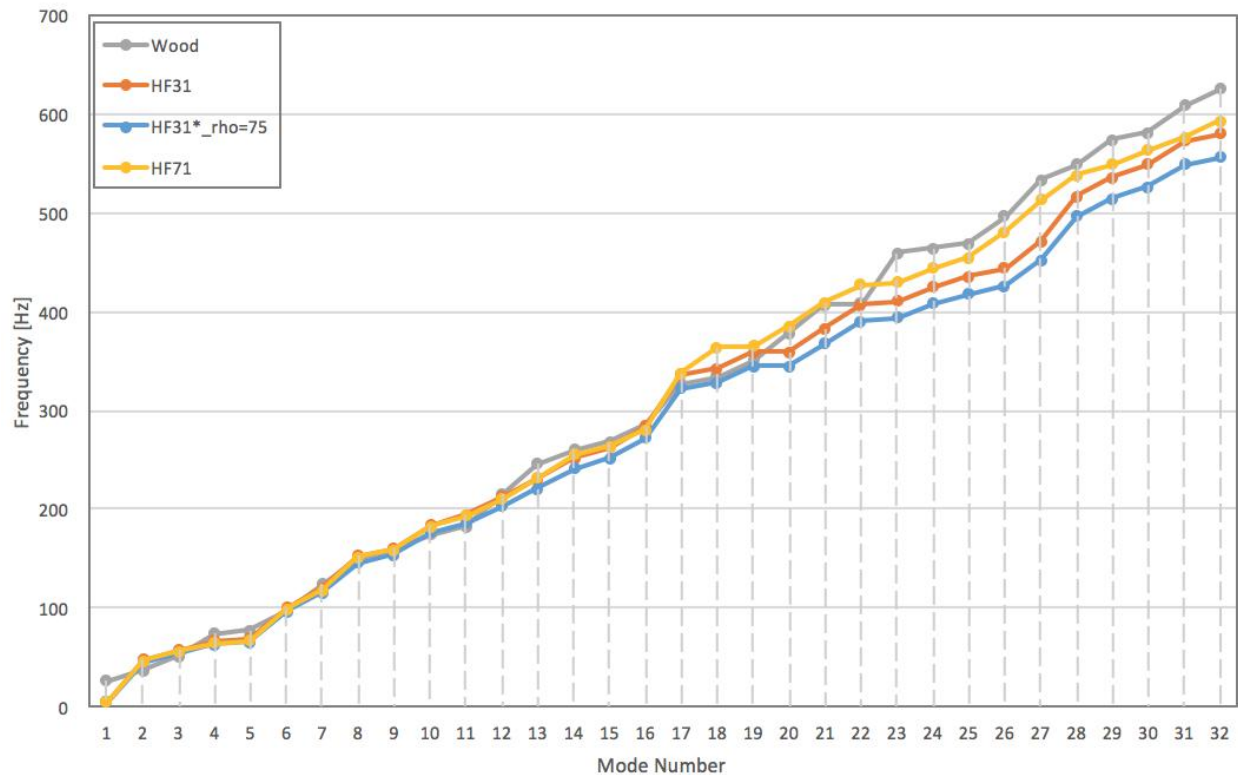
Figure 4.8: Visualizing the effect of varying the density of the top plate core foam (HF 31) to a hypothetical value of 75 $[kg/m^3]$, compared to when the core foam is replaced with HF 71 of the same thickness. HF 71 has slightly higher G and E values, compared to those of HF 31.

Notice that the eigen-frequencies of the top plate with a HF 71 core foam are higher than those of the hypothetical HF 31*_rho75, which is believed to be due to the higher G of HF 71 (92 [MPa]), compared to that of HF 31 (13 [MPa]). To better match the eigen-frequencies of the wooden top plate, a core foam with a slightly larger G was desired. Rohacell Rist 71 was therefore chosen as a candidate. The eigen-frequencies of the top plate with a 1.7 [mm] Rohacell Rist 71 core foam are shown in Fig. 4.9, compared to those of the HF 71 top plate. The masses of these top plates are also listed in Table 4.2.

Table 4.2: Masses of the FUD top plates considered.

Material	Mass [g]
Wooden Top Plate	114.0
FUD/1.275 mm HF31/FUD	115.0
FUD/1.7 mm HF31/FUD	117.0
FUD/1.7 mm Rist71/FUD	127.0

One thing that must be pointed out is that considering the mentioned FUD top plate layups, it was noticed that while the top plate with 1.7 [mm] Rist 71 core foam generally matched the wooden top plate in eigen-frequencies, regardless of the core thickness or density, the first eigen-frequency of these FUD top plates were found to be quite low compared to that of the wooden top plate (25.96 [Hz]). This was one of the reasons why we were interested in looking into the use of NCT321 as a potential composite layer in the top plate as well.
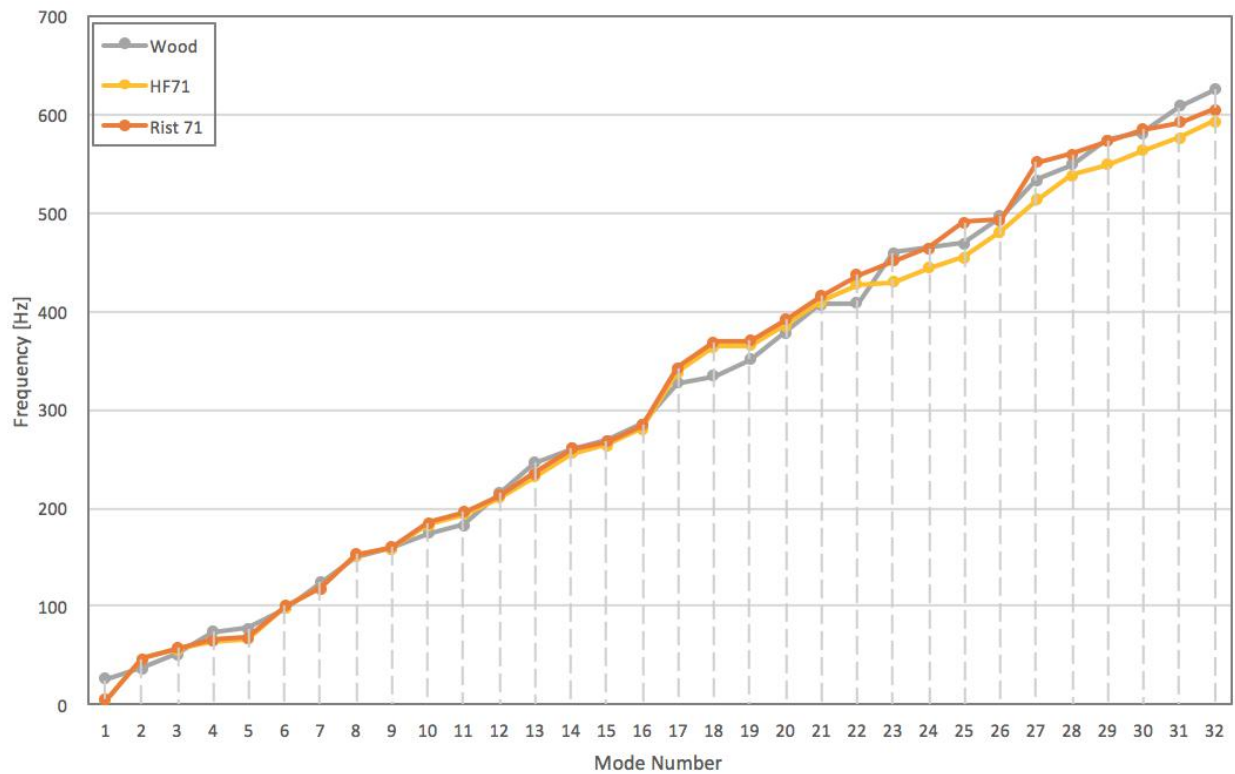

Figure 4.9: The effect of replacing HF 71 with Rist 71 of the same thickness, but with a slightly larger G.

NCT321

Similar to the above analysis, the possibility of making the top plate from NCT321 face layers was also analyzed. NCT321 pre-preg plies have higher stiffness and density values compared to those of FUD180, but they come in smaller thicknesses. The optimum core thickness and core properties would therefore be different from those obtained for the FUD180 top plate sandwich.

As explained in Sec. 3.4.3, the core thickness considered for use in the NCT top plate sandwich was 0.84 [mm]. For this sandwich to have a mass equal to that of the wooden top plate, the foam had to have a density of 400 $[kg/m^3]$. There were, however, a number of problems associated with the stated thickness and density:

1. Among the rigid foams offered by Rohacell, the heaviest foams have a density of 205 $[kg/m^3]$.

2. The foams available are not commercially available in thicknesses of less than 1 [mm].

3. The heaviest rigid foams offered by Rohacell (e.g. SL 200 and Hero 200) do not come in thicknesses of less than 6 [mm].

Despite the issues stated above, the effect of varying the ρ to hypothetical values were still monitored on the eigen-frequencies of the top plate. Considering the fact that the desired density for a 0.84 [mm] core is 400 $[kg/m^3]$, the desired density for the core foam with a thickness of 1 [mm] was determined to be 335 $[kg/m^3]$, which again, was higher than the foams available to us. The eigen-frequencies of the top plates made from the heaviest 1 [mm] foam cores available were therefore determined. Notice that the eigen-frequencies of these top plates are all generally higher than those of the wooden top plate.
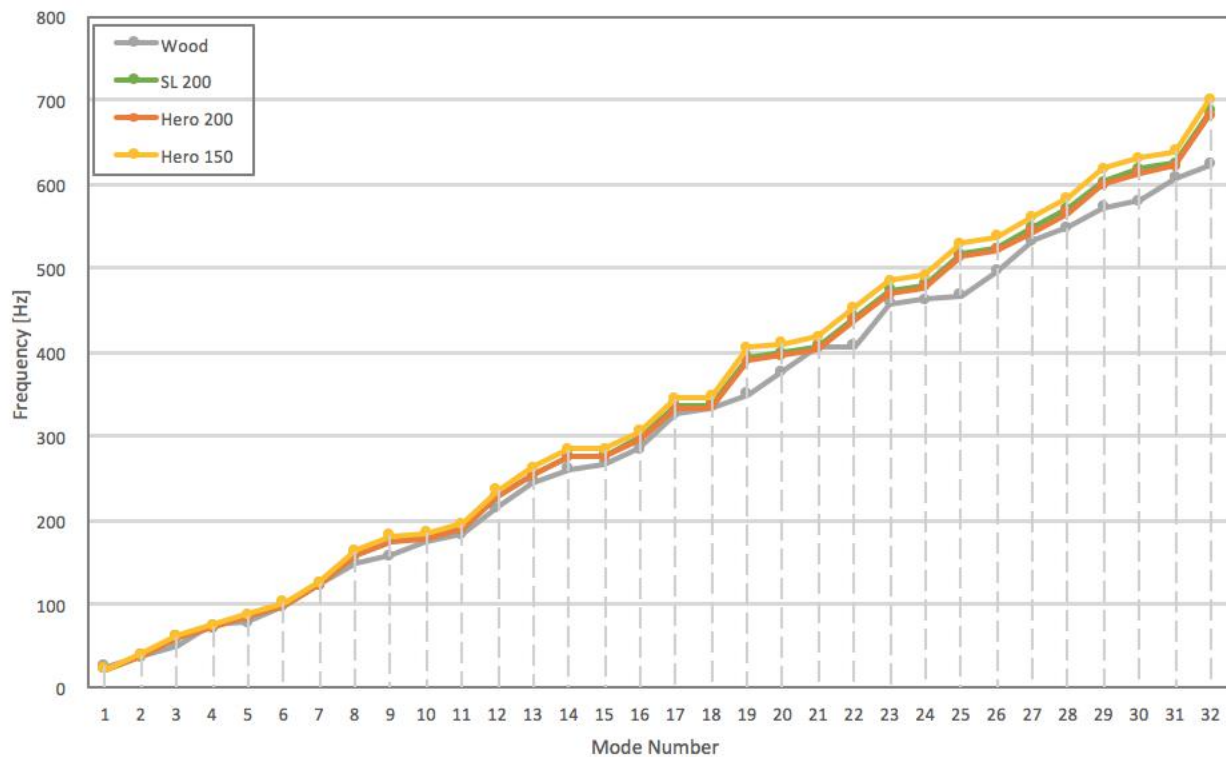
Figure 4.10: The eigen-frequencies of NCT top plates with foams of high density. In reality, these foams are not commercially available in thicknesses of below 6 [mm].

As explained earlier, none of the foams mentioned in Fig. 4.10 are available in 1 [mm] thicknesses. For that reason, the foams that had relatively high density and were available in 1 [mm] thicknesses were considered next. The eigen-frequencies of the top plates containing these foams are presented below.
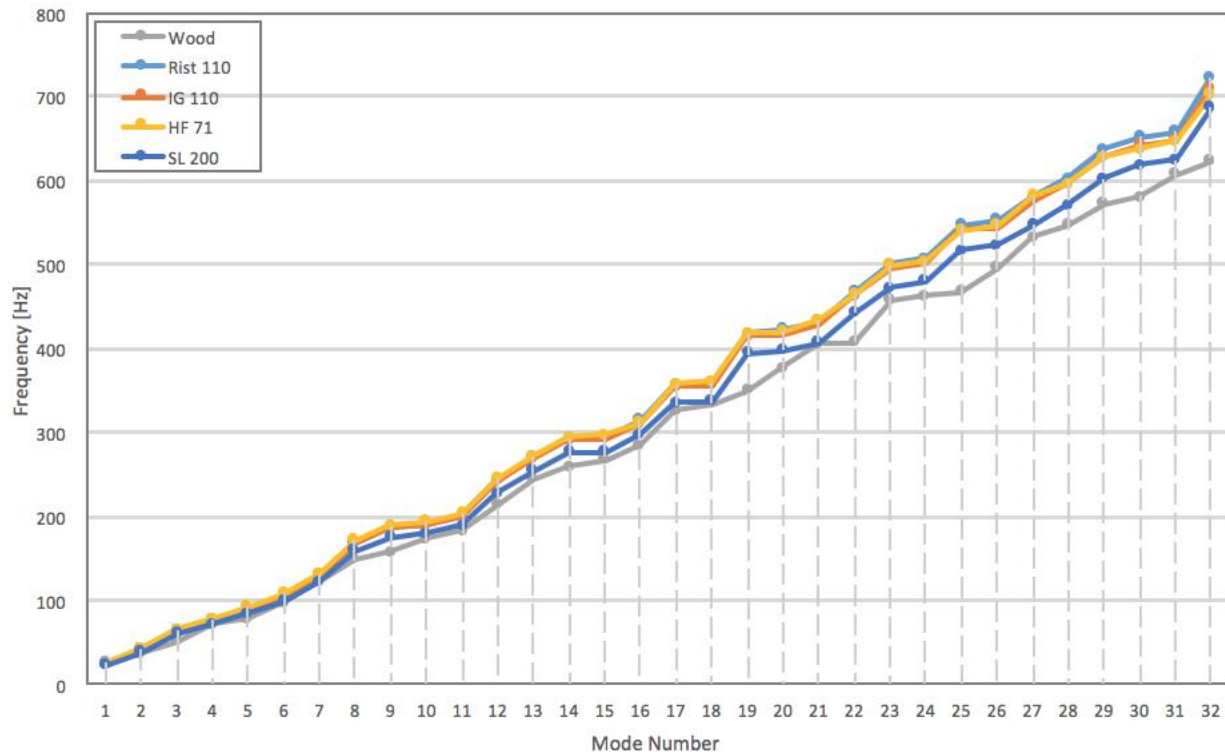
Figure 4.11: Eigen-frequencies of NCT top plates with foams of high density available in 1 [mm] thickness. Notice that in case of 1 [mm] core thickness top plates, the thickness of the core is so small that a density change from 71 $[kg/m^3]$ to 110 $[kg/m^3]$ does not result in a significant change in mass. Also note that SL 200 is only provided for reference, and that it is not available in thicknesses of < 6 [mm].

Following the comparison between the eigen-frequencies, the first 10 mode-shapes of the suggested FUD top plate and an NCT top plate were compared with those of the wooden top plate in Fig. 4.12. It is important to realize that neither the eigen-frequencies nor the mode-shapes of the composite top plate being similar to those of the wooden top plate guaranteed that the eigen-frequencies and the mode-shapes of the braced soundboard were going to match after adding the braces.

By now, we had therefore come to realize that the choice had to be made between using FUD180 with a 1.7 [mm] Rist 71 core foam, or using NCT321 with a 1 [mm] core foam of relatively high density, i.e. 71-110 $[kg/m^3]$. At this point, it seemed to us that FUD/1.7mmRist71/FUD would be a better candidate, but upon adding the braces in the simulations (in Sec. 4.3), it became clear to us that the braced soundboards including the stated FUD top plate would have significantly lower eigen-frequencies compared to those of the wooden soundboard.

Figure 4.12: The simulated mode-shapes for the wooden and composite top plates under free BCs. Left: wood. Middle: NCT/1mmRist110/NCT. Right: FUD/1.7mmHF71/FUD
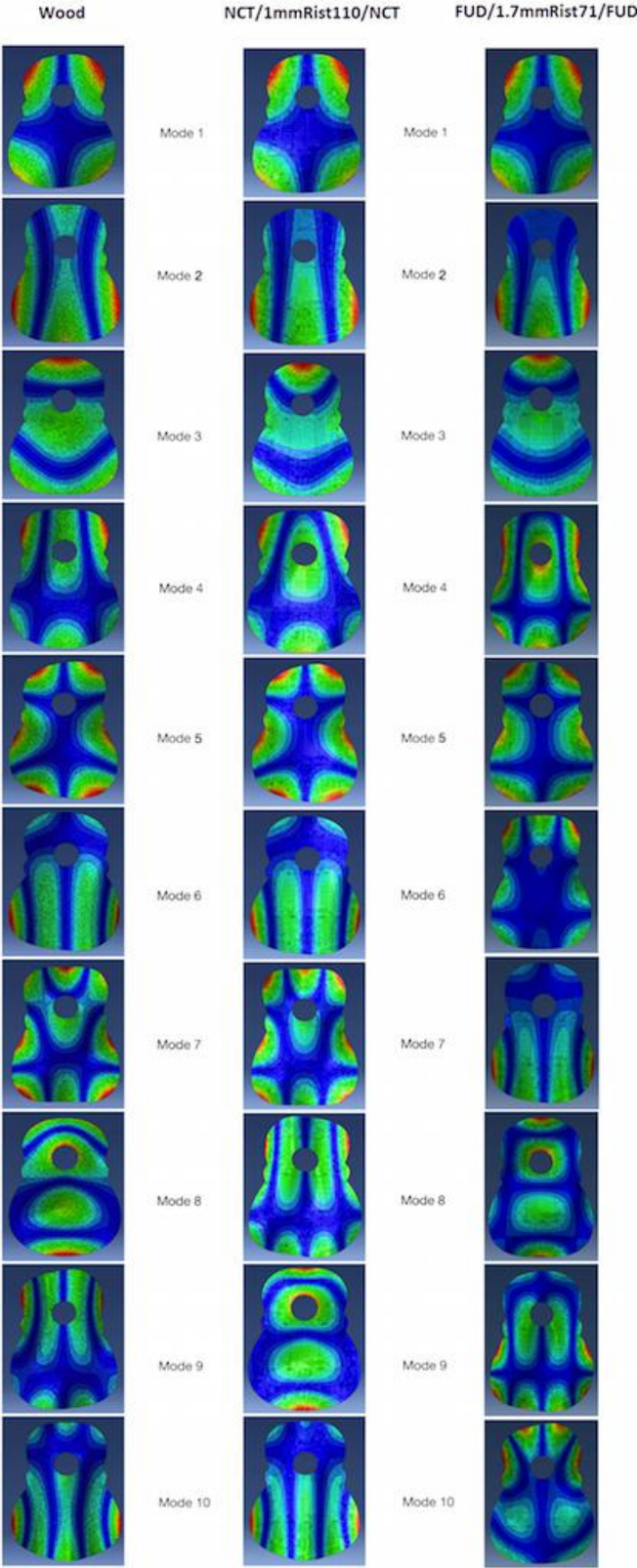
4.3 Addition of the Braces: Simulation Results

With the proposed top plates, the material properties and the thickness of the layers used in the bracing sandwiches (Fig. 3.15) were varied in the available ranges. Upon adding braces to the NCT top plates, the foams listed in Table 4.2 were considered and inserted into the numerical model of the braces with thicknesses of 2-10 [mm]. The eigen-frequencies of the potential soundboards with different bracing layups were compared under free and hinged Boundary Conditions (BCs). The ultimate goal here was to come up with a set of bracing sandwiches that would result in the hinged composite soundboard to have similar eigen-frequencies to those of the hinged wooden soundboard.

Among the bracing layups considered, two sets of layups, referred to as *C1* and *CZ*, were found to give the hinged composite soundboard eigen-frequencies relatively similar to those of the hinged wooden soundboard. Figure 4.13 presents the eigen-frequency vs. mode-number plots for the wooden soundboard and the two mentioned composite soundboards under free and hinged BCs. Figure 4.14 presents the top plate used in both of these composite soundboards, and Figures 4.15 and 4.16 show the sandwich layups used in *C1* and *CZ*, respectively.
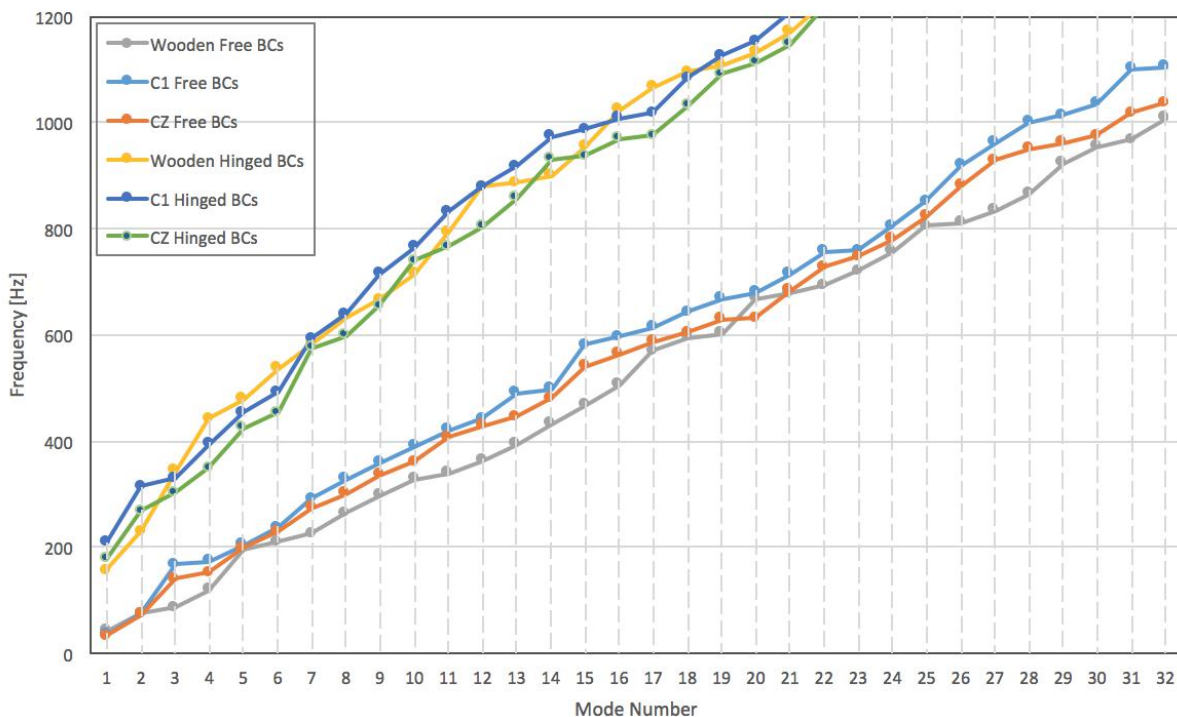

Figure 4.13: Eigen-Frequencies of two potential NCT soundboards and the wooden soundboard under free and hinged BCs, plotted vs. mode number.
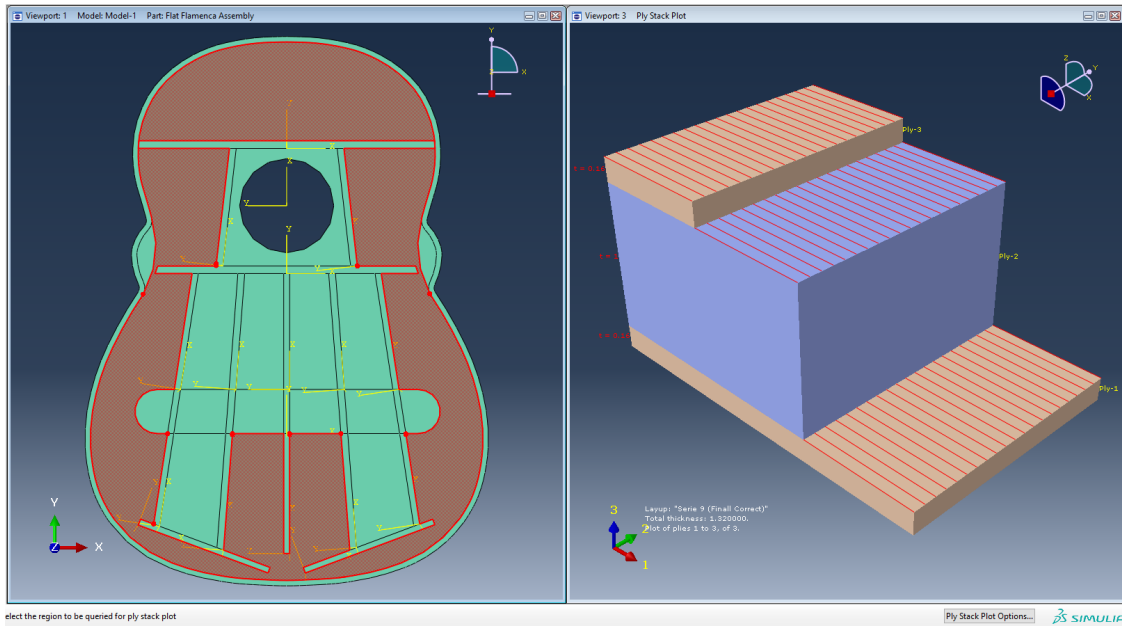
Figure 4.14: The sandwich layup of the NCT top plate used in *C1* and *CZ*. Note that this layup is for the whole top plate, and not only the red area.
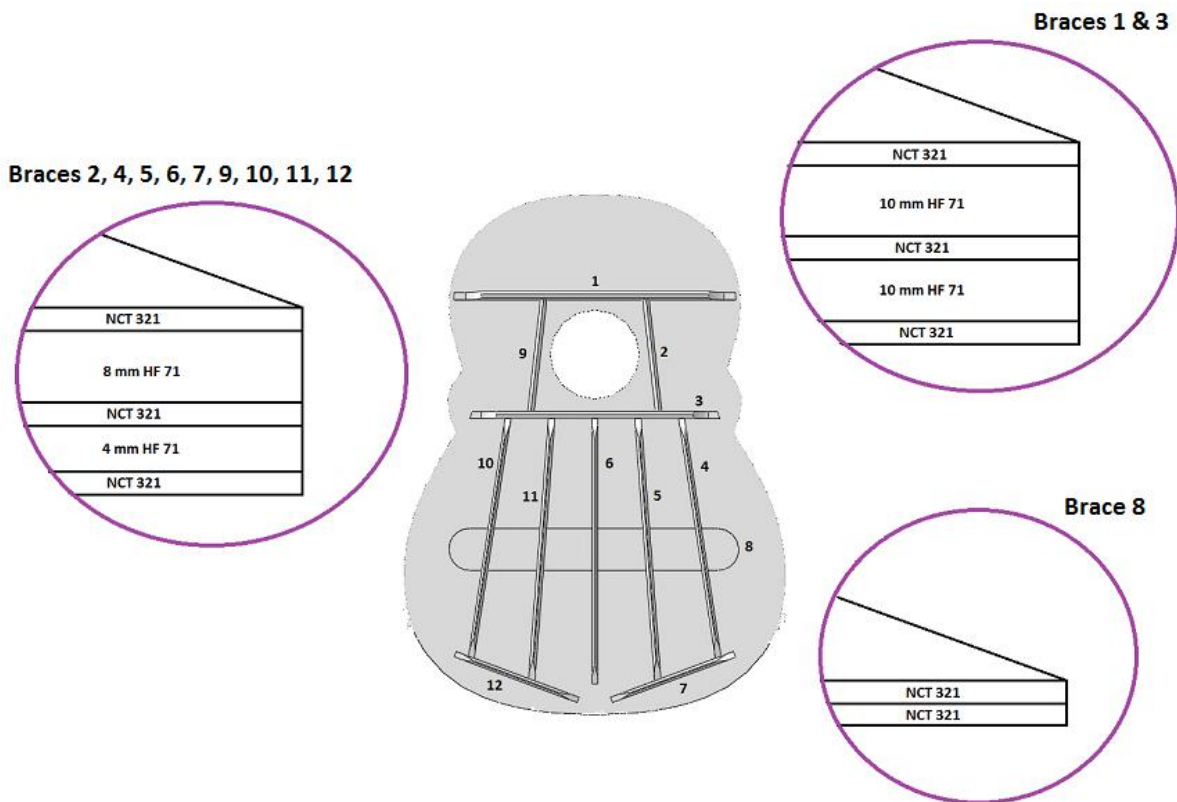

Figure 4.15: Layup diagram of *C1*. Note: diagram is not to scale.
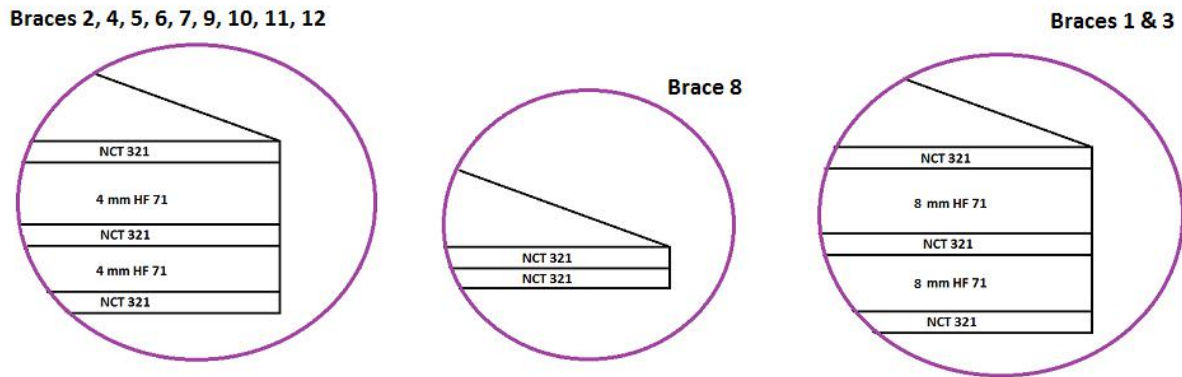
Figure 4.16: Layup diagram of *CZ*. Note: diagram is not to scale.

In Fig. 4.13, notice that even though *CZ* appears to be a better match for the wooden soundboard when compared under free BCs, *C1* is seen to be a better candidate when compared under hinged BCs. Since the soundboard under hinged BCs is a closer representation of the soundboard attached to the instrument body, the similarity between the hinged composite soundboard and the hinged wooden soundboard was used as the main design criteria. Based on these results, the sandwich layup of *C1* was therefore considered a reasonable candidate for use with an NCT top plate for now. Note that in this case, *CZ* was simply presented as a representative of the other possible sandwich layups that were considered.

One might question why some of the braces in *C1* and *CZ* are not symmetric through their thickness, and whether a symmetric layup would have resulted in a different set of eigen-frequencies. The eigen-frequencies of *C1* with a symmetric through-thickness layup were found to be quite similar to those of *C1*. The only reason a non-symmetric layup was selected was that initially a third potential sandwich layup was also considered for use, in which brace 8 was made from a 3 layer sandwich, and it would have been easier if the thickness of the lower foam of the overlapping braces was equal to the thickness of brace 8. The foams ordered were chosen so that both *C1* and *CZ* layups could be built, if desired. *C1* was later on selected as the layup set of choice.

FUD

Next, different bracing layups were considered for use with the proposed FUD top plate (FUD/1.7mmRist71/FUD). Figure 4.17 presents the eigen-frequencies of the soundboard with two different bracing layups used with the mentioned FUD top plate. Note that the braces used in *FZ1* were those of *C1* introduced above, and the braces used in *F22* are presented in Fig. 4.18.
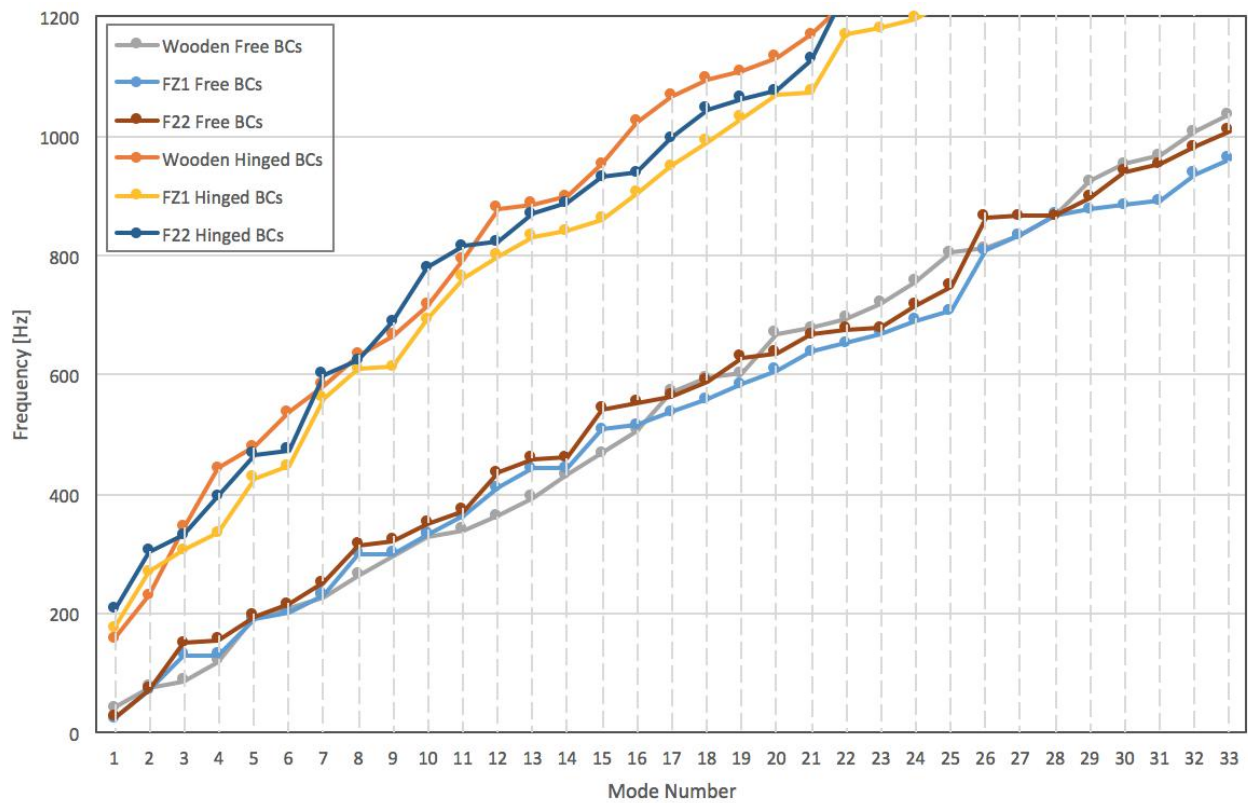
Figure 4.17: Eigen-frequencies of *FZ1* and *F22* compared to those of the wooden soundboard.
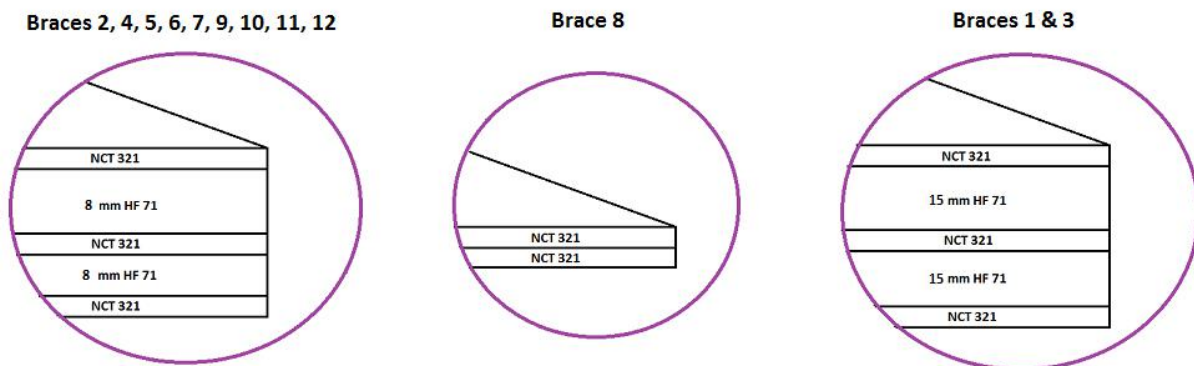
Figure 4.18: Layup diagram of *F22*. Note: diagram is not to scale.

It is curious that even using considerably thick braces, like those in *F22*, has not increased the eigen-frequencies of the soundboard to the desired extent under hinged BCs. To increase the eigen-frequencies of the soundboard containing the FUD top plate, many bracing sandwiches were considered. Among these layups were some containing more than 3 composite plies, some containing significantly thicker foams, and some including only FUD,

only NCT or a combination of the two. Using more than 3 composite layers seemed to make the structure too heavy, causing the eigen-frequencies to decrease even further, and using significantly thicker foams seemed to have little effect on the eigen-frequencies, as can be seen in *F22* of Fig. 4.17, regardless of the type of the composite layers used. By this point, we were convinced that for the soundboard, made from an FUD top plate, to have reasonably high eigen-frequencies under hinged BCs, the thickness of the top plate core foam would need to be increased.

Based on the above observations, it was decided to make the composite soundboard from an NCT top plate (NCT/1mmRist110/NCT) and *C1* braces. It is worth noting that replacing the Rist 110 core foam of the top plate with HF 71 or IG 110 would not have made a significant difference in the eigen-frequencies, and the only reason Rist 110 was chosen over the other two was that one Rohacell Rist 110 was already available to us in the Structures and Composite Materials Laboratory. The mass of this simulated composite soundboard was determined to be 111 [g], which is lighter than that of the wooden soundboard (151 [g]).

The first 10 mode-shapes of the selected composite soundboard were then compared to those of the wooden one under free and hinged BCs in Figures 4.19 and 4.20, respectively. Notice the difference in the mode-shapes of the wooden and the composite soundboards, their order of appearance, and how the mode-shapes change upon being constrained by the BCs.

Figure 4.19: Simulated mode-shapes of the wooden and the designed composite soundboards under free BCs. Left: wood. Right: composite.
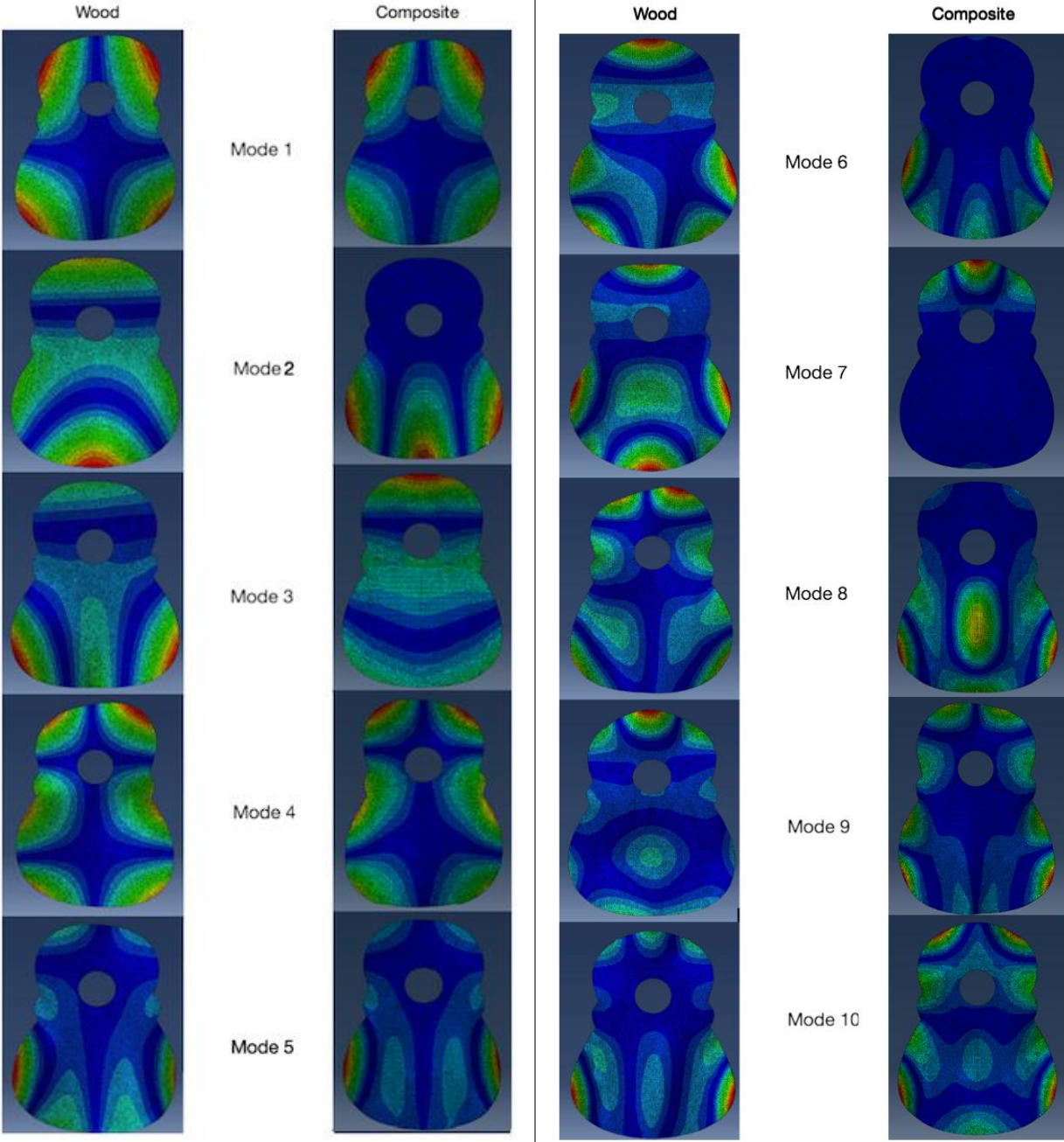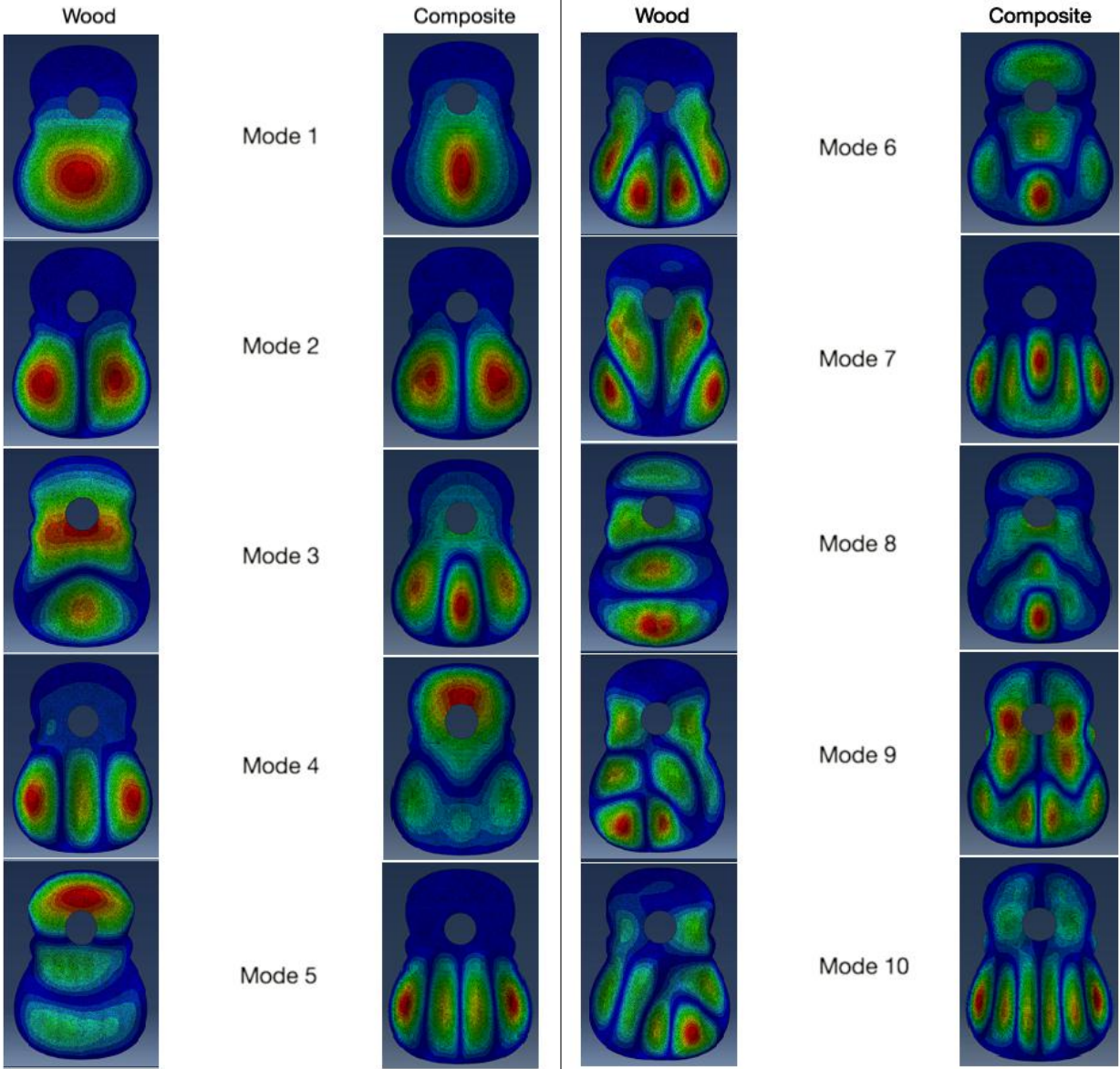
Figure 4.20: Simulated mode-shapes of the wooden and the designed composite soundboards under hinged BCs. Left: wood. Right: composite.

4.4 The Composite Top Plate: Experimental Results

4.4.1 The Masses

According to Abaqus, the mass of the composite top plate was predicted to be 82.5 [g], while that of the constructed top plate was measured to be 85.4 [g]. The thickness of the constructed top plate was also measured to be 1.6 [mm], while it was expected to be 1.32 [mm], which was most probably due to the uncertainty in the thickness of the core foam. The difference observed in mass was therefore believed to be due the thickness of the core foam being larger than assumed, and perhaps slightly due to cutting the outline of the top plate slightly larger than the intended outline, when using the Dremel.

Table 4.3: Mass of the top plates: simulation vs. experimental.

Part	Mass [g]
Wooden Top Plate (Simulation)	114.0
Composite Top Plate (Simulation)	82.5
Composite Top Plate (Constructed)	85.4

Notice that although as a starting point, the density of the foam was chosen such that the top plate would have a mass equal to that of the wooden top plate, from then on, when matching the mode-frequencies was chosen as the main goal, the mass of the wooden top plate was solely considered an upper bound for the mass of the composite top plate.

4.4.2 The Modes

From the 32 eigen-frequencies predicted for the composite top plate with free BCs in the 0-740 [Hz] range, 30 modes appeared as peaks in the FRFs obtained experimentally. As can be seen in Fig. 4.21, the experimental natural frequencies were seen to be similar to the predicted eigen-frequencies in the lower frequency range, and they start to diverge from the predicted values as frequency increases. This divergence could be due to the excess 0.28 [mm] thickness of the core foam. Table 4.5 presents the numerical and the experimental mode-frequencies of the composite top plate, and their absolute differences.
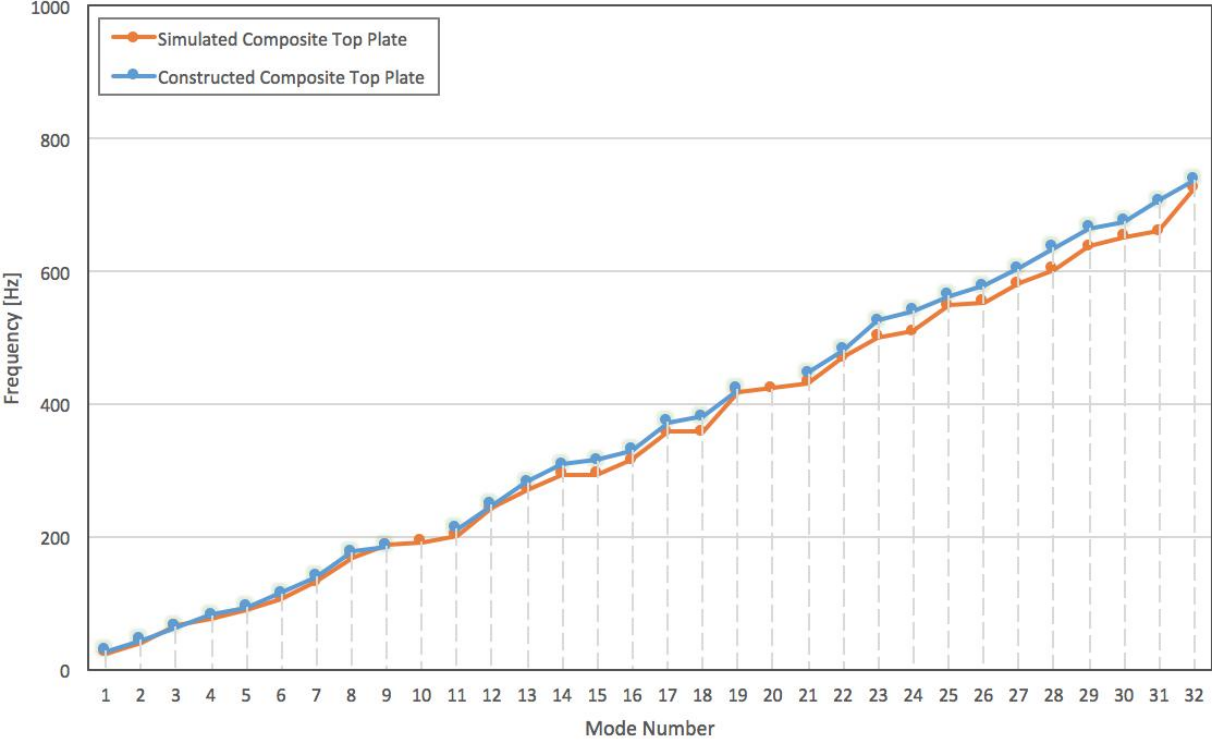
Figure 4.21: Experimental and simulated mode-frequencies of the composite top plate under free BCs, plotted vs. mode number.

Table 4.4: Simulation and experimental mode-frequencies of the composite top plate.

Mode Number	Simulation [Hz]	Experimental [Hz]	Absolute Difference [Hz]
1	23.926	27.6	3.67
2	41.624	44.3	2.68
3	65.158	63.5	1.66
4	77.713	81.5	3.79
5	90.678	93.5	2.82
6	106.31	114	7.70
7	130.96	139	8.04
8	169.75	177	7.25
9	187.71	186	1.71
10	191.39	-	-
11	202.16	212	9.84
12	243.5	248	4.5
13	271.16	283	11.84
14	294.19	308	13.81
15	294.63	316	21.37
16	315.36	330	14.64
17	357.79	373	15.21
18	358.79	381	22.21
19	419.46	422	2.54
20	423.28	-	-
21	432.75	447	14.25
22	468.95	482	13.05
23	501.69	526	24.31
24	508.68	540	31.32
25	548.39	563	14.61
26	553.88	578	24.12
27	581.61	604	22.39
28	603.66	636	32.34
29	638.17	666	27.83
30	652.59	676	23.41
31	659.59	706	46.41
32	724.68	738	13.32

Note that in this case, it was rather easy to know which modes are missing in the experimental results, because the experimental and the numerical curves were seen to follow a similar trend. If the curves followed largely different trends, it would have been difficult to know which modes are missing and which modes must be paired and compared. Furthermore,

the experimental mode-shapes were seen to differ from those predicted by the simulation beyond the 9th mode, or they were seen to appear in a different order, so the pairs being compared do not necessarily correspond to the same mode-shapes. Fig. 4.21 is therefore meant to show the spread of the natural-frequencies of the constructed top plate in the frequency region displayed, compared to its numerical model. The modal density of the constructed top plate in the 0-740 [Hz] range is therefore 30 modes, whereas the numerical model of the composite top plate had predicted a modal density of 32 modes in this range.

Finally, Fig. 4.22 presents the first 10 mode-shapes of the composite soundboard determined by the simulation and obtained experimentally. We can see that the first 9 mode-shapes obtained experimentally match those determine by the simulation. The 10th mode having a different mode-shape could perhaps be expected, since its frequency was also missing from the set of the experimental natural frequencies in Fig. 4.21.
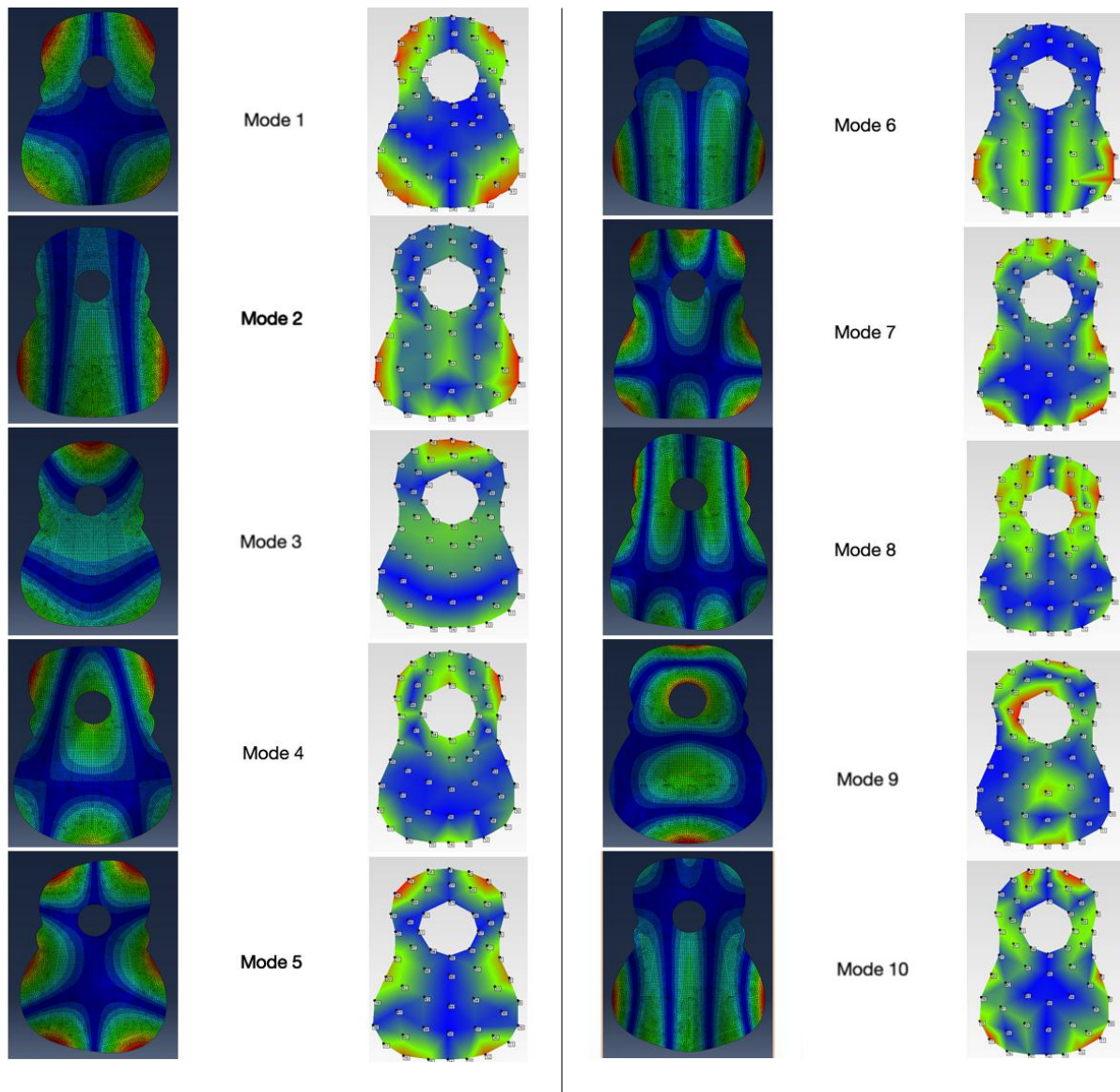
Figure 4.22: Mode-shapes of the composite top plate under free BCs. Left: simulation. Right: experimental.

4.5   The Composite Soundboard: Experimental Results

In attaching the braces, one practical modification had been made in the bracing layup of the soundboard. In the numerical model of the composite soundboard, a thickness of 0.32 [mm] was removed from the base of braces 4, 5, 6, 10 and 11, in the areas where they overlapped brace 8. This was for simplicity in the numerical model, so that the braces could be placed on top of brace 8 without a gap between the braces and the top plate. In reality, however,

the overlapping areas were not removed, as we feared that creating 0.32mm-deep slots at the base of the braces with the wet saw might damage the braces further than intended. Other than that, these slots had to be created at precise angles in the braces, so that no extra parts overlapped brace 8, and creating them at precise angles would have been rather difficult.

In the process of making the braces with the wet saw, a large portion of the bracing sandwiches was thrown away, due to the high uncertainty of the saw. Mistakes in cutting the braces would have therefore required us to cure and cut more braces, or perhaps even order more foams. It was due to the risks associated with making the slots as well as time constraints that it was decided to not create the slots and directly attach the braces on top of brace 8. The gaps between the braces and the top plate were therefore to be filled with glue and pressure applied to the ends of the braces. Unfortunately, the effect of not creating these 0.32mm-deep slots could not be determined before construction, as it was not possible to define a slanted gap between the composite layups on Abaqus. The result was therefore yet to be determined experimentally.

4.5.1 The Masses

The simulated and the measured masses of the wooden and the composite soundboards are presented in Table 4.6. In this table, notice that despite having tried to use as little glue as possible, it was expected that the mass of the constructed soundboard would still be higher than that predicted by Abaqus, even if the top plate and the braces were cut to the exact intended size. This is simply because the glue used was not introduced in the numerical model of the composite soundboard, and neither was its mass.

Table 4.5: The predicted and the measured mass of the wooden soundboard, the braces and the composite soundboard.

Part	Mass [g]
Wooden Soundboard (Simulated)	151.0
Wooden Soundboard (Existing)	152.0
Composite Soundboard (Simulated)	110.0
Composite Soundboard(Constructed)	121.6
Composite Braces (Simulated)	29.4
Composite Braces (Constructed)	32.7

Based on the values reported in Tables 4.5 and 4.6, the total mass of the glue used in the soundboard was calculated as:

$$121.6 - 85.4 - 32.7 = 3.5 \text{ [g]}$$
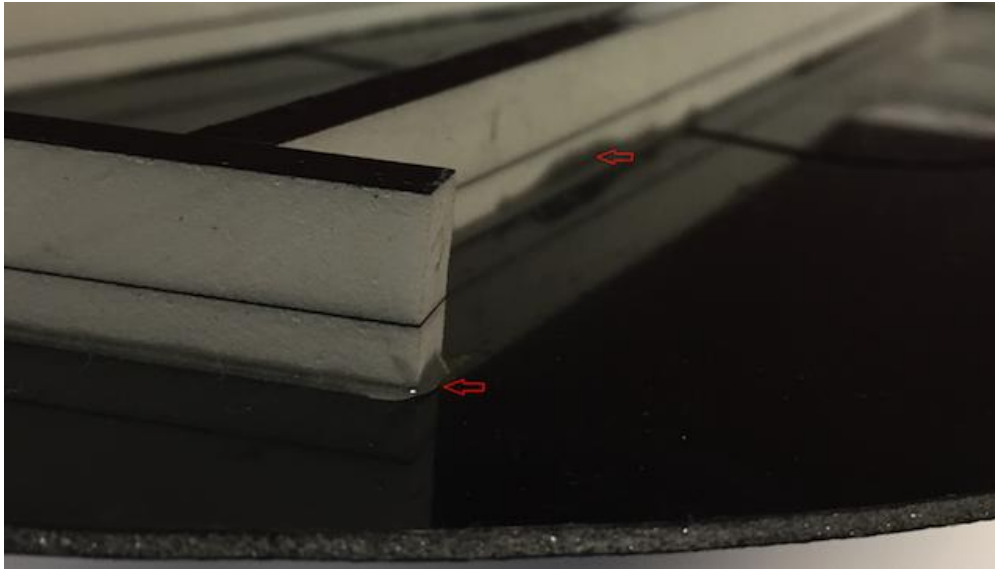
Figure 4.23: The excess glue observed at the points of attachment of the braces and the top plate.

4.5.2   The Modes

From the 32 modes predicted numerically for the composite soundboard (with free BCs) in the range of 1-1000 [Hz], 29 appeared as peaks in the measured FRFs. The frequencies of these modes were seen to differ from the predicted values by 1.5 to 48.63 [Hz] (avg. of 19.3 [Hz]), among which the lower frequencies showed larger differences. The differences observed between the numerical and the experimental mode-frequencies, especially in the low-frequency region, are thought to be due to (1) the thickness of the top plate being larger than assumed. (2) the top plate silhouette being slightly larger than intended. (3) the presence of the glue in the composite soundboard and its effect on the total mass, mechanical properties and the modal behaviour of the soundboard, and (4) the 0.32mm-deep slots not having been created in braces 4, 5, 6, 10 and 11. Table 4.7 presents these numerical and experimental mode-frequencies and their absolute differences.
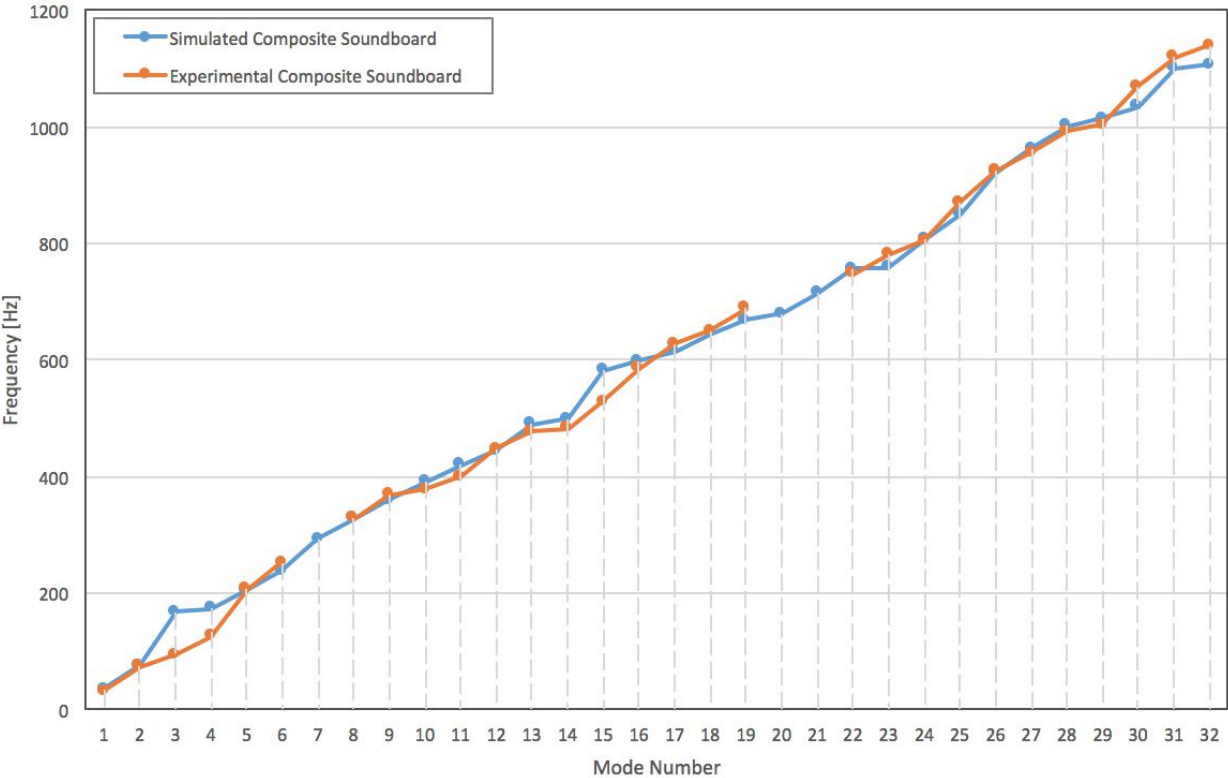
Figure 4.24: Experimental and simulated mode-frequencies of the composite soundboard under free BCs, plotted vs. mode number.

Table 4.6: Simulation and experimental mode-frequencies of the composite composite soundboard.

Mode Number	Simulation [Hz]	Experimental [Hz]	Absolute Difference [Hz]
1	35.352	31.2	4.15
2	76.109	73.1	3.01
3	167.36	94.7	72.66
4	173.63	125	48.63
5	204.5	206	1.5
6	237.56	252	14.44
7	291.77	-	-
8	327.77	327	0.77
9	359.68	368	8.32
10	391	378	13.00
11	420.16	400	20.16
12	442.88	447	4.12
13	490.53	477	13.53
14	498.96	482	16.96
15	581.68	529	52.68
16	597.65	585	12.65
17	615.05	627	11.95
18	644.1	650	5.9
19	668.6	688	19.4
20	680.06	-	-
21	713.84	-	-
22	757.36	747	10.36
23	758.65	780	21.35
24	806.26	804	2.26
25	851.14	871	19.86
26	920.12	924	3.88
27	961.95	956	5.95
28	1000.7	992	8.7
29	1013.8	1003	10.8
30	1034.6	1070	35.4
31	1100.6	1120	19.4
32	1105.5	1140	34.5

The mode-shapes and the modal damping ratios of the first 10 modes of the constructed composite soundboard (with free BCs) are presented in Figures 4.25 and 4.26, respectively. Notice that the first 6 experimental mode-shapes are found to match the predicted ones, and

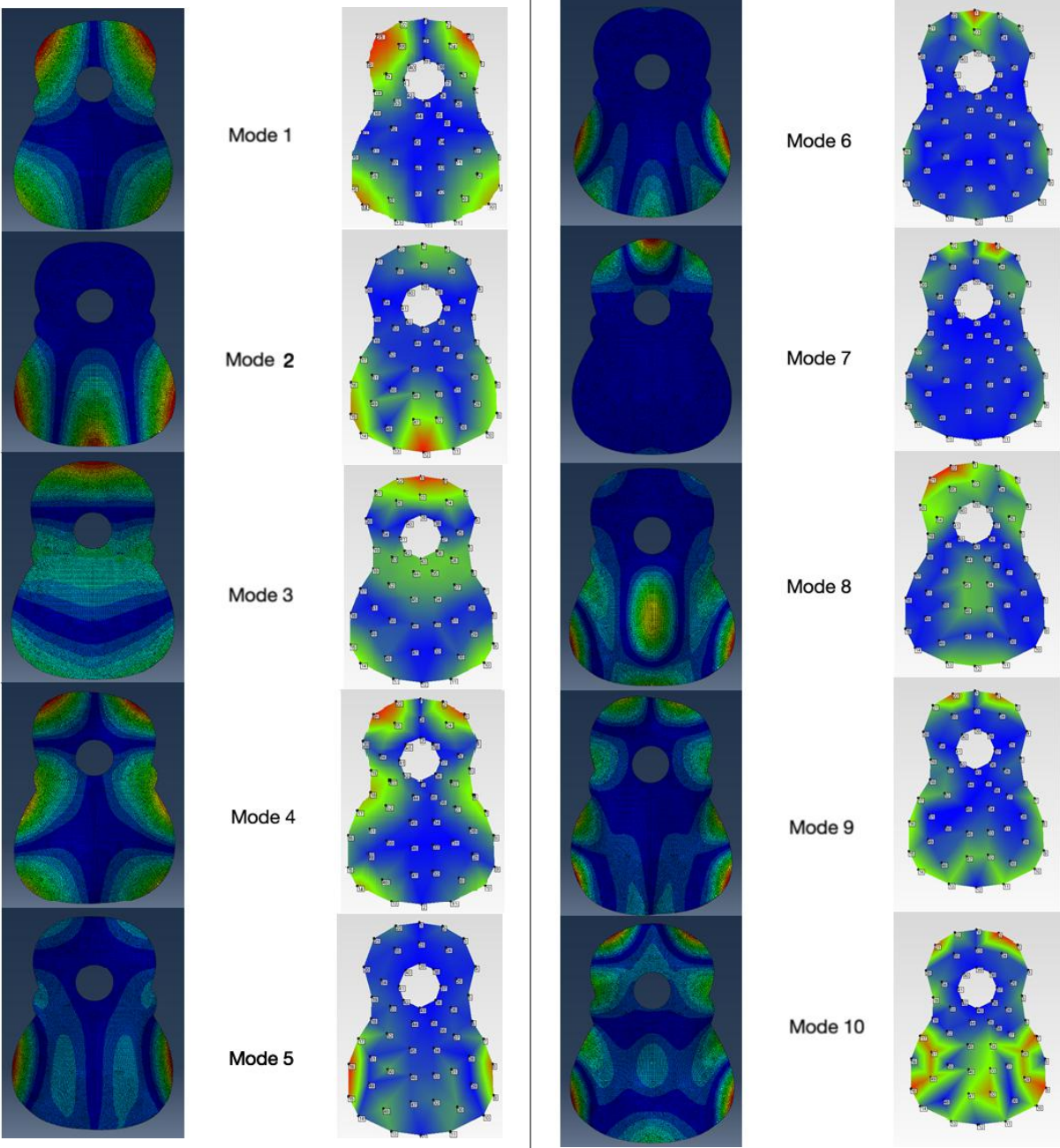modes 7 to 10 are seen to be similar with some local differences in shape.

Figure 4.25: Experimental and simulated mode-shapes of the composite soundboard under free BCs.

	Select Mode	Frequency (Hz)	Damping (Hz)	Damping (%)
1	No	31.7	0.261	0.824
2	No	74	0.449	0.607
3	No	95.6	0.532	0.556
4	No	126	0.617	0.491
5	No	207	1.21	0.585
6	No	252	1.56	0.621
7	No	328	1.63	0.496
8	No	378	2.19	0.579
9	No	402	2.7	0.671
10	No	448	2.35	0.525

Figure 4.26: The experimental natural frequencies and the modal damping values for the first 10 modes of the constructed composite soundboard, obtained from ME'scope.

It must be pointed out that unlike the case seen in Sec. 4.4.2, despite a reasonable agreement observed between the experimental and the predicted mode-shapes, the experimental and the numerical frequency vs. mode-number curves of the composite soundboard (shown in Fig. 4.24) were seen to follow rather different trends, especially in the lower frequency region. This made it difficult for us to know which modes were missing, and which modes from the numerical set had to be compared with every experimental mode. It was only after comparing the experimental mode-frequency trend of the constructed composite soundboard with that of the wooden soundboard that a similarity was observed between the trends, allowing us to decide which pairs had to be compared. Figure 4.27 presents the numerical and the experimental mode-frequencies of the wooden and the composite soundboards. One interesting observation in this comparison is that while the first five natural-frequencies of the constructed composite soundboard were seen to differ from those predicted numerically, they are found to be really similar to the first five mode-frequencies of the wooden soundboard (both the existing soundboard and its numerical model).
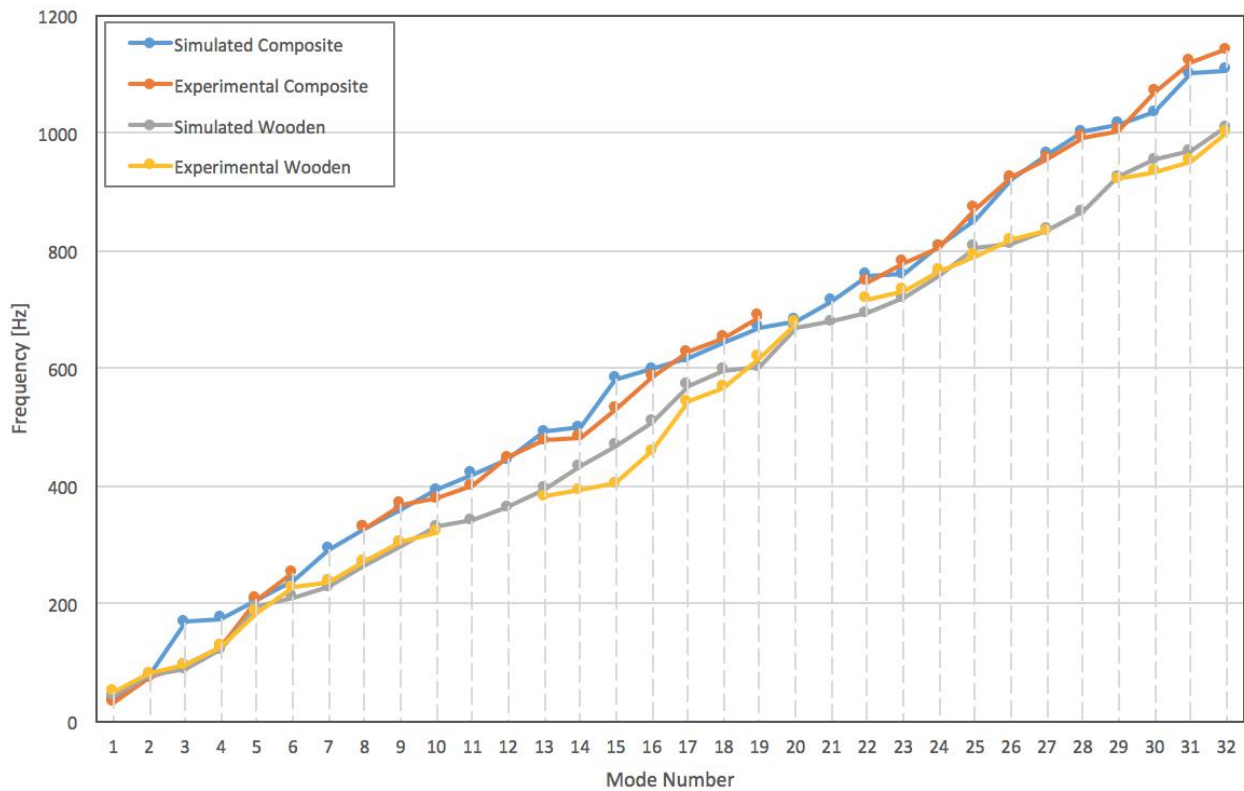
Figure 4.27: Experimental natural frequencies of the wooden and the composite soundboards under free BCs, plotted vs. mode number. Notice that the orange curve is superimposed on the grey and the yellow curves in the first 4 modes.

The FRFs obtained from a similar point on both soundboards are presented in Fig. 4.28. Keep in mind that our aim when designing the composite soundboard was not to match the natural frequencies at this stage, but rather to match them under hinged BCs, so the differences in the mode-frequencies were expected, and the FRFs are presented simply to observe the mode-amplitudes and search for similarities.
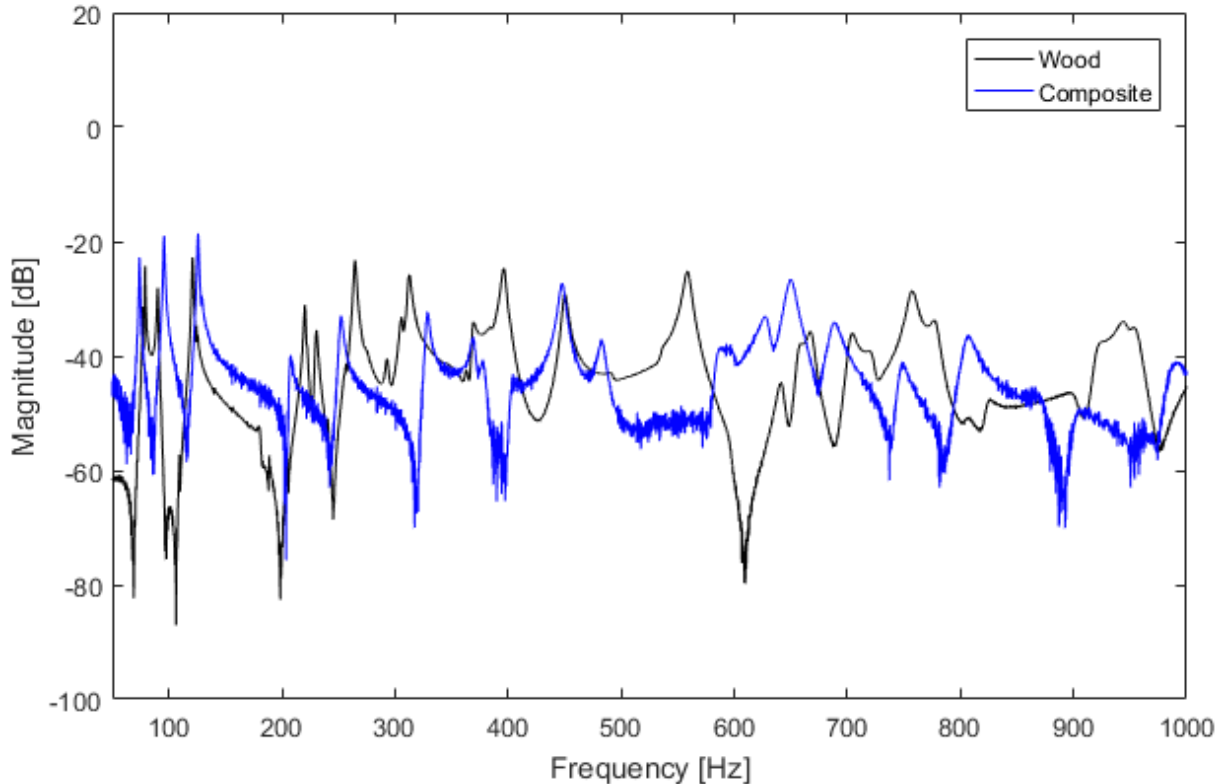
Figure 4.28: FRFs corresponding to the wooden and the composite soundboard. The measurement point was identical between the two soundboards, as well as the impact points.

4.6   Sources of Error

Considering the discussions elaborated in this chapter, the following are some of the factors that may have resulted in differences between the experimental and the simulation results:

○ The frequency and the occurrence of peaks in the experimental FRFs are both sensitive to boundary conditions, the tapping and measurement locations, the resolution of the sensors used and human errors while conducting the experiments. The very act of choosing FRF peaks as experimental natural frequencies for a structure can therefore be subject to a number of errors.

○ Aside from the errors associated with the process of experimental modal analysis, performing the experiments on an unpolished wooden structure like the wooden soundboard was seen to be subject to changes due to humidity and temperature variations. If the results of the experiments on the first day were taken as the reference for the wooden soundboard, the mode-frequencies would have differed from those predicted by the model.

○ Considering the variability observed in the material properties of Picea Abies reported in different sources, the extent to which we can rely on the reported physical, geometric and elastic properties of Picea Abies is still questionable. A more reliable way of determining these properties would have been to extract them experimentally. The same applies to the foams and the composite materials used.

○ As explained earlier, the thickness of the foams being used in the soundboard (especially that of the top plate) played a role in the experimental mode-frequencies being different from those predicted by the numerical model. The silhouette of the top plate being slightly larger than the intended outline could have also been a source of mismatch in mode-frequencies and mode-shapes.

○ The presence of the glue in the constructed composite soundboard, and the 0.32mm-deep slots not having been created in the overlapping braces is believed to play a role in the differences observed between the experimental and the numerical mode-frequencies and mode-shapes of the composite soundboard.

4.7 Limitations Faced

The following are some of the limitations faced throughout the course of this project:

○ Our design process mostly relied on simulation results, and the experiments on the composite parts were only meant for comparison and verification purposes, rather than being used as a part of the design process. This was simply because not all the potential materials considered were at our disposal throughout the project.

One consequence of this limitation was that a number of parameters that could be extracted experimentally and could also be considered in the design process had to be disregarded, e.g., loss coefficient and modal damping values, as it was not possible to determine them numerically or analytically for a complex structure like the guitar, prior to construction.

Another consequence was that we could not foresee possible mismatches between the expected geometric, mechanical and physical properties, and those of the delivered parts, or mismatches between the numerical model and the constructed parts.

○ Although it is possible to create FRFs on Abaqus from the determined modal data, creating an accurate FRF with correct modal damping values required us to have the modal damping ratios for every determined mode. These damping ratios can be determined experimentally,

but not numerically prior to construction. It was therefore not possible to determine FRFs with correct damping values on Abaqus.

○ A closer look at the eigen-frequecies of the different introduced numerical models reveals that some of the neighbouring eigen-frequencies are less than 1 Hz apart. This means that if these modes appear as peaks in the measured FRFs, the interaction between the two would not allow us to identify them as two separate peaks.

○ Although a wooden soundboard was used as the reference for our design, if there are certain acceptable degrees of dissimilarities between different wooden soundboards, we are unaware of the extent of these variations in their natural frequencies and modal parameters. Therefore, although the natural frequencies and the modal properties of the constructed composite soundboard are slightly different from the reference wooden one, its natural frequencies and modal parameters might still fall within the acceptable range of variations of wooden soundboards. To know whether that is the case or not, we would have needed to perform experimental modal analyses on a number of similar wooden soundboards with the same bracing pattern, material and geometry.

○ Comparing experimental mode-frequencies to the predicted mode-frequencies depended on whether the frequency vs. mode-number plot trends were somewhat similar. In cases where the trends were seen to differ to large extents, it was difficult to know which modes had to be compared, especially since the mode-shapes start to appear at different orders as frequency increases, and comparing modes based on mode-shapes becomes an unreliable method at high frequencies.

Chapter 5

Conclusions and Future Work

5.1 Conclusions

The aim of this project was to use the Finite Element Method (FEM) to design and manufacture the soundboard of a nylon-string guitar from sandwich-structured composites, with reference to an existing wooden soundboard, and to evaluate the accuracy of the numerical models of the wooden soundboard, the brace-less composite top plate and the braced composite soundboard by means of experimental modal analysis.

The modal behaviour of the existing wooden soundboard was first studied through experimental modal analysis, where the natural frequencies of the wooden soundboard were obtained in the range of 0-1000 [Hz] under free Boundary Conditions (BCs), as well as its first 10 mode-shapes and modal damping values. The 3D CAD model of the soundboard was then built, followed by a numerical simulation of the modal behaviour of the soundboard. The natural frequencies of the wooden soundboard obtained experimentally were found to vary to large extents over time, which was believed to be due to the variations of temperature and humidity.

The bending stiffness, mass and the strength of the wooden top plate were first used as guidelines for an initial composite top plate design. Using FEM, the effect of varying certain physical, geometric and elastic properties of the materials used in the top plate were determined on its natural frequencies under free BCs. The effect of varying the bracing materials was then determined on the mode-frequencies of the composite soundboard under free and hinged BCs. The composite soundboard that was determined to have natural frequencies relatively similar to those of the wooden soundboard under hinged BCs, and could be built from commercially available materials was constructed. To verify the results

predicted numerically, experimental modal analyses were performed on the composite top plate and the composite soundboard under free BCs.

The composite soundboard constructed was made up of a top plate sandwich layup containing pre-preg carbon fibre face layers (Newport 321 plies) and a Rohacell Rist 110 core foam (NCT321/1mmRist110/NCT321), and braces of different thicknesses containing Newport 321 plies and Rohacell HF 71 core foams.

The experimental mode-frequencies of the constructed composite top plate were seen to match those predicted numerically in the lower frequency range, slightly diverging from the numerical values as frequency increases, while following a similar trend. In the first 9 modes, the experimental and the numerical frequencies were seen to differ by 1.66 to 8.04 [Hz] from the predicted eigen-frequencies (avg. of 4.37 [Hz] absolute difference), which we consider a successful match. The higher natural frequencies, however, were found to be further from the predicted values, i.e. 2.54 to 46 [Hz] away from the predicted eigen-frequencies (avg. of 19.20 [Hz] absolute difference). This was believed to be due to the thickness of the top plate core foam being slightly larger than previously assumed. The 10th and the 20th modes predicted were not excited, therefore the modal density of the constructed top plate in the range of 0-740 [Hz] was 30 modes, while the predicted value was 32. Furthurmore, among the first 10 mode-shapes of the constructed composite top plate, the first 9 were found to match the predicted shapes.

In analyzing the results of the experiments on the braced composite soundboard, the first 6 mode-shapes were found to match those predicted by the simulation, and modes 7 to 10 were found to be similar with some local differences. The experimental mode-frequencies up to 1200 [Hz] were found to differ from the predicted values by 0.77 to 52.68 [Hz] (avg. of 17.22 [Hz]), with the low and mid-frequency modes exhibiting more significant mismatches. The numerical and the experimental frequency vs. mode-number curves in this case were seen to follow less similar trends. Modes 7, 19 and 20 were not excited, making the modal density of the top plate 29 over the 0-1200 [Hz] range, while the predicted value was 32. Surprisingly, the first few experimental mode-frequencies of the constructed composite top plate were seen to follow a more similar trend to that of the wooden soundboard, than to that of the numerical model of the composite soundboard.

Overall, the agreement observed between the numerical and the experimental results were considered satisfactory, the use of the FEM was found useful and reasonably accurate in the design of a soundboard made from sandwich-structured composites, and the objectives of the project were met.

5.2 Future Work

Studying the modal parameters of a guitar soundboard only gives us a partial idea about the timbre of the instrument, and as explained in Chap. 2, once the soundboard is attached to the rest of the body, the interaction between the soundboard and the body through the boundaries will change the modal parameters of the soundboard. In order to determine the vibrational behaviour of the instrument as a whole, it would be required to attach the soundboard to the body and repeat the experiments on a full instrument. The loss coefficient and the damping ratios associated with the different modes could also be monitored, in order to better describe the vibrational behaviour of the soundboard. This could be followed with a psychoacoustic analysis of the sound of the constructed instrument. In fact, a psychoacoustic analysis on the instrument would ultimately be the point where we can determines whether we have succeeded in imitating the wooden soundboard, and if not, in what terms and to what extent the sound of the instrument is different from that of the reference wooden instrument.

One further analysis that can be carried out in continuation of this study is a stress analysis on the wooden and the composite soundboard using the Finite Element Method. For that, the bridge and the saddle of the instrument would need to be included in the numerical model of the soundboard, and the exact tension of the strings will need to be known.

Another component that could add value to this research is the study of the effect of temperature and humidity variations on the modal parameters of wooden soundboards, where the temperature and the humidity of the space the soundboard is stored and tested in is controlled and monitored over time, as well as the initial moisture content of the wood and the heat treatments it has gone through.

Although a number of studies have been done on the variation and categorization of wooden guitars, e.g. [14], as explained in Sec. 4.7, one thing that remains unknown to us is the extent of variations conventionally observed between the vibrational behaviour of wooden nylon-string guitar soundboards. It would therefore be useful to perform experimental modal analyses on a large number of wooden soundboards, in order to have an idea about the extent of these variations.

It is worth mentioning that even though sandwich-structured composites with the proposed layup may be a reasonable replacement for wood in the construction of nylon-string guitar soundboards, it is highly possible that creating custom-made composites, as opposed

to pre-preg plies, can give us the freedom to create parts with specifically designed density, thickness and elastic properties.

Last but not least, an idea that is worth exploring is the use of the genetic algorithm and machine learning techniques in coming up with an optimized design for the composite soundboard. As mentioned in Sec. 3.4, this project was not treated as an optimization problem, mainly because there were technically infinite possibilities that could be tested. The genetic algorithm has only recently been used in material selection problems like ours, which is based on multi-objective functions with infinite possible solutions. In the case of this project, the genetic algorithm could come up with a large number of possible soundboard designs, and depending on how we define our optimization criteria, machine learning techniques could be used to choose the most promising designs.

Bibliography

[1] T. D. Rossing, Ed., *Science of String Instruments.* Springer, 2010, vol. New York.

[2] (2012, February) Vanishing tonewoods. Living On Earth. [Online]. Available: http://www.loe.org/shows/segments.html?programID=12-P13-00005&segmentID=6

[3] Ovation 1187-247. [Online]. Available: http://www.dreamguitars.com/detail/3785-ovation_1187247_59/

[4] R. M. French, *Technology of the Guitar.* Springer, 2012.

[5] The emerald guitar story. [Online]. Available: http://emeraldguitars.com/the-emerald-guitars-story/?v=3e8d115eb4b3

[6] T. Ono and D. Isomura, "Acoustic characteristics of carbon fiber-reinforced synthetic wood for musical instrument soundboards," *Acoustical science and technology*, vol. 25, no. 6, pp. 475–477, 2004.

[7] S. M. Probert, "Design, manufacture and analysis of a carbon fiber epoxy composite acoustic guitar design," Master's thesis, University of Washington, 2007.

[8] M. Roest, "Design of a composite guitar," Master's thesis, Delft University of Technology, August 2016.

[9] E. Davis, "On the structural acoustic design of guitar soundboards," Ph.D. dissertation, University of Washington, 1990.

[10] J. L. Romanillos and M. H. Winspear, *Antonio De Torres: Guitar Maker - His Life and Work.* Westport, CT: Bold Strummer, 1997.

[11] R. Reynolds. Classical guitars by randy reynolds. [Online]. Available: http://www.reynoldsguitars.com/dcon.shtml

[12] 1998 boaz/majkowski kasha-schneider concert guitar - classical guitar. [Online]. Available: http://www.dreamguitars.com/detail/1739-boaz_majkowski_kashaschneider_concert_guitar_lisa_5/

[13] Ortega m200cs-c nemesis series classical guitar with spruce nomex double top and solid madagascar rosewood for. [Online]. Available: https://www.amazon.co.uk/d/cj6/Ortega-M200CS-C-Nemesis-Classical-Guitar-Madagascar-Rosewood/B00DUQT782

[14] H. Mansour, V. Fréour, C. Saitis, and G. P. Scavone, "Post-classification of nominally identical steel-string guitars using bridge admittances," *Acta Acustica united with Acustica*, vol. 101, no. 2, pp. 394–407, 2015.

[15] C. Besnainou, "From wood mechanical measurements to composite materials for musical instruments: New technology for instrument makers," *MRS Bulletin*, vol. 20, no. 3, pp. 34–36, 1995.

[16] What's the deal with carbon fiber guitars? pros vs cons. [Online]. Available: http://www.guitaradventures.com/carbon-fiber-guitars-pros-vs-cons

[17] Gibson launches first composite-fingerboard guitars. [Online]. Available: http://www.musicroom.com/blog/gibson-launches-first-composite-fingerboard-guitars

[18] Ws1000n2. [Online]. Available: http://www.rainsong.com/classic/ws6.html

[19] Alan. (2017, May) X20 nylon amber artisan gallery. [Online]. Available: http://emeraldguitars.com/gallery/x20-nylon-amber-artisan-gallery/?v=3e8d115eb4b3

[20] About us. [Online]. Available: https://luisandclark.com/about/

[21] "Carbony celtic winds," Company Overview, Carbony Celtic Winds. [Online]. Available: https://carbony.com/

[22] A. Lenz, "Identifying drone reeds," Santa Cruz, California, 2001-2014. [Online]. Available: http://bagpipejourney.com/articles/dronereedsid.shtml

[23] The violin. Luis and Clark. [Online]. Available: https://luisandclark.com/the-instruments/the-violin/

[24] T. Ono, "Frequency responses of wood for musical instruments in relation to the vibrational properties," *Journal of the Acoustical Society of Japan (E)*, vol. 17, no. 4, pp. 183–193, 1996.

[25] T. Ono, S. Miyakoshi, and U. Watanabe, "Acoustic characteristics of unidirectionally fiber-reinforced polyurethane foam composites for musical instrument soundboards," *Acoustical Science and Technology*, vol. 23, no. 3, pp. 135–142, 2002.

[26] Y. Lu, "Comparison of finite element method and modal analysis of violin top plate," Master's thesis, McGill University, 2013.

[27] A. Damodaran, H. Mansour, L. Lessard, G. Scavone, and A. S. Babu, "Application of composite materials to the chenda, an indian percussion instrument," *Applied Acoustics*, vol. 88, pp. 1–5, 2015.

[28] R. Viala, V. Placet, and S. Cogan, "Model-based effects screening of stringed instruments, numerical prototyping art and craft domains," 34th edition of IMAC Presentation, January 2016.

[29] Frequently asked questions. [Online]. Available: https://www.guitarsalon.com/faq.php

[30] N. H. Fletcher and T. D. Rossing, *The Physics of Musical Instruments*, 2nd ed. New York: Springer Science, 1998.

[31] J. O. S. III, "The dispersive 1d wave equation," Appendix, 2010. [Online]. Available: https://ccrma.stanford.edu/~jos/pasp/Dispersive_1D_Wave_Equation.html

[32] B. Colosi. Costum guitar saddles by bob colosi. [Online]. Available: http://www.guitarsaddles.com/gen_info.asp

[33] F. Mueller. Fritz Mueller, luthier 7210 Tatlayoko Road Tatlayoko Lake, British Columbia British Columbia, Canada. [Online]. Available: http://www.classicalguitars.ca/features.htm

[34] How does a guitar work? [Online]. Available: https://newt.phys.unsw.edu.au/music/guitar/guitarintro.html

[35] U. G. Wegst, "Wood for sound," *American Journal of Botany*, vol. 93, no. 10, pp. 1439–1448, 2006.

[36] R. C. Hibbeler, *Mechanics of Materials*, 8th ed. Boston: Prentice Hall, 2011.

[37] Module 3 constitutive equations. Module Notes. [Online]. Available: http://web.mit.edu/16.20/homepage/3_Constitutive/Constitutive_files/module_3_with_solutions.pdf

[38] F. C. Campbell, *Structural Composite Materials.* Materials Park, Ohio: ASM International, 2010.

[39] M. Avitabile, "Experimental modal analysis," *Society of Experimental Mechanics*, vol. 22, no. 2, Mar/Apr 1998.

[40] P. Dunham. Introduction to dynamic simulation. [Online]. Available: http://www.ni.com/tutorial/11606/en/

[41] G. Caldersmith, "Guitar as a reflex enclosure," *The Journal of the Acoustical Society of America*, vol. 63, no. 5, pp. 1566–1575, 1978.

[42] O. Christensen and B. B. Vistisen, "Simple model for low-frequency guitar function," *The Journal of the Acoustical Society of America*, vol. 71, no. S1, pp. S8–S8, 1982.

[43] J. E. Popp, "Four mass coupled oscillator guitar model," *The Journal of the Acoustical Society of America*, vol. 131, no. 1, pp. 829–836, 2012.

[44] J. Dean. Introduction to the finite element method (fem) lecture 2 first and second order one. [Online]. Available: http://www.ccg.msm.cam.ac.uk/images/FEMOR_Lecture_2.pdf

[45] T. Rees. (2009) Chladni plates: the first step towards visualizing sound. [Online]. Available: http://www.sites.hps.cam.ac.uk/whipple/explore/acoustics/ernstchladni/chladniplates/

[46] W. Hossak, "Topic 9: Holographic interferometry," Teaching Slides. [Online]. Available: http://www2.ph.ed.ac.uk/~wjh/teaching/mo/slides/holo-interferometry/holo-inter.pdf

[47] J. Thomas. Property comparison. [Online]. Available: http://classes.mst.edu/civeng5260/concept/04/04/property_comparison/index.html

[48] F. Ford. Grain runout. [Online]. Available: http://www.lutherie.net/frankford.runout.html

[49] M. Mehdi Jalili, S. Yahya Mousavi, and A. S. Pirayeshfar, "Investigating the acoustical properties of carbon fiber-, glass fiber-, and hemp fiber-reinforced polyester composites," *Polymer Composites*, vol. 35, no. 11, pp. 2103–2111, 2014.

[50] E. R. G. Tapia, *Simulating a Classical Acoustic Guitar, Finite Elements and Multi-physics Modelling*, 2002.

[51] M. Elejabarrieta, A. Ezcurra, and C. Santamaría, "Evolution of the vibrational behavior of a guitar soundboard along successive construction phases by means of the modal analysis technique," *The Journal of the Acoustical Society of America*, vol. 108, no. 1, pp. 369–378, 2000.

[52] ——, "Vibrational behaviour of the guitar soundboard analysed by the finite element method," *Acta Acustica united with Acustica*, vol. 87, no. 1, pp. 128–136, 2001.

[53] M. Elejabarrieta, C. Santamaria, and A. Ezcurra, "Air cavity modes in the resonance box of the guitar: the effect of the sound hole," *Journal of Sound and vibration*, vol. 252, no. 3, pp. 584–590, 2002.

[54] M. Elejabarrieta, A. Ezcurra, and C. Santamarıa, "Coupled modes of the resonance box of the guitar," *The Journal of the Acoustical Society of America*, vol. 111, no. 5, pp. 2283–2292, 2002.

[55] Consistent units. [Online]. Available: http://www.dynasupport.com/howtos/general/consistent-units

[56] S. Marburg, "Discretization requirements: How many elements per wavelength are necessary?" in *Computational Acoustics of Noise Propagation in Fluids-Finite and Boundary Element Methods.* Springer, 2008, pp. 309–332.

[57] A. J. Jerri, "The shannon sampling theorem—its various extensions and applications: A tutorial review," *Proceedings of the IEEE*, vol. 65, no. 11, pp. 1565–1596, 1977.

[58] S. S. Tavallaey, "Wave propagation in sandwich structures," 2001.

[59] M. F. Ashby and D. Cebon, "Materials selection in mechanical design," *Le Journal de Physique IV*, vol. 3, no. C7, pp. C7–1, 1993.

[60] E. E. Gdoutos and I. M. Daniel, "Failure mechanisms of composite sandwich structures," September 2009.

[61] "Technical data sheet - flaxply," Technical Data Sheet, Lineo. [Online]. Available: http://www.lineo.eu/download/2015-TDS-FlaxPly.pdf

[62] "Spruce/whitewood (picea abies)," Sweden.

[63] F. W. Schwarze, M. Spycher, and S. Fink, "Superior wood for violins–wood decay fungi as a substitute for cold climate," *New Phytologist*, vol. 179, no. 4, pp. 1095–1104, 2008.

[64] I. M. Daniel, E. E. Gdoutos, and Y. D. Rajapakse, *Major accomplishments in composite materials and sandwich structures: an anthology of ONR sponsored research.* Springer Science & Business Media, 2009.

[65] "Negative poisson's ratio materials," Research Notes. [Online]. Available: http://silver.neep.wisc.edu/~lakes/Poisson.html

[66] *Rohacell Rist-HT Technical Information*, Rohacell, June 2016. [Online]. Available: http://www.rohacell.com/sites/lists/RE/DocumentsHP/ROHACELL-RIST-HT-technical-information-en.pdf

[67] *Rohacell HF Technical Information*, Rohacell, February 2017. [Online]. Available: http://www.rohacell.com/sites/lists/RE/DocumentsHP/ROHACELL%20HF%20Product%20Information.pdf

[68] Rubi dx-350-n 1300 laser and level bridge wet saw 110v. [Online]. Available: http://www.protilertools.co.uk/rubi-wet-saws/1835/rubi-dx-350-n-1300-laser-level-bridge-wet-saw-110v-52917

[69] Vibrant learning lab - 7/23/2014 - curve fitting using me'scope. [Online]. Available: https://www.youtube.com/watch?v=GhvSjySH0cU